



The Journal of Gemmology

Volume 36 / No. 7 / 2019



Diamond Verification Instrument
Testing by the Assure Program

Inclusions in Thai Rubies

Gem Exploration in Canada

Images Seen Through Calcite

SSEF

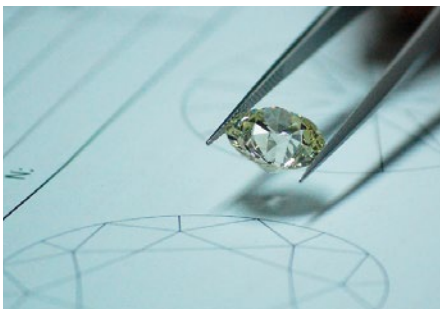
SCHWEIZERISCHES GEMMOLOGISCHES INSTITUT
SWISS GEMMOLOGICAL INSTITUTE
INSTITUT SUISSE DE GEMMOLOGIE



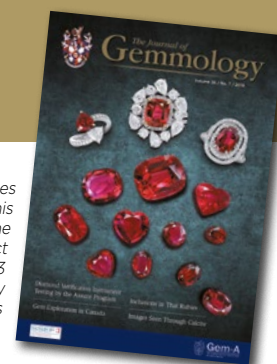
ORIGIN DETERMINATION · TREATMENT DETECTION

DIAMOND GRADING · PEARL TESTING

EDUCATION · RESEARCH



THE SCIENCE OF GEMSTONE TESTING™



Cover photo: Thai rubies are rarely mined today, although the stones continue to circulate in the market. An article on pp. 634–645 of this issue provides a detailed view of the inclusions in these rubies. The heat-treated stones shown here include loose rubies weighing 3–24 ct (courtesy of a private collector) and diamond rings set with 3.58, 4.43 and 3.26 ct centre stones (left ring courtesy of Thai Lapidary International Co. Ltd, Bangkok, Thailand, and the center and right rings are from Prima Gems, Bangkok). Photo by Chanchai Kamemakanon.

COLUMNS

Editorial 577

What's New 578

3DPro 360° Video Imaging System | DiaTrue CS, CL and CM | GLIS Mini | Q-Chk++ | Smart-Raman Portable Spectrometer | Varna-D Diamond Colour-Grading Instrument | Gemlogis Vista | 2017 and 2018 Dallas Mineral Collecting Symposium Presentations | Diamond Disclosure Reports from De Beers | Gemmological Society of Japan 2019 Annual Meeting Abstracts | Jewelry Development Impact Index Report on Emerald Mining in Colombia and Zambia | MSA Centennial Symposium Presentations | MJSa Expo Seminar Presentations | Platinum Jewellery Business Review 2019

Gem Notes 582

Albite from Brazil | Dark Blue Beryl from Pakistan | Emerald from Nunavut, Canada | Mesolite Cabochons from India | Quartz from Brazil with Biotite Inclusions | Quartz from Brazil with Dendritic Inclusions | Sapphire with Unusual Inclusion Scenery | Scapolite from Brazil | Spessartine Reportedly from Ethiopia | Diamond Mining at Theindaw, Myanmar | Early Illustration of Sparkle in Diamonds | Nur al-Ayn Diamond Rephotographed | Cultured Abalone Pearls from Chile | Pearls from *Tutufa bubo* | Eulytine Inclusions in Manufactured Glass | Opal Doublets from Slovakia | Heated Sapphires with Unstable Colour Centres | 2019 Rough Stone Sales in Myanmar

ARTICLES

Selecting a Diamond Verification Instrument Based on the Results of the Assure Program: An Initial Analysis 606

By Harold Dupuy and Jon C. Phillips

Adding Logic to Luck: Recent Advances in Coloured Stone Exploration in Canada 620

By Lee A. Groat

An Update on Mineral Inclusions and Their Composition in Ruby from the Bo Rai Gem Field in Trat Province, Eastern Thailand 634

By Supparat Promwongnan and Chakkaphan Sutthirat

Doubling and Differential Magnification of Images Seen Through Calcite and Other Uniaxial Materials 646

By Harold Killingback



Photo by Jeff Scovil



Photo courtesy of Hillberg & Berk

Conferences 656

Scottish Gemmological Association Conference | 5th Mediterranean Gemmological & Jewellery Conference | AGA Las Vegas Conference | 7th European Gemmological Symposium

Gem-A Notices 664 **New Media** 670

Learning Opportunities 666 **Literature of Interest** 674

The Journal is published by Gem-A in collaboration with SSEF and with the support of AGL.



The Journal of Gemmology

EDITOR-IN-CHIEF

Brendan M. Laurs
brendan.laurs@gem-a.com

EXECUTIVE EDITOR

Alan D. Hart

EDITORIAL ASSISTANT

Carol M. Stockton

EDITOR EMERITUS

Roger R. Harding

ASSOCIATE EDITORS

Ahmadjan Abduriyim, *Tokyo Gem Science LLC, Tokyo, Japan*; Raquel Alonso-Perez, *Harvard University, Cambridge, Massachusetts, USA*; Edward Boehm, *RareSource, Chattanooga, Tennessee, USA*; Maggie Campbell Pedersen, *Organic Gems, London*; Alan T. Collins, *King's College London*; John L. Emmett, *Crystal Chemistry, Brush Prairie, Washington, USA*; Emmanuel Fritsch, *University of Nantes, France*; Rui Galopim de Carvalho, *PortugalGemas Academy, Lisbon, Portugal*; Lee A. Groat, *University of British Columbia, Vancouver, Canada*; Thomas Hainschwang, *GGTL Laboratories, Balzers, Liechtenstein*; Henry A. Hänni, *GemExpert, Basel, Switzerland*; Jeff W. Harris, *University of Glasgow*; Alan D. Hart, *Gem-A, London*; Ulrich Henn, *German Gemmological Association, Idar-Oberstein*; Jaroslav Hýršl, *Prague, Czech Republic*; Brian Jackson, *National Museums Scotland, Edinburgh*; Mary L. Johnson, *Mary Johnson Consulting, San Diego, California, USA*; Stefanos Karamelas, *Bahrain Institute for Pearls & Gemstones (DANAT), Manama*; Lore Kiefert, *Gübelin Gem Lab Ltd, Lucerne, Switzerland*; Hiroshi Kitawaki, *Central Gem Laboratory, Tokyo, Japan*; Michael S. Krzemnicki, *Swiss Gemmological Institute SSEF, Basel*; Shane F. McClure, *Gemmological Institute of America, Carlsbad, California*; Jack M. Ogden, *London*; Federico Pezzotta, *Natural History Museum of Milan, Italy*; Jeffrey E. Post, *Smithsonian Institution, Washington DC, USA*; Andrew H. Rankin, *Kingston University, Surrey*; Benjamin Rondeau, *University of Nantes, France*; George R. Rossman, *California Institute of Technology, Pasadena, USA*; Karl Schmetzer, *Petershausen, Germany*; Dietmar Schwarz, *Federated International GemLab, Bangkok, Thailand*; Menahem Sevdemish, *Gemewizard Ltd, Ramat Gan, Israel*; Andy H. Shen, *China University of Geosciences, Wuhan*; Guanghai Shi, *China University of Geosciences, Beijing*; James E. Shigley, *Gemmological Institute of America, Carlsbad, California*; Christopher P. Smith, *American Gemmological Laboratories Inc., New York, New York*; Evelyn Stern, *London*; Elisabeth Strack, *Gemmologisches Institut Hamburg, Germany*; Tay Thye Sun, *Far East Gemmological Laboratory, Singapore*; Pornsawat Wathanakul, *Kasetsart University, Bangkok*; Chris M. Welbourn, *Reading, Berkshire*; Bert Willems, *Leica Microsystems, Wetzlar, Germany*; Bear Williams, *Stone Group Laboratories LLC, Jefferson City, Missouri, USA*; J. C. (Hanco) Zwaan, *National Museum of Natural History 'Naturalis', Leiden, The Netherlands*.

CONTENT SUBMISSION

The Editor-in-Chief is glad to consider original articles, news items, conference/excursion reports, announcements and calendar entries on subjects of gemmological interest for publication in *The Journal of Gemmology*. A guide to the various sections and the preparation of manuscripts is given at <https://gem-a.com/index.php/news-publications/journal-of-gemmology/submissions>, or contact the Editor-in-Chief.

SUBSCRIPTIONS

Gem-A members receive *The Journal* as part of their membership package, full details of which are given at <https://gem-a.com/membership>. Laboratories, libraries, museums and similar institutions may become direct subscribers to *The Journal*.

ADVERTISING

Enquiries about advertising in *The Journal* should be directed to advertising@gem-a.com. For more information, see <https://gem-a.com/news-publications/media-pack-2019>.

DATABASE COVERAGE

The Journal of Gemmology is covered by the following abstracting and indexing services: Clarivate Analytics' (formerly Thomson Reuters/ISI) Science Citation Index Expanded (also known as SciSearch, in the Web of Science), *Journal Citation Reports (Science Edition)* and *Current Contents (Physical, Chemical and Earth Sciences)*; Elsevier's Scopus; Australian Research Council's Excellence in Research for Australia (ERA) Journal List; China National Knowledge Infrastructure (CNKI Scholar); EBSCO's Academic Search Ultimate; ProQuest (Cambridge Scientific Abstracts); GeoRef; CrossRef; Chemical Abstracts (CA Plus); Mineralogical Abstracts; Index Copernicus ICI Journals Master List; Gale Academic OneFile; British Library Document Supply Service; and Copyright Clearance Center's RightFind application.

Science Citation Index
Expanded

Web of Science

Clarivate
Analytics

COPYRIGHT AND REPRINT PERMISSION

For full details of copyright and reprint permission contact the Editor-in-Chief. *The Journal of Gemmology* is published quarterly by Gem-A, The Gemmological Association of Great Britain. Any opinions expressed in *The Journal* are understood to be the views of the contributors and not necessarily of the publisher.

Design & production by Zest Design, www.zest-uk.com

Printed by DG3 Group (Holdings) Ltd

© 2019 Gem-A (The Gemmological Association of Great Britain)
ISSN 1355-4565 (Print), ISSN 2632-1718 (Online)

Mixed Sources
Product group from well-managed
forests and other controlled sources
www.fsc.org Cert no. TIC-COC-1024
© 1996 Forest Stewardship Council



Gem-A
THE GEMMOLOGICAL ASSOCIATION
OF GREAT BRITAIN

21 Ely Place
London EC1N 6TD
UK

t: +44 (0)20 7404 3334
f: +44 (0)20 7404 8843
e: information@gem-a.com
w: <https://gem-a.com>

Registered Charity No. 1109555
A company limited by guarantee and
registered in England No. 1945780
Registered office: Palladium House,
1-4 Argyll Street, London W1F 7LD

PRESIDENT

Maggie Campbell Pedersen

VICE PRESIDENTS

David J. Callaghan
Alan T. Collins
Noel W. Deeks
Andrew H. Rankin

HONORARY FELLOWS

Gaetano Cavalieri
Andrew Cody
Terrence S. Coldham
Emmanuel Fritsch

HONORARY DIAMOND MEMBER

Martin Rapaport

CHIEF EXECUTIVE OFFICER

Alan D. Hart

COUNCIL

Justine L. Carmody – Chair
Nevin Bayoumi-Stefanovic
Kathryn L. Bonanno
Louise Goldring
Joanna Hardy
Philip Sadler
Christopher P. Smith

BRANCH CHAIRMEN

Midlands – Louise Ludlam-Snook
North East – Mark W. Houghton
South East – Veronica Wetten
South West – Richard M. Slater

Editorial

THE JOURNAL JOINS THE PRESTIGIOUS SCIE DATABASE

I am very pleased to announce that *The Journal of Gemmology* has been accepted for coverage in the Science Citation Index Expanded (SCIE) database, in the Web of Science Core Collection. This indicator of academic excellence for scientific journals is a landmark accomplishment for *The Journal*, which passed a rigorous selection process involving numerous evaluative criteria to ensure that it meets high standards of academic quality.

The SCIE is a comprehensive database covering more than 9,200 scientific journals across 178 disciplines. Along with *The Journal's* coverage in the SCIE, it is also included in Clarivate Analytics' *Journal Citation Reports* and its *Current Contents—Physical, Chemical and Earth Sciences*.

Importantly, coverage in the SCIE will allow *The Journal* to obtain an impact factor (a measure of citation activity). Although *The Journal* was previously included in the Web of Science through its coverage in the Emerging Sources Citation Index, that database does not include an impact factor. Since authors from some academic institutions can only receive 'credit' for articles published in journals with an impact factor, *The Journal's* coverage in the SCIE will allow it to attract even more high-quality research from around the world.

A journal's impact factor is calculated by counting the number of citations to the articles it published in the previous two years, and dividing this number by the total citable articles that it published during those two years. *The Journal's* initial impact factor will thus be determined by adding up the number of citations received during 2019 for articles published in 2017 and 2018, and dividing this by the total number of articles published in 2017 and 2018. Clarivate Analytics will perform the calculations in early 2020, and the impact factor will be published in the

Journal Citation Reports (and posted on *The Journal's* website) in approximately June 2020.

Specialised publications such as *The Journal* typically have relatively low impact factors compared to those covering mainstream disciplines such as chemistry and physics. This is certainly understandable, considering that citations are only counted from journals already in the SCIE. There is currently only one other gemmological journal in that database (*Gems & Gemology*), although some citation activity would also be expected from earth and materials science journals in the SCIE.

As for any title covered by the SCIE, *The Journal* must continue to maintain its quality and impact criteria, as judged by Clarivate Analytics, in order to remain in this database. The evaluation process and selection criteria are described at <https://clarivate.com/webofsciencengroup/journal-evaluation-process-and-selection-criteria>.

The Journal's coverage in the SCIE reflects Gem-A's core values of providing high-quality gemmological education and sharing cutting-edge research with the gemmological and earth science communities. Inclusion of *The Journal* in the SCIE will help

elevate gemmology even further with scientists and academics. I thank *The Journal's* Associate Editors for sharing their expertise and maintaining high scientific standards while reviewing articles submitted for publication. I am also grateful to our authors for sharing their research and for their perseverance during the review process. Finally, I thank our readers for their ongoing support. Please join me in celebrating this important milestone for *The Journal of Gemmology*.

Brendan M. Laurs FGA
Editor-in-Chief

Science Citation Index
Expanded

Web of Science 

What's New

INSTRUMENTATION



3DPro 360° Video Imaging System

In April 2019, ImaGem Inc. (Ardmore, Pennsylvania, USA) released 3DPro, a digital photo box designed to capture videos of mounted and unmounted gemstones during a 360° rotation. The 23 × 23 × 23 cm box comes with a built-in rotary stage, lighting, camera, software and 12-volt adapter usable worldwide. Operation requires a laptop computer. Lighting, background colour, and camera position can all be modified. Output is 5 MP in a variety of graphic formats. For additional information and sample videos, visit <https://imageminc.com/3d>.

DiaTrue CS, CL and CM

In the first half of 2019, OGI Systems Ltd. (Israel) launched its latest models in the line of DiaTrue diamond detectors, accompanied by updates to the entire DiaTrue line, which enable all of the models to simultaneously scan and identify CVD- and HPHT-grown synthetic diamonds, as well as CZ and synthetic moissanite. DiaTrue CS is a compact desktop unit with a 5 × 5 cm tray that can accommodate small melee parcels or ring-mounted samples in the D-K colour range. A scan takes approximately 7–10 seconds. The unit measures 26.5 × 21 × 22.5 cm and weighs 6.5 kg. DiaTrue CL is the largest of the three; the tray is 20 × 20 cm and the unit measures 28 × 25 × 50 cm (8.5 kg). DiaTrue CM is intermediate in size and capacity between the CS and CL. All models can save test data and create printable DiaTrue reports. Visit www.ogisystems.com/diatrucecs.html (for the CS), www.ogisystems.com/diatruexl.html (for the CL) and www.ogisystems.com/diatrue.html (for the CM).



GLIS Mini

A portable version of the GLIS-3000 (see What's New section, Vol. 35, No. 4, 2016, p. 271) was released in early 2019. The GLIS Mini weighs ~3 kg and can test small batches of loose or mounted diamonds within an area measuring 5 × 6 cm. As with the GLIS-3000, the GLIS Mini uses UV fluorescence and phosphorescence to determine natural vs. synthetic (CVD and HPHT) origin, yielding results in approximately 10 seconds. Visit www.glistmachines.com/collections/frontpage/products/mini-glis.

Q-Chk++

Released in 2019, the third generation of this synthetic diamond detector from GII Arotek (Gemmological Institute of India and Arotek Scientific Instruments) features expanded capabilities. It can distinguish HPHT- and CVD-grown synthetic diamonds of any shape, size and colour grade, both loose and mounted (including pavé), within an area of 11 × 6 cm. It can reportedly test up to 1,000 samples in as little as 7 seconds based on UV fluorescence and photoluminescence together with 'optically stimulated luminescence'. The unit has a footprint of about 60 × 60 cm. Visit <https://giionline.com/q-chk-adc> or www.arotekscientific.com/lan-grown-diamond-detector.html.



Smart-Raman Portable Spectrometer

From Napco Precision Instruments (China) comes this 2019 Raman unit packed in a portable case (40 × 31 × 17 cm), including laser, detector, cooling unit and laptop computer with dedicated software and a Raman database. It features a 100–500 mW continuously adjustable laser, 3950–150 cm⁻¹ range and 8 cm⁻¹ resolution. It is powered by AC voltage or rechargeable lithium batteries with an operating life of about 3 hours. The unit can display printable Raman spectra with customisable features, and can enable a trained gemmologist to identify a variety of gem materials and screen diamonds. Visit www.napcobalances.com/product_view_152_162.html.



Varna-D Diamond Colour-Grading Instrument

ImaGem Inc. released the Varna-D diamond colour-grading instrument in April 2019. The self-contained unit grades faceted diamonds in the colour range D–L from 0.25–5 ct with a repeatable accuracy of ±½ colour grade. It is able to take into account fluorescence, zoning and secondary hues. The unit measures 15.2 × 10.8 × 8.9 cm, weighs 1 kg, and operates on a USB-chargeable Li-ion battery, making it relatively portable. An external battery pack and stone calibration sets are available separately. Visit <https://imageminc.com/products/varna-d>.

Vista

In May 2019, Gemlogis (Hong Kong) released the Vista for separating HPHT- and CVD-grown synthetic from natural diamonds. This portable instrument can test both loose and mounted samples (open- or closed-back settings) in the colour range D–J as small as 0.02 ct. The unit weighs 0.73 kg and measures 16.5 × 16.5 × 12.7 cm. The small size of the unit limits its capability to one stone or jewellery piece at a time. It is powered by a rechargeable lithium battery and also comes with an AC adapter. For additional information and to view the video on the device, visit www.gemlogisusa.com/gemlogis-vista.html.

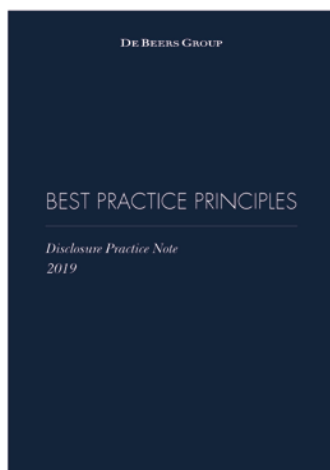


NEWS AND PUBLICATIONS

2017 and 2018 Dallas Mineral Collecting Symposium Presentations



The Dallas Mineral Collecting Symposium is held annually in August in Dallas, Texas, USA, and attracts mineral enthusiasts from around the world. Presentations from the 2017 and 2018 Symposia are now available online at www.dallassymposium.org/videos, and include topics such as gem minerals of Myanmar, colour in minerals, treasures from Pakistan, notable gems and minerals in French museums, and the history of the discovery and mining of tsavorite.



Diamond Disclosure Reports from De Beers

On 29 March 2019, the De Beers Group released two reports on disclosure: *Standard Guidance: Undisclosed Synthetic Diamonds* and *Best Practice Principles: Disclosure Practice Note 2019*. The first of

these addresses the increased occurrence of undisclosed synthetic diamonds within the diamond supply chain and the potential damage they may cause to the diamond industry, and proposes modifications to the De Beers Group's Best Practice Principles (BPP). Download the full report at www.debeersgroup.com/~media/Files/D/De-Beers-Group/documents/reports/library/2019/Standard-Guidance_Undisclosed-Synthetic-Diamonds-2019.pdf. The second report is a companion to the BPP that provides guidance to Sight-holders and Accredited Buyers on how to reduce the risk of trading in undisclosed synthetic diamonds. It includes various approaches to screening and testing, with references to De Beers' AMS2 and SYNTHdetect instruments. This report is available at www.debeersgroup.com/~media/Files/D/De-Beers-Group/documents/reports/library/2019/Disclosure-Practice-Note-2019.pdf.

Abstract of Papers Presented at Annual Meeting of the Gemmological Society of Japan

Gemmological Society of Japan 2019 Annual Meeting Abstracts

Abstracts of Special Lectures presented at the 2019 Annual Meeting of the Gemmological Society of Japan are now available online. The 22 abstracts cover a wide variety of topics, including synthetic diamond research and identification, diamond fluorescence, origin determination of gem corundum from Luc Yen (Vietnam), jadeite from the Polar Urals (Russia), red corals (origins and trace-element composition) and more. To download the abstracts from this and previous conferences, visit www.jstage.jst.go.jp/browse/gsj/list/-char/en.

Jewelry Development Impact Index Report on Emerald Mining in Colombia and Zambia

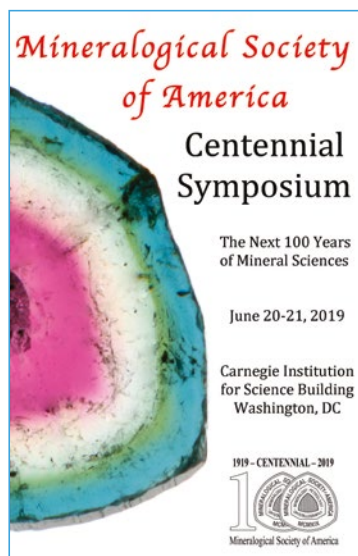


In May 2019, researchers from the American

University School of International Service produced *Jewelry Development Impact Index: A Comparative Case Study of Emerald Mining in Colombia and Zambia*. The 88-page report examines the historical and cultural background of emerald mining in these two countries, and then provides numerical scores on a variety of areas (governance, economics, environment, health and human rights) for both localities. Download this and other recent JDI publications at www.sustainablegemstones.org/jewelry-development-index-jdi.

MSA Centennial Symposium Presentations

The Mineralogical Society of America celebrated its 100th anniversary with a Centennial Symposium, held 20–21 June 2019 in Washington DC, USA. Sessions of interest to gemmologists included ‘Scientific Characterization of High-Value Gemstones’, ‘Mineral Inclusions in Diamonds from the Deep Earth’ and ‘Advances in Mineral Analysis’. Videos of all the presentations and a report of the symposium are available at www.minsocam.org/MSA/Centennial/MSA_Centennial_Symposium.



MJSA Expo Seminar Presentations

Videos of presentations and panel discussions from the March 2019 Manufacturing Jewelers & Suppliers of America (MJSA) Expo are available at https://mjsa.org/eventsprograms/mjsa_expo/expo_seminars. Presentations featuring experts in jewellery marketing and design include ‘Where does custom design go from here?’, ‘What’s new in responsible sourcing?’, ‘You’ve lost that handcrafted feeling’, ‘Celebrating the American jewelry design movement’ and ‘Tracking your digital advertising’.

Platinum Jewellery Business Review 2019

Platinum Guild International released their 2019 Platinum Jewellery Business Review on 15 May with a review of the 2018 market and outlook for 2019. It identifies the jewellery industry as the second largest market for platinum and emphasises the value of marketing to drive demand. In the four largest markets, Japan continued to show a slight

(1%) growth of retail sales through 2018, the USA had notable (11%) growth, China experienced a decline (7%) and India demonstrated significant growth (17%). The predictions for 2019 are that these trends will continue. Download the report at <https://platinumguild.com/research-publications/platinum-jewellery-business-review>.

Transforming metal into meaning



Platinum Jewellery Business Review

London, 15th May 2019

PLATINUM GUILD
INTERNATIONAL

What's New provides announcements of new instruments/technology, publications, online resources and more. Inclusion in What's New does not imply recommendation or endorsement by Gem-A. Entries were prepared by Carol M. Stockton unless otherwise noted.

Gem Notes

COLOURED STONES

Albite from Minas Gerais, Brazil

During the February 2019 Tucson gem shows in Arizona, USA, Dr Marco Campos Venuti (Seville, Spain) had some new faceted albite from Brazil. He obtained 50 kg of rough material in August 2018 while visiting Brazil, and was told that it was mined near Teófilo Otoni in Minas Gerais State. He processed the rough into 5 kg of cuttable material and then faceted several hundred carats of the albite. The largest clean gems weighed ~6.5 ct and the more-included stones ranged up to 10 ct.

Dr Campos Venuti kindly donated a 2.50 ct faceted albite to Gem-A (Figure 1), and it was characterised by author AC for this report. The stone was colourless and transparent with a vitreous lustre. The hydrostatic SG was 2.65, the RIs were 1.535–1.542 (birefringence 0.007) and the stone had a uniaxial positive optic character. These properties are consistent with albite, and this identity was confirmed by Raman analysis using a Horiba LabRam II confocal Raman microspectrometer equipped with a 532 nm laser and a high-resolution diffraction grating. The stone fluoresced moderate reddish under short-wave UV radiation and was inert to long-wave UV.



Figure 1: This 2.50 ct albite from Brazil contains conspicuous linear features. Gift of Dr Marco Campos Venuti; photo by A. Costanzo.



Figure 2: In addition to containing two sets of lamellar twinning with slightly different orientations, the albite hosts elongate hollow inclusions that appear to be etched dislocations. Photomicrograph by A. Costanzo; image width 2.6 mm.

The most common internal feature was parallel-planar lamellar twinning. A subordinate set of the twin planes was angled at a slightly different orientation (Figure 2), perhaps because the sample also contained another twin law. Even more conspicuous than the twinning were roughly textured linear features that were parallel to the main set of twin planes (again, see Figure 2). Raman microspectroscopy only yielded patterns for the host albite, suggesting that these inclusions consisted of etched dislocation channels running along twin/cleavage planes. Their hollow nature was supported by the presence of dark foreign material (probably polishing residue) where they intersected the surface of the stone.

*Dr Alessandra Costanzo FGA DGA
(alessandra.costanzo@nuigalway.ie)
National University of Ireland Galway, Ireland*

Brendan M. Laurs FGA



Figure 3: Shown from the side and top views, this deeply etched dark blue beryl crystal (236.7 g and 61 × 50 × 49 mm) is from Khyber Pakhtunkhwa in northern Pakistan. Courtesy of 3090 Gems; photos by Sara Rey.

Dark Blue Beryl from Pakistan

Pakistan is a well-known source of aquamarine, which commonly occurs as lustrous, well-formed crystals that are prized by mineral collectors. Most of the aquamarine comes from the Shengus–Dassu (or Shingus–Dusso) and Chumar Bakhoo areas of Gilgit-Baltistan (Kazmi *et al.* 1985; Appiani 2007). During the February 2019 Tucson gem shows, Meg Berry (Megagem, Fallbrook, California, USA) showed one of the authors (BML) some interesting dark blue beryl from a new find in Pakistan. According to her supplier, Bryan Lichtenstein (3090 Gems, San Francisco, California, USA), it comes from Khyber Pakhtunkhwa in northern Pakistan. The initial discovery was made in September 2018 by Raza Shah (Gems Parlor, Fremont, California), who has partnered with Lichtenstein in providing the material to the gem trade. Only a limited amount has been produced so far, mostly as 1–2 g pieces, but some are in the 30–50 g range. The largest crystal known so far weighs 236.7 g (Figure 3). The rough material is heavily etched, and some pieces are colour zoned in dark blue to dark blue-green.

Berry cut a cabochon (Figure 4) from one of the larger pieces of this beryl, and two offcuts from that sample were provided to one of the authors (GRR) for analysis. Semi-quantitative energy-dispersive X-ray fluorescence (EDXRF) chemical analysis using an INAM Expert 3L unit yielded an iron-rich composition with ~2.5 and 3.6 wt.% Fe in the two samples, as well as relatively high

levels of Cs (1.5 and 2.3 wt.% Cs). Also present were minor amounts of Mg and traces of Mn, Rb, S, Zn, Cu, Ga, Ni and V.

Visible-near infrared (Vis-NIR) spectroscopy of one of the beryl specimens was accomplished with a combination of silicon-diode and InGaAs array microspectrometers. The spectrum shows that the beryl's dark blue colour is due to an absorption minimum in the 450–500 nm region that is bounded by absorption bands in the visible region that arise from the presence of abundant Fe (Figure 5). Absorption features centred near 830 and 1080 nm are from Fe²⁺ while the band near 600 nm is due to Fe²⁺–Fe³⁺ intervalence charge transfer. These absorptions are strongly polarised, and are much more prominent in the spectrum taken with light polarised parallel to the c-axis. A weak, sharper feature near 440 nm is due to Fe³⁺. A series of sharp absorptions near 1400 nm arise from overtones of the vibrations of water molecules in the channels of the beryl structure. Additional weaker water-related features appear near 970 and 1160 nm (Wood & Nassau 1967). None of the absorptions commonly seen in Maxixe beryl were recorded in the spectra of this material from Pakistan.

Brendan M. Laurs FGA

Dr George R. Rossman
California Institute of Technology
Pasadena, California, USA



Figure 4: This cabochon of dark blue-green beryl from Pakistan weighs 7.49 ct. Pinpoint reflections are created by iridescent feathers in the stone. Photo by Orasa Weldon.

References

- Appiani, R. 2007. Pink fluorite from an exceptional new find at Chumar Bakhoo, Pakistan. *Mineralogical Record*, **38**(2), 95–100.
- Kazmi, A.H., Peters, J.J. & Obodda, H.P. 1985. Gem pegmatites of the Shingus-Dusso area, Gilgit, Pakistan. *Mineralogical Record*, **18**(5), 393–411.
- Wood, D.L. & Nassau, K. 1967. Infrared spectra of foreign molecules in beryl. *Journal of Chemical Physics*, **47**(7), 2220–2228, <https://doi.org/10.1063/1.1703295>.

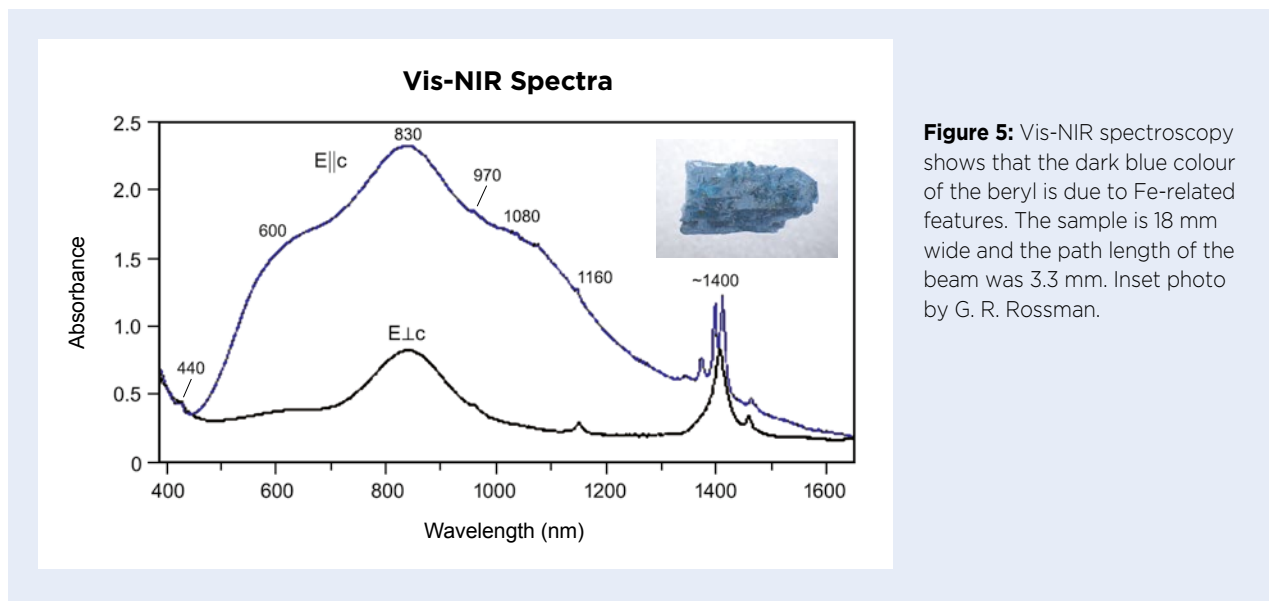


Figure 5: Vis-NIR spectroscopy shows that the dark blue colour of the beryl is due to Fe-related features. The sample is 18 mm wide and the path length of the beam was 3.3 mm. Inset photo by G. R. Rossman.

Emerald from the Anuri Prospect, Nunavut, Canada

In the summer of 2012, a geologist working for North Country Gold Corp. identified significant amounts of emerald in drill core obtained in 2005 and 2006 from the Anuri gold-and-silver prospect in Nunavut, Canada. The prospect is located at 66° 27.4' N, 92° 31.0' W, approximately 410 km north of Rankin Inlet, and is accessible only by air. The area is underlain by the Committee Bay Greenstone Belt, which forms part of the Rae domain of the western Churchill Province, within the Neoproterozoic volcano-sedimentary Prince Albert Group.

The emeralds occur in potassic-altered komatiites (ultramafic, high-Mg volcanic rocks) and are associated with highly elevated Be values. Similar rocks have been documented up to 7 km east of the Anuri prospect (Turner 2007), which has implications for the potential extent of emerald mineralisation in the area.

The emerald was found in seven ~1 m intervals from three drill holes, from 76 to 180 m depth. Ten polished thin sections of the seven intervals were studied with a petrographic microscope, scanning electron microscope and electron microprobe. The results show that the beryl occurs within a texturally and mineralogically variable matrix of phlogopite, muscovite, actinolite, plagioclase and pyrite, with occasional quartz, calcite and accessory minerals such as fluorapatite, titanite, rutile, chalcopyrite, molybdenite and rare tellurides.

The beryl can occur as large, slightly altered grains in coarse-textured, hydrothermally altered, silicified zones, as well as at altered protolith contacts, as

inclusions in other minerals (such as amphibole), and as a fine-grained, pervasive overprint that may represent a sodic alteration event. In most cases the emerald is present as rims on near-colourless beryl, and there appears to be an association of emerald with molybdenite veinlets; some even have molybdenite inclusions.

Refractive indices of $n_e = 1.583 \pm 0.001$ and $n_o = 1.591 \pm 0.001$, yielding a birefringence of 0.008, were measured from an emerald crystal. Electron microprobe analyses (245 points) of the beryl showed a wide range of compositions, but the dominant chromophore in the emerald was Cr (with essentially no V), with a maximum of 2.62 wt. % Cr_2O_3 , equivalent to 0.20 Cr per formula unit (pfu). The emerald also contained unusually high concentrations of Mg (up to 3.41 wt. % MgO or 0.48 Mg pfu) and Fe (up to 1.99 wt. % FeO or 0.16 Fe pfu). The highest Mg contents were observed in beryl inclusions in the cores of euhedral amphibole crystals. Only emeralds from the Ianapera deposit in Madagascar (Vapnik *et al.* 2010) show more substitution at the Al site. The Anuri emerald also showed unusually high concentrations of Na (up to 2.66 wt. % Na_2O or 0.49 Na pfu).

Electron microprobe analyses identified the micas as F-rich phlogopite, fluorophlogopite and muscovite. Amphiboles ranged between tremolite and ferri-magnesian hornblende, and were enriched in F and Na (0.2–1.2 F pfu; ≤ 0.42 Na pfu). The plagioclase was albite to oligoclase (≤ 0.2 Ca pfu). Titanite had elevated contents of F and Al (≤ 0.17 F pfu, ≤ 0.14 Al pfu).



Figure 6: Emeralds were recovered from drill cores at the Anuri gold-and-silver prospect in Nunavut, Canada. Shown here are (a) a 13.16 ct cabochon of emerald-bearing rock and (b) a 0.27 ct opaque faceted emerald containing dark amphibole and brassy pyrite inclusions. Both pieces were cut by Bradley S. Wilson (Alpine Gems, Kingston, Ontario, Canada). Photos by Tom Fa/Panotora.

The emerald likely formed via the interaction of the komatiite with Be-, F- and Na-bearing fluids from an unexposed pegmatite dyke or hydrothermal vein, with later overprinting by a metamorphic event. The dyke

or vein is probably associated with a nearby tonalite dated $2,718 \pm 2$ million years (Skulski *et al.* 2003) that intrudes the komatiite and was intersected by a drill hole approximately 100 m south of the main area investigated (Turner 2007).

The emerald-bearing rock has been polished into a small number of cabochons, and one opaque emerald containing amphibole and pyrite inclusions has been faceted (Figure 6). It is unlikely that more material will become available unless fieldwork shows that the emerald-bearing horizons extend up to the surface.

Dr Lee A. Groat (groat@mail.ubc.ca)
and Allison Brand

University of British Columbia, Vancouver, Canada

Dr Jan Cempírek
Masaryk University, Brno, Czech Republic

Dr Joel Grice and Willow Wight
Canadian Museum of Nature
Ottawa, Ontario, Canada

References

- Skulski, T., Sandeman, H., Sanborn-Barrie, M., MacHattie, T., Young, M., Carson, C., Berman, R., Brown, J. *et al.* 2003. *Bedrock Geology of the Ellice Hills Map Area and New Constraints on the Regional Geology of the Committee Bay Area, Nunavut*. Geological Survey of Canada, Current Research 2003-C22, 13 pp., http://publications.gc.ca/collections/collection_2013/rncan-nrcan/M44-2003-C22-eng.pdf.
- Turner, A.J. 2007. *2006 Exploration Summary Report, Committee Bay Project, Nunavut, Canada*. Unpublished company report, Committee Bay Resources Ltd, Vancouver, British Columbia, Canada, 127 pp.
- Vapnik, Y., Sabot, B. & Moroz, I. 2010. Fluid inclusions in Ianapera emerald, southern Madagascar. *International Geology Review*, 47(6), 647–662, <http://doi.org/10.2747/0020-6814.47.6.647>.

Aesthetic Mesolite Cabochons from India

Well known amongst mineral collectors, zeolite minerals are sometimes encountered as collector gemstones (e.g. pollucite, leucite, natrolite, analcime, etc.). Specimen- and gem-grade zeolites commonly form as secondary minerals within cavities in basalts, and perhaps the most famous deposits are hosted by the Deccan volcanic province in India (Ottens *et al.* 2019). During the past few years, white cabochons composed of radiating

crystal clusters described as scolecite (a zeolite of the natrolite subgroup) have been available from India. Early in 2019, similar stones with mixed white and orangey pink ('salmon') colouration exhibiting aesthetic patterns entered the market from India's Maharashtra State. Two such samples (28.10 and 36.73 ct) were characterised for this report (Figure 7).

Natrolite-subgroup zeolites are composed of three



Figure 7: The cabochons from Maharashtra State in India examined for this study (28.10 ct, bottom, and 36.73 ct, top) show aesthetic patterns due to differently coloured mesolite aggregates. Photo by T. Cathelineau.

main species: scolecite ($\text{CaAl}_2\text{Si}_3\text{O}_{10} \cdot 3\text{H}_2\text{O}$), natrolite ($\text{Na}_2\text{Al}_2\text{Si}_3\text{O}_{10} \cdot 2\text{H}_2\text{O}$) and mesolite ($\text{Na}_2\text{Ca}_2\text{Si}_9\text{Al}_6\text{O}_{30} \cdot 8\text{H}_2\text{O}$). They commonly form attractive sprays of slender radiating crystals up to 30 cm in size, in colourless, white, grey, brown, bluish, yellowish, or more rarely pink or orange. The orthorhombic natrolite and the monoclinic mesolite and scolecite all form pseudo-tetragonal prisms with an almost square section. If a cabochon of such aggregates is cut perpendicular to the prisms, a chequered pattern may result, as shown by the 28.10 ct stone in Figure 7. When cut parallel to the slender crystals, they

produce a radiating acicular pattern, as shown by the 36.73 ct cabochon in Figure 7.

The 36.73 ct sample showed the following properties: colour—‘salmon’ and white; diaphaneity—translucent in the ‘salmon’ areas and opaque in the white ones; RI—1.505; birefringence—could not be determined from the RI readings (see below); hydrostatic SG—2.23; magnetism—diamagnetic; Chelsea Colour Filter reaction—none; fluorescence—faint white in white areas and inert in ‘salmon’ portions when exposed to short-wave UV radiation, and inert to long-wave UV; and spectroscopy spectrum—strong absorption in the violet and blue regions with moderate absorption in the green. The 28.10 ct stone showed the same properties except that it was opaque and had an SG value of 2.18; no RI or spectrum could be obtained. Both stones increased in weight when left immersed in water for several minutes. The RI and SG values are consistent with those reported for mesolite by O’Donoghue (2006). (Although mesolite is biaxial positive, all three RI values are ~ 1.505 , so birefringence is almost unobservable with a gemmological refractometer.)

Infrared reflectance spectra were collected from several spots on the cabochons (both ‘salmon’ and white areas), and all yielded the same pattern (e.g. Figure 8). The spectra are characteristic of a silicate mineral, and comparison with the author’s Spec4Gem database (www.spec4gem.info/databases/irs/40) revealed an exact match with mesolite samples analysed a few years ago. The identification of the earlier samples as mesolite was achieved by comparing their IR spectra to those of the natrolite subgroup in the RRUFF database and to the

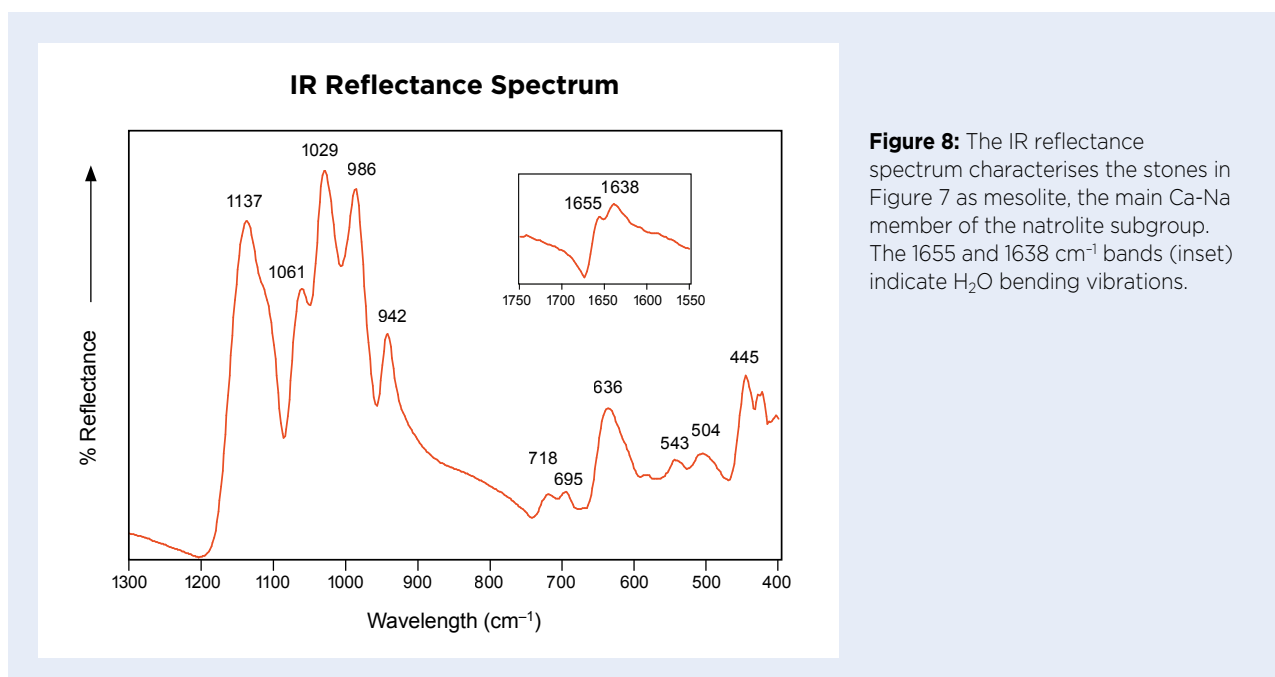


Figure 8: The IR reflectance spectrum characterises the stones in Figure 7 as mesolite, the main Ca-Na member of the natrolite subgroup. The 1655 and 1638 cm^{-1} bands (inset) indicate H_2O bending vibrations.

IR transmission spectra published by Chukanov (2014, pp. 846, 848, 869). The 1655 and 1638 cm^{-1} bands are associated with H_2O bending vibrations (Geiger 2012).

A Vis-NIR spectrum (Figure 9) was collected from a translucent 'salmon' area of the 36.73 ct cabochon with the beam oriented nearly perpendicular to the mesolite prisms. It showed strong absorption in the violet, blue and green regions with an edge in the yellow-green region caused by a prominent band at ~ 535 nm. Also present was a moderate band at ~ 665 nm (red region), a weak band at ~ 855 nm and a moderate band at ~ 980 nm (NIR). The overall spectral pattern displayed an absorption continuum towards the UV, which is responsible for the 'salmon' colouration. Iron is easily incorporated into zeolites, as demonstrated by Suhartana *et al.* (2018); Fe-bearing zeolite is generally orange-brown, which is similar to the 'salmon' colouration seen in the present samples, although the author is not aware of any corresponding Vis-NIR spectra. The 980 nm band is very likely due to OH second overtones, as deduced by the author from the OH stretching vibrations of H_2O between 3600 and 3100 cm^{-1} (Geiger 2012).

Photoluminescence of the white areas of the cabochons was studied using 254 nm excitation, in accordance with the fluorescence observations mentioned above. (Other wavelengths at 377, 405 and 447 nm did not produce any photoluminescence.) The 254 nm source induced a broad but very weak emission peaking at 480 nm (Figure 10). This spectrum is similar to those of zeolites published without explanation by Gorobets & Rogojine (2002, p 150). It is possible that the luminescence could be related to organic molecules and/or an oxygen centre.

Thierry Cathelineau
(thierry.cathelineau@spec4gem.info)
Paris, France

References

- Chukanov, N.V. 2014. *Infrared Spectra of Mineral Species*. Springer, Dordrecht, The Netherlands, 1,726 pp., <http://doi.org/10.1007/978-94-007-7128-4>.
- Geiger, C.A. 2012. A low-temperature IR spectroscopic investigation of the H_2O molecules in the zeolite mesolite. *European Journal of Mineralogy*, **24**(3), 439–445, <http://doi.org/10.1127/0935-1221/2012/0024-2176>.
- Gorobets, B.S. & Rogojine, A.A. 2002. *Luminescent Spectra of Minerals*. All-Russia Institute of Mineral Resources, Moscow, Russia, 300 pp.
- O'Donoghue, M. (ed) 2006. *Gems*, 6th edn. Butterworth-Heinemann, Oxford, 873 pp.
- Ottens, B., Götze, J., Schuster, R., Krenn, K., Hauzenberger, C., Zsolt, B. & Vennemann, T. 2019. Exceptional multi stage mineralization of secondary minerals in cavities of flood basalts from the Deccan volcanic province, India. *Minerals*, **9**(6), article 351 (41 pp.), <http://doi.org/10.3390/min9060351>.
- Suhartana, Sukmasari, E. & Azmiyawati, C. 2018. Modification of natural zeolite with Fe(III) and its application as adsorbent chloride and carbonate ions. *IOP Conference Series: Materials Science and Engineering*, **349**, article 012075 (12 pp.), <http://doi.org/10.1088/1757-899x/349/1/012075>.

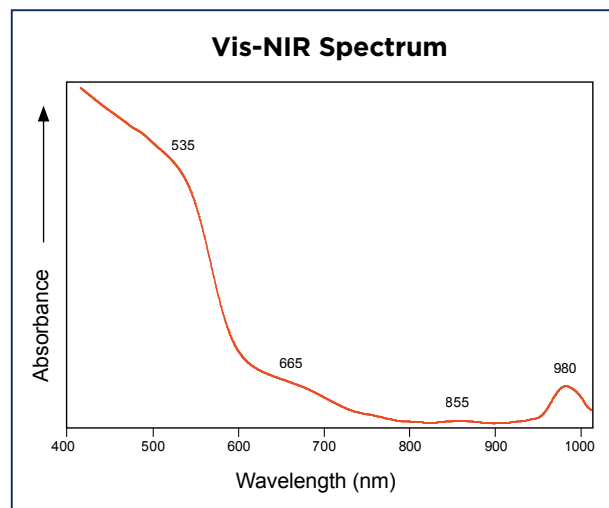


Figure 9: This Vis-NIR spectrum was collected from a 'salmon'-coloured area of the 36.73 ct mesolite cabochon. A continuum of absorption in the violet, blue and, to a lesser extent, green regions gives the stone its 'salmon' colouration.

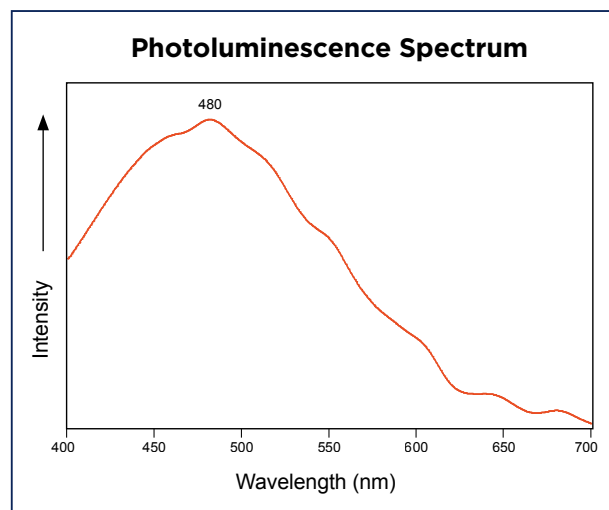


Figure 10: The photoluminescence spectrum of a white area of the 36.73 ct mesolite obtained with 254 nm excitation shows a broad but weak emission centred at 480 nm.

Quartz from Brazil with Biotite Inclusions

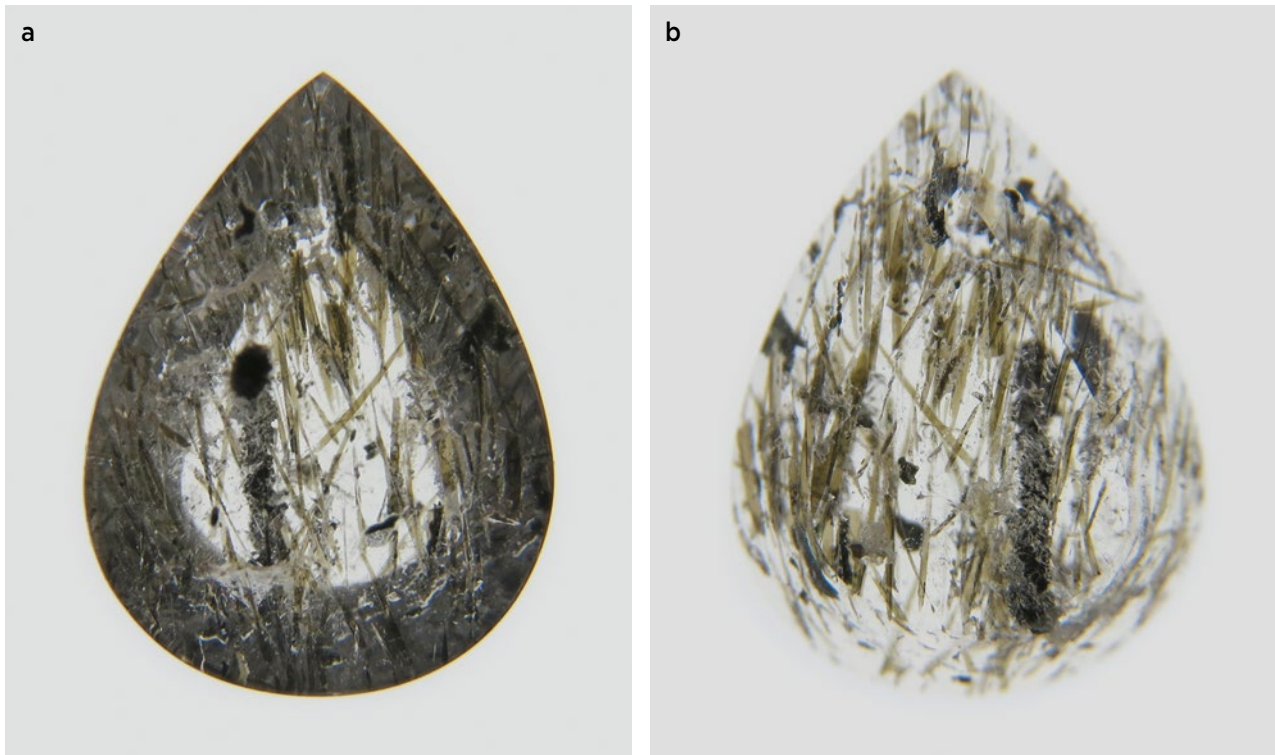


Figure 11: This 2.70 ct buff-top quartz, shown in (a) table-up and (b) table-down positions, contains abundant greenish brown inclusions that proved to be biotite. Also visible is a large etch channel filled with a dark-coloured foreign substance. Gift of Dr Marco Campos Venuti; photos by A. Costanzo.

During the August 2018 Feira Internacional de Pedras Preciosas (FIPP) gem show in Teófilo Otoni, Brazil, stone dealer Dr Marco Campos Venuti obtained some new rough quartz from Minas Gerais containing abundant inclusions. Only a few of these quartz crystals were available, and from them he cut 30–40 stones (both faceted and buff tops), yielding a total of about 100 carats. Dr Campos Venuti displayed the gems at the February 2019 Tucson gem shows, and he kindly donated a 2.70 ct specimen to Gem-A for examination (Figure 11).

The pear-shaped buff-top quartz was colourless and heavily included with elongate greenish brown flakes (Figure 12). They were mostly sub-parallel, but some were present in different orientations. Observation with a petrological microscope indicated the inclusions were composed of a dark mica (e.g. biotite) showing high-order interference colours in cross-polarised light and straight optical extinction. The identification as biotite was confirmed with Raman microspectroscopy using a Horiba LabRam II confocal Raman spectrometer equipped with a 532 nm laser and a high-resolution diffraction grating. Also present in the quartz were numerous liquid-rich two-phase (liquid and

vapour) inclusions, as well as solid-rich three-phase (liquid, vapour and solid) inclusions. In addition, a large etch channel filled with a dark-coloured foreign substance (probably polishing compound) formed a prominent columnar inclusion in the quartz (again, see Figure 11).

Although quartz and biotite are both common

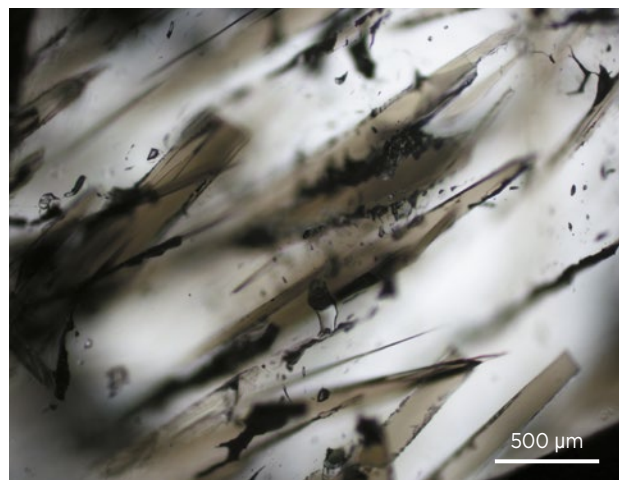


Figure 12: The biotite inclusions in the Brazilian quartz form elongate flakes accompanied by smaller fluid inclusions. Photomicrograph by A. Costanzo.

rock-forming minerals, it is somewhat unusual to encounter quartz in the gem trade containing monomineralic biotite inclusions. Hyrsl & Niedermayr (2003, p. 205) documented quartz from Alpine-type veins in the Ganesh Himal region of Nepal that contained large biotite plates up to several centimetres long and 1 cm wide.

*Dr Alessandra Costanzo FGA DGA
and Brendan M. Laurs FGA*

Reference

Hyrsl, J. & Niedermayr, G. 2003. *Magic World: Inclusions in Quartz*. Bode, Haltern, Germany, 240 pp.

Quartz from Brazil with Dendritic Inclusions

Brazil is one of the most prolific sources of quartz containing interesting inclusions. During the February 2019 Tucson gem shows, Frederico de Vasconcelos (MultiGemas/Vasconcelos Brazil, Governador Valadares, Brazil) displayed two new finds of quartz with dendritic inclusions from Minas Gerais. He reported that quartz

with black dendritic inclusions (Figure 13) was discovered in December 2018 by miners looking for aquamarine near Leopoldina in south-eastern Minas Gerais near the border with Rio de Janeiro State. The largest quartz crystal recovered weighed 500 kg, and was cut into seven larger polished stones and approximately 3,000 carats of smaller gems. The dendrites range from dark grey to black and commonly show a plant-like appearance.

Just prior to this discovery, in November 2018, quartz with red-orange dendritic inclusions (Figure 14) was found at an unspecified locality in Minas Gerais. So far, approximately 20,000 carats have been cut into stones ranging from 10 to 60 ct each. The dendrites in this quartz form delicate patterns, and they are commonly accented by a granular-appearing white coating within some of the fractures (Figure 15).

Brendan M. Laurs FGA

Nathan D. Renfro FGA

*Gemological Institute of America (GIA)
Carlsbad, California, USA*



Figure 13: These quartz specimens (64 × 81 and 44 × 50 mm) from Leopoldina, Brazil, contain dendritic inclusions with a somewhat plant-like appearance. Photo by Jeff Scovil.



Figure 14: Brazil is also the source of this 41 × 25 mm quartz with red-orange dendrites. Photo by Robison McMurtry, © GIA.



Figure 15: The red-orange dendrites in the quartz are accompanied by a granular-appearing white material in the fractures. Photo by N. D. Renfro, © GIA; image width 12.9 mm.

Sapphire with Unusual Inclusion Scenery

Recently, the authors examined an unheated blue sapphire of ~2 ct, presumably from Myanmar (Burma), which displayed unusual inclusion scenery. Raman microspectroscopy of the inclusions was carried out at the DSEF German Gem Lab using a Renishaw inVia Raman microscope, at room temperature with 514 and 785 nm laser excitations in confocal mode.

One side of the sapphire contained hundreds of colourless, transparent, doubly refractive crystal inclusions with a euhedral, short-prismatic habit. These were identified as scapolite. Scapolite is rarely seen as inclusions in gem corundum, although it was documented in ruby by Gübelin & Koivula (2008). One of the larger scapolite inclusions attracted our attention because it contained some negative crystals filled with CO₂ together with some (unidentified) daughter crystals (Figure 16).

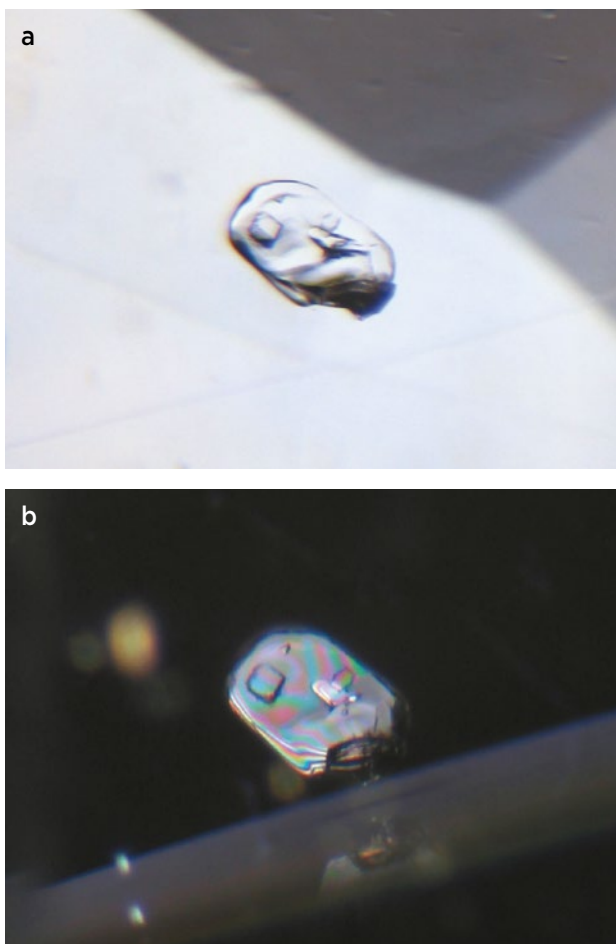


Figure 16: (a) This inclusion in a blue sapphire was identified as scapolite, which contains negative crystals filled with CO₂ and unidentified daughter crystals. (b) Viewed with crossed polarisers, the doubly refractive nature of the scapolite (and some of its inclusions) is evident. Photomicrographs by T. Stephan; image widths 3.2 mm.

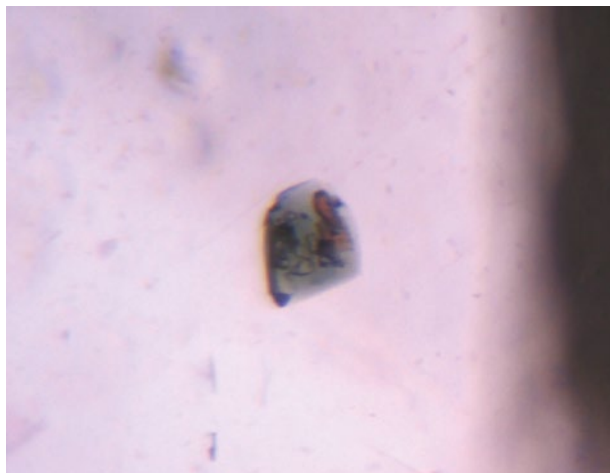


Figure 17: This greenish mineral in the blue sapphire was identified as spinel, which itself contains inclusions of dolomite, feldspar, mica and primary rutile. Photomicrograph by T. Stephan; image width 2.1 mm.

Near the scapolite inclusions, the sapphire also hosted a greenish mineral, the colour of which reminded us of amphibole inclusions commonly seen in gem corundum from East Africa. We identified it as spinel, which is known to occur in sapphires from Myanmar (Gübelin & Koivula 2008; Smith 2018). However, this particular spinel inclusion was of further interest because it hosted several crystals showing various shapes and colours (Figure 17), which consisted of rhombohedral colourless dolomite, rounded colourless feldspar, brownish mica flakes and primary rutile grains. Raman analysis also showed the presence of CO₂ in the spinel inclusion.

These two multi-phase inclusions reflect the complex geological formation environment of this sapphire. It is fortunate that the stone did not undergo high-temperature heat treatment, which would have destroyed these interesting internal features.

Tom Stephan (t.stephan@dgemg.com)
German Gemmological Association
Idar-Oberstein, Germany

Stefan Müller
DSEF German Gem Lab, Idar-Oberstein

References

- Gübelin, E.J. & Koivula, J.I. 2008. *Photoatlas of Inclusions in Gemstones*. Opinio Publishers, Basel, Switzerland, 672 pp.
- Smith, C.P. 2018. Gem Notes: Sri Lankan sapphire with spinel inclusions. *Journal of Gemmology*, **36**(4), 291.

Scapolite from Brazil with Interesting Inclusions

Various localities in Brazil have produced gem-quality light yellow scapolite. Espírito Santo State is a source of facetable scapolite crystals, which are sometimes fairly large (up to ~6 g), although they usually contain numerous long thin tubes (Sauer 1982). Gem scapolite is also known from Minas Gerais State, and was chemically analysed by Dunn *et al.* (1978). Furthermore, Zwaan & Arps (1980) reported gemmological and powder X-ray diffraction data for a scapolite from an unspecified locality in Brazil.

During the February 2019 Tucson gem shows, Dr Marco Campos Venuti debuted a new production of light yellow scapolite from an unspecified locality in Brazil. He obtained ~3–4 kg of rough while visiting Brazil in August 2018, from which approximately 1,000 carats of faceted stones were produced. The gems consisted of mostly clean stones up to 20 ct (typically 2–10 ct). Dr Campos Venuti kindly donated to Gem-A an elongate cushion weighing 5.50 ct (Figure 18), which was characterised by author AC for this report.

The stone was transparent with a vitreous lustre, and exhibited weak dichroism in slightly greenish yellow and yellow. It luminesced strong red under short-wave UV radiation and displayed faint yellowish fluorescence to long-wave UV. The RIs were 1.545–1.560, yielding a birefringence of 0.015, and the stone showed a uniaxial negative optic character. Hydrostatic measurements yielded an SG value of 2.64.

The scapolite group includes an isomorphous series between the end members marialite ($\text{Na}_4\text{Al}_3\text{Si}_9\text{O}_{24}\text{Cl}$) and meionite ($\text{Ca}_4\text{Al}_6\text{Si}_6\text{O}_{24}\text{CO}_3$), and both the optical properties and SG of scapolite vary with the relative

amounts of Na and Ca (Zwaan & Arps 1980; Deer *et al.* 2004). The properties obtained for the present scapolite specimen correspond to a marialite composition, and are comparable (though with slightly higher RI and SG values) to the data for Brazilian marialite given by Zwaan & Arps (1980). By contrast, Dunn *et al.* (1978) indicated a meionite composition for scapolites from Minas Gerais and Espírito Santo.

The 5.50 ct stone contained conspicuous inclusions, consisting of elongate parallel arrays of brown to black particles (Figure 19). Some of the black inclusions had a skeletal growth appearance. Unfortunately, these particles could not be identified by laser Raman microspectroscopy due to their small size.

*Dr Alessandra Costanzo FGA DGA
and Brendan M. Laurs FGA*

References

- Deer, W.A., Howie, R.A., Wise, W.S. & Zussman, J. 2004. *Rock-Forming Minerals, Vol. 4B: Framework Silicates—Silica Minerals, Feldspatoids and Zeolites*, 2nd edn. The Geological Society of London, Bath, 982 pp.
- Dunn, P.J., Nelen, J.E. & Norbert, J. 1978. On the composition of gem scapolites. *Journal of Gemmology*, **16**(1), 4–10, <http://doi.org/10.15506/jog.1978.16.1.4>.
- Sauer, J.R. 1982. *Brazil, Paradise of Gemstones*. Gemological Institute of America, Santa Monica, California, USA, 135 pp.
- Zwaan, P.C. & Arps, C.E.S. 1980. Properties of gemscapolites [sic] from different localities. *Zeitschrift der Deutschen Gemmologischen Gesellschaft*, **29**(1/2), 82–85.



Figure 18: This 5.50 ct Brazilian scapolite has a marialite composition and contains parallel trails of dark inclusions. Gift of Dr Marco Campos Venuti; photo by A. Costanzo.

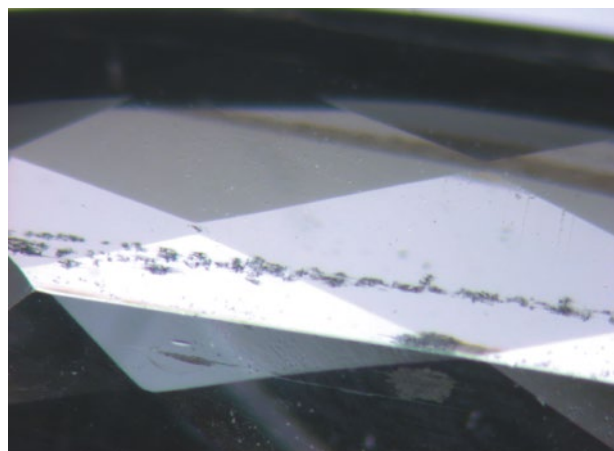


Figure 19: Black skeletal inclusions form an elongate array in the scapolite. Photomicrograph by A. Costanzo; image width 5 mm.

Spessartine Reportedly from Ethiopia

Ethiopia has become an important source of coloured stones such as opal, sapphire and emerald. Recently, the authors examined various rough samples, reportedly from Ethiopia, which were provided by Sascha Weiß (Ethio Star, Germany). These included several (mostly red) garnets, two greenish brown clinzoisites, one brown epidote and a green sapphire. We were especially interested in a bright orange 6.46 g stone (Figure 20), which was identified by Raman spectroscopy as spessartine. The SG was measured hydrostatically as 4.24 and the RI was ~1.80 (measured from a small polished surface with a Presidium digital reflectometer). Microscopic examination revealed mainly fluid inclusions (some multi-phase) and growth structures.

The semi-quantitative chemical composition of the sample was obtained by EDXRF spectroscopy with a Thermo Scientific ARL Quant'X instrument, and compared (along with RI and SG data) to that for spessartine from other localities (Table I; see also Laurs & Knox 2001; Milisenda *et al.* 2010). The data reveal a particularly



Figure 20: This 6.46 g spessartine, reportedly from Ethiopia, was examined for this report. Photo by T. Stephan.

Mn-rich composition ($\text{Sps}_{91.5}\text{Alm}_{6.2}\text{Pyr}_{1.3}\text{Grs}_{0.9}$) that is typical of some spessartine from granitic pegmatites (e.g. in Nigeria). The absorption spectrum of this sample is

Table I: RI, SG and chemical data for spessartine from various localities.^a

Property	Namibia	Pakistan	Nigeria	Tanzania	Ethiopia
	Lind <i>et al.</i> (1994); Lind (2002)	Qasim Jan <i>et al.</i> (1995); Henn (1996); Lind (2002)	Lind & Henn (2000); Lind (2002)	Milisenda <i>et al.</i> (2010)	This work
RI ^b	1.790-1.797	1.798-1.802	1.801-1.803	1.777-1.785	~1.80
SG	4.09-4.16	4.05-4.23	4.15-4.22	4.02-4.08	4.24
Oxide (wt.%)					
SiO ₂	33.93-38.48	35.01-36.80	36.01-37.04	37.33-37.48	36.92
TiO ₂	nd-0.22	nd-0.08	0.01-0.09	0.06-0.08	0.01
Al ₂ O ₃	18.87-21.23	19.92-20.68	20.63-21.48	21.06-21.23	17.76
Cr ₂ O ₃	nd-0.06	nd-0.008	nd-0.07	nd-0.03	nd
FeO _{tot}	nd-1.13	4.45-6.88	0.62-5.93	nd	2.86
MnO	35.56-42.45	33.28-36.98	37.67-43.08	34.75-34.88	41.64
MgO	2.47-4.32	nd-0.01	0.03-0.99	4.32-5.14	0.35
CaO	0.35-0.98	1.55-1.60	0.09-0.41	1.34-1.79	0.33
End member (mol.%)^b					
Sps	81.5-87.0	80.3-85.3	86.3-96.7	75.8-76.5	91.5
Alm	0-2.5	10.1-14.8	1.4-13.2	—	6.2
Pyr	9.5-17.4	—	0.1-4.1	18.8-19.8	1.3
Grs	1.0-2.5	4.6-4.8	0.3-1.2	3.7-5.0	0.9

^a Abbreviations: Alm = almandine, Grs = grossular, nd = not detected, Pyr = pyrope and Sps = spessartine.

^b The RI and end-member compositions also include data from Milisenda *et al.* (2010).

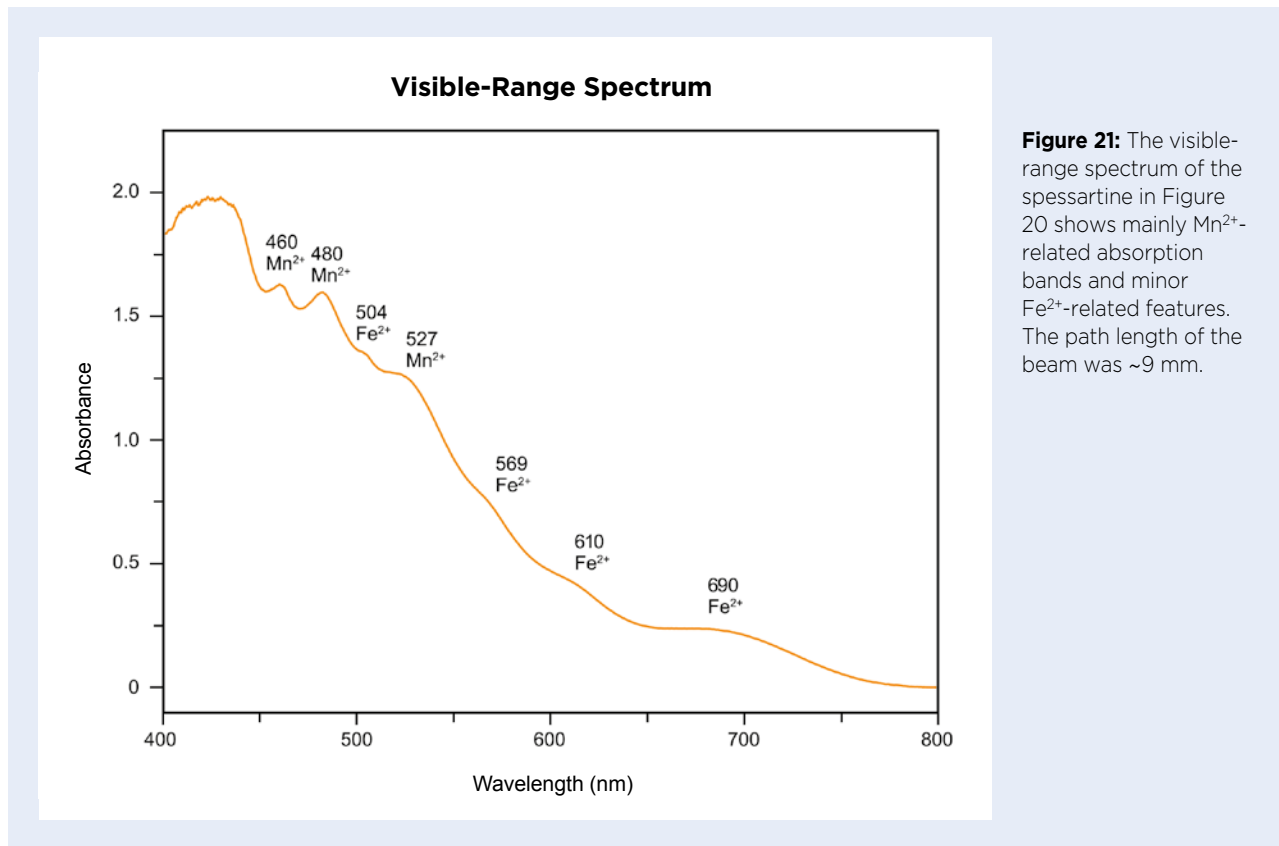


Figure 21: The visible-range spectrum of the spessartine in Figure 20 shows mainly Mn^{2+} -related absorption bands and minor Fe^{2+} -related features. The path length of the beam was ~9 mm.

shown in Figure 21. In addition to absorptions attributed to Mn^{2+} , bands associated with Fe^{2+} are present, as expected for spessartine (cf. Lind 2015).

The spessartine sample described here reportedly came from the Shakiso region of southern Ethiopia, which is also a source of emerald, pyrope, aquamarine, ruby, sapphire and tourmaline (S. Weiß, pers. comm., 2019). Spessartine has been previously reported from highly evolved granite–pegmatite rocks in the Kenticha area near Shakiso (Mohammedyasin 2017), but this is the first time that the authors have seen gem-quality spessartine from Ethiopia.

Tom Stephan, Thomas Lind and Benjamin Huaysan
German Gemmological Association

Stefan Müller
DSEF German Gem Lab, Idar-Oberstein

References

- Henn, U. 1996. Spessartine aus Pakistan. *Gemmologie: Zeitschrift der Deutschen Gemmologischen Gesellschaft*, **45**(2), 93–94.
- Laurs, B.M. & Knox, K. 2001. Spessartine garnet from Ramona, San Diego County, California. *Gems & Gemology*, **37**(4), 278–295, <http://doi.org/10.5741/gems.37.4.278>.
- Lind, T. 2002. *Kristallchemie und Farbe von Granaten kommerzieller Edelsteinvorkommen*. Ph.D. thesis, Johannes Gutenberg University of Mainz, Germany, 377 pp.
- Lind, T. 2015. Kristallchemie und Farbe von Granaten kommerzieller Edelsteinvorkommen. *Gemmologie: Zeitschrift der Deutschen Gemmologischen Gesellschaft*, **64**(1/2), 1–41.
- Lind, T. & Henn, U. 2000. A new find of spessartine garnets in Nigeria. *Journal of Gemmology*, **27**(3), 129–132, <http://doi.org/10.15506/JoG.2000.27.3.129>.
- Lind, T., Henn, U. & Bank, H. 1994. Leuchtend orangefarbige Spessartine aus Namibia. *Zeitschrift der Deutschen Gemmologischen Gesellschaft*, **43**(1/2), 39–47.
- Milisenda, C.C., Lind, T. & Henn, U. 2010. Spessartin: Vom Sammlerstein zum Topseller. *Gemmologie: Zeitschrift der Deutschen Gemmologischen Gesellschaft*, **59**(1/2), 3–18.
- Mohammedyasin, M.S. 2017. Geology, geochemistry and geochronology of the Kenticha rare metal granite pegmatite, Adola belt, southern Ethiopia: A review. *International Journal of Geosciences*, **8**(1), 46–64, <http://doi.org/10.4236/ijg.2017.81004>.
- Qasim Jan, M., Malik, R.H. & Ahmad, K.S. 1995. Gem garnet in pegmatites from Neelum Valley, Azad Kashmir. *Geological Bulletin of the University of Peshawar*, **28**, 9–14.

DIAMONDS

Diamond Mining at Theindaw, Myanmar

For decades, diamonds have occasionally been recovered from alluvial sediments in various parts of Myanmar, including the Momeik Valley (near Mogok), the Tanintharyi region in the south and the Hukawng Valley in the north (e.g. Mitchell 2018). Some of the mining sites include Bokpyin, Dawei (old name: Tavoy), Theindaw, Kyauk-O Chaung (south-east of Taungoo) and Nambyu (in the Tanai area). The diamonds are typically recovered as by-products of mining the alluvial deposits for other commodities such as tin, tungsten and coloured stones.

In June 2019, one of the authors (TTS) visited a small privately owned mining operation in the Theindaw area of the Tanintharyi region. (There is also a government-owned mine at Theindaw, which provides employment for the local community.) From the town of Myeik it took more than four hours to reach the mining area. The trip (during the rainy season) included two hours by car on paved and muddy roads, a river crossing by ferry, and then another two hours riding a motorbike on a slippery, muddy road.

In the Theindaw area the miners mainly seek tin and tungsten, and occasionally they find diamond and gold. The area is mainly underlain by Carboniferous sedimentary rocks and rare Permian limestones, and is locally intruded by lamprophyre dykes; the primary source of the alluvial diamonds in these ‘headless placers’ is unknown. During the author’s visit, a crew of three workers hydraulically mined a small open pit (Figure 22), and the slurry was pumped to a sluice where the heavier minerals were removed by hand.

The mine manager displayed an approximately 0.50 ct diamond that was found some years ago at that location (Figure 22, inset). The pale brown rounded tetrahedron was consistent in appearance with typical diamonds from Myanmar, which are commonly brown to reddish brown or yellow, and sometimes colourless (Griffin *et al.* 2001). Also, most Theindaw diamonds are rounded and contain percussion marks, lamination lines, pits and stepped growth faces (trigons). In order of abundance, the diamond forms are the octahedron, dodecahedron and trisoctahedron, and less commonly



Figure 22: In the Theindaw area of southern Myanmar, miners searching for tin and tungsten occasionally recover diamonds (see, e.g., the 0.50 ct stone in the inset) from small alluvial mining operations. Photos by Tay Thye Sun.

the hexoctahedron, tetrahexahedron, hexatetrahedron, various combinations of forms, aggregates and fragments (Nyunt 2002). According to the knowledge of authors NH and TTN, from 1985 to 1990 the average diamond content of the alluvium was 0.44 carats per 100 cubic yards and the average stone weight was 0.77 ct. Available records from the Myanmar Gems Enterprise for diamond production from Theindaw during the period July 1985 to March 1992 indicate a total of 1,886 stones recovered with a total weight of 1,458 carats; the smallest diamond was 0.02 ct and the largest was 72.55 ct. No production records have been kept for diamonds from Myanmar since 2002.

Acknowledgements: Author TTS sincerely thanks U Kyaw Kyaw (group leader), U Han Min Ko, U Thant

Zin Oo and driver U Kyaw Htoo for providing a safe journey to the mining area.

*Tay Thye Sun FGA (tay@gem.com.sg)
Far East Gemological Laboratory, Singapore*

*U Nyunt Htay
Myanmar Geosciences Society
Yangon, Myanmar*

*Dr Thet Tin Nyunt
Myanmar Gems Enterprise, and Department of
Geological Survey and Mineral Exploration,
Ministry of Natural Resources and
Environmental Conservation,
Nay Pyi Daw, Myanmar*

References

- Griffin, W.L., Win, T.T., Davies, R., Wathanakul, P., Andrew, A. & Metcalfe, I. 2001. Diamonds from Myanmar and Thailand: Characteristics and possible origins. *Economic Geology*, **96**(1), 159–170, <https://doi.org/10.2113/gsecongeo.96.1.0159>.
- Mitchell, A. 2018. Chapter 17: Popa–Loimye Arc, correlations with Tibet, and alluvial diamonds in

Myanmar. Geological Belts, Plate Boundaries, and Mineral Deposits in Myanmar, Elsevier, Amsterdam, The Netherlands, 473–482, <http://doi.org/10.1016/b978-0-12-803382-1.00017-1>.

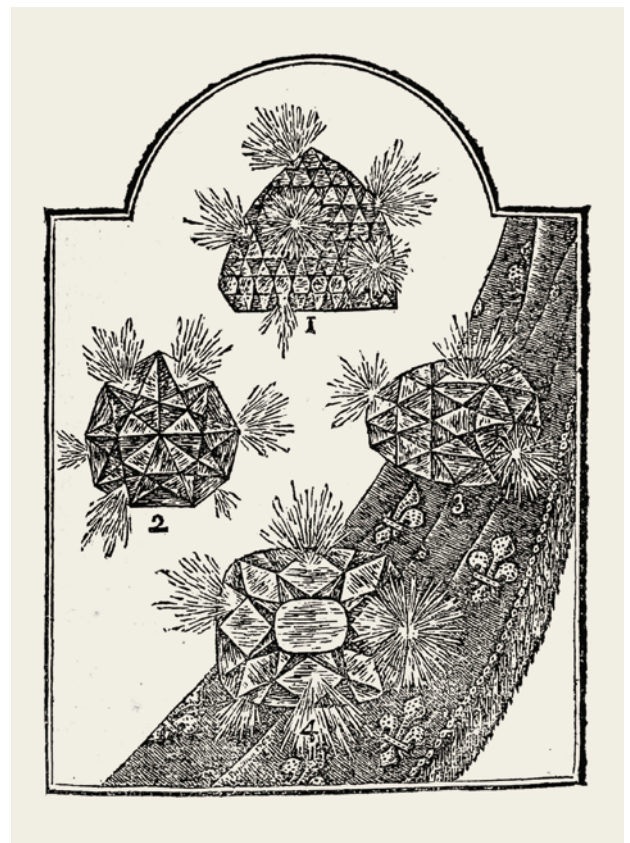
Nyunt, T.T. 2002. *Petrology and economic geology of Theindaw area, Tanintharyi Township*. Master's thesis, Department of Geology, University of Yangon, Myanmar, 45 pp.

Drawing Fire: An Early Illustration of Sparkle in Diamonds

Photographers of diamonds and other gems are well aware of the challenge posed by reflections. Excellent return of light might be a positive feature for a diamond, but not where photography is concerned; too many reflections obscure the form and appearance of the gem. In the days before photography, illustrators had exactly the opposite problem. How might they render the fire and sparkle of a diamond in a drawing?

In 1766, French wood engraver and illustrator Jean Michel Papillon wrote a comprehensive treatise on the craft of engraving wood blocks used in printing. In the second volume, he described one way to indicate sparkle in diamonds (Papillon 1766, pp. 279–285). He shows what he describes as the four most beautiful diamonds in the world, with their sparkle rendered as radiating lines of irregular length (Figure 23). These gems, as numbered in his plate, are (1) the Grand Mogul's diamond, (2) the Duke of Tuscany's diamond, (3) the Sancy and (4) the Regent.

Figure 23: This illustration by Papillon (1766, p. 281) renders the sparkle associated with what he considered the four most beautiful diamonds in the world.



For comparison, he referred the reader to his earlier drawing that was published by Antoine-Joseph Dézallier d'Argenville in 1755, showing these same four diamonds unembellished with 'sparkle' (Figure 24).

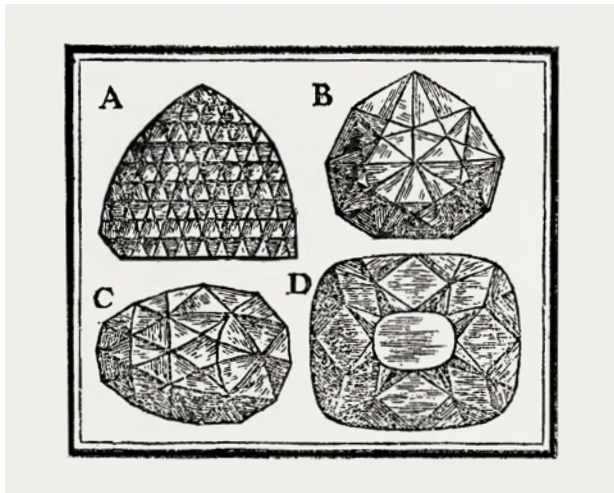


Figure 24: An earlier drawing by Papillon of the same four diamonds (published by Dézallier d'Argenville 1755, p. 157), shown without 'sparkle', was mentioned by Papillon (1766) for comparison.

The use of radiating lines in drawings to represent light was nothing new. You could argue that the same approach was used in representations of the sun several millennia earlier, in Egypt, for example. Similar radiating lines were also used in medieval art for fire and explosions, but applying such lines to gems was a novel idea. Whether Papillon's method is effective is a matter for the viewer to decide, but it is worth noting that it does not appear to have been adopted by other illustrators.

Dr Jack M. Ogden FGA (jack@striptwist.com)
London

References

- Dézallier d'Argenville, A.-J. 1755. *L'Histoire Naturelle Eclaircie dans une de ses Parties Principales, l'Oryctologie, qui Traite des Terres, des Pierres, des Métaux, des Minéraux, et Autres Fossiles (...)*. De Bure l'Ainé, Paris, France, 560 pp.
- Papillon, J.M. 1766. *Traité Historique et Pratique de la Gravure en Bois*, Vol. 2. Pierre-Guillaume Simon, Paris, France, 388 pp.

The Nur al-'Ayn Diamond, Rephotographed

During the preparation of the recent article in *The Journal* on the history of the Hornby diamond (Vol. 36, No. 6, 2019, 512–522), the author attempted to obtain a new photo of the ~60 ct brilliant-cut Nur al-'Ayn diamond, which is set in a tiara made by Harry Winston in the 1950s (Figure 25). The only image available at the time was taken in the 1960s by Canadian gemmologists Victor Meen and Arlotte Tushingham when they studied the Iranian Crown Jewels in what is now the National Jewelry Treasury (or Treasury of National Jewels) in the Central Bank of the Islamic Republic of Iran, Tehran.

By good fortune, David Brough (editor and co-founder of *Jewellery Outlook*) put the author in touch with Iranian gemmologist Dr Vahid Ahadnejad of the Gemmology Center, Shahid Beheshti University, in Tehran. Dr Ahadnejad graciously agreed to explore the possibility of obtaining a new photograph. Unfortunately, it was not a simple process, and when it seemed that a new photo was unlikely to be available in the short term, the author decided to use the Meen and Tushingham photo, which Nicola Woods at the Royal Ontario Museum (Toronto, Ontario, Canada) kindly provided.

Figure 25: This recent photo shows the ~60 ct Nur al-'Ayn pink brilliant diamond in the centre of a tiara designed by Harry Winston for Farah Diba to wear at her marriage to Shah Mohammed Reza in 1958. Photo courtesy of the National Jewelry Treasury, Central Bank of the Islamic Republic of Iran.



Dr Ahadnejad subsequently forwarded an excellent new photo of the tiara that he arranged through the management of the National Jewelry Treasury in Tehran (again, see Figure 25). It is important to show it here not simply because it illustrates what is quite possibly the largest brilliant-cut pink diamond in the world, but because it also

reveals that the older photo, as supplied by the Royal Ontario Museum, was reversed. The new photo shows the correct orientation and provides a far clearer view of this slightly misshapen but highly important diamond.

Dr Jack M. Ogden FGA

PEARLS

Cultured Abalone Pearls from Chile

Chile is an important aquaculture producer of abalone meat for the Asian market, with exports reaching 1,000 tonnes per year. In 2012, a research project for producing cultured abalone pearls was started by the University of Antofagasta in northern Chile under the leadership of authors RAV and JMZ. The goal was to develop a new source of income for Chilean abalone farmers. First attempts led to the successful production of prototype blister and whole cultured pearls (e.g. Figure 26), and international patent applications followed (e.g. Araya Valencia *et al.* 2017).

In 2016, one of the larger abalone companies in Patagonia made available about 800 of the animals for grafting with spherical beads (6 mm in diameter). In August 2018, after a growth period of 16 months, about 14% of the molluscs produced whole cultured pearls with nacreous outer layers of 0.5–0.6 mm thickness. About 50% of them were of acceptable gem quality and showed a variety of colours, often combining hues of gold, blue, silver and green.

Importantly, nearly all of the abalone survived the grafting process; the mortality rate was only ~1%, thus

demonstrating to abalone farmers that culturing pearls would, in the long run, not disturb their main business of producing meat. It is hoped that this initiative will eventually evolve into a Chilean cultured abalone pearl industry that will successfully market its own ‘Abalone Patagonia Pearls’, although more research is needed to achieve this aim. For example, one of the next steps will focus on increasing the ratio of nacre to organic substance secreted by the mantle cells when coating the bead, thus improving the quality of the cultured pearls.

*Elisabeth Strack FGA (info@strack-gih.de)
Gemmologisches Institut Hamburg
Hamburg, Germany*

*Dr Rubén Araya Valencia
University of Antofagasta, Chile*

*Jaime Maturana Zuñiga
Proyecta Consultores, Providencia, Chile*

Reference

Araya Valencia, R., Saucedo Lastra, P., Rojas Figueroa, A. & Maturana Zuñiga, J. 2017. Production of Free Pearls in Abalone. U.S. Patent Application US 2018/0077910 A1, filed 16 November, published 22 March 2018.

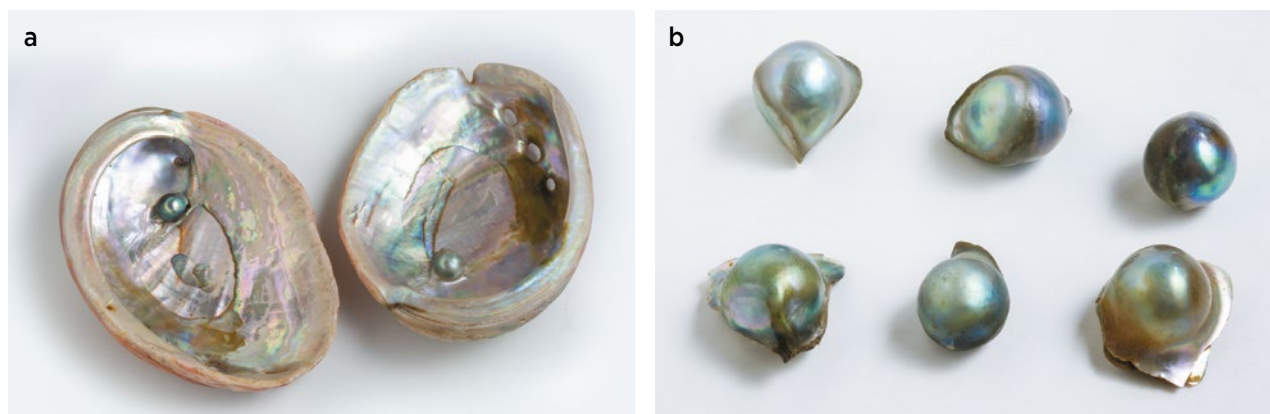


Figure 26: Experimental culturing of abalone pearls in Patagonia, Chile, yielded (a) these blisters attached to the shells (which are 10 and 12 cm long) and (b) this assortment of whole cultured pearls. Both the blisters and the whole cultured pearls were produced using 6-mm-diameter beads and are overgrown by a layer of nacre that is 0.5–0.6 mm thick. Photos courtesy of R. Araya Valencia and J. Maturana Zuñiga.

Pearls from *Tutufa bubo*

During the February 2019 Tucson gem shows, Pacific Coast Pearls (Petaluma, California) displayed for the first time natural pearls from the marine gastropod *Tutufa bubo*, commonly known as the giant frog snail (Figure 27). Named by Carl Linnaeus in 1758, the species is notable for its large size, as the shell can attain a length of more than 30 cm. It lives in relatively shallow waters (up to 180 m deep) of the Red Sea and Indo-Pacific region, where it feeds primarily on sea stars (see www.marine-species.org/aphia.php?p=taxdetails&id=476597).



Figure 27: The giant frog snail *Tutufa bubo* (here, approximately 20 cm long) is the source of the pearls described in this report. Photo courtesy of the Rankin family/Pacific Coast Pearls.



Figure 28: These rare pearls from *Tutufa bubo* weigh 31 ct (left) and 38 ct (right). Photo courtesy of the Rankin family/Pacific Coast Pearls.

The two pearls shown in Tucson, weighing 31 and 38 ct, represent true novelties (Figure 28). Both had symmetrical pear shapes, the larger (about 30 mm long) being more pointed than the other. The larger pearl showed an evenly distributed orange colour that became yellow at the broader end, while the smaller pearl had an overall yellowish colour. Both had porcelaneous lustre, with a barely perceptible flame structure (comparable to that of conch and *Tridacna* pearls) that was visible in places. The pearls reportedly originated from the Indo-Pacific Ocean, but no information was available as to their specific location or date of discovery.

Elisabeth Strack FGA

SYNTHETICS AND SIMULANTS

Eulytine Inclusions in a Manufactured Glass—A Rare Encounter

In November 2018, the American Gemological Laboratories (AGL) received two faceted samples for identification. They were slightly brownish orange and lacked lustre and shine (Figure 29). Both were acquired by Marcus McCallum FGA, a gem dealer in Hatton Garden, London, who purchased them already cut from a merchant based in southern Africa. The merchant, in turn, had reportedly bought them from an ‘itinerant’ source in Zimbabwe. Unfortunately, we were unable to obtain further information regarding their origin. McCallum provided the samples to Charles Evans (Gem-A, London) and Kerry

Gregory (Gemmology Rocks, Rochester), who then sent them to AGL for further testing.

Both pieces displayed numerous eye-visible inclusions, which were dipyrmidal and colourless (Figure 30). The samples were singly refractive (1.645 and 1.650), and we measured hydrostatic SG values of 3.16 and 3.11. The higher SG corresponded to the greater abundance of inclusions in the pear-shaped specimen. The RI and SG data proved inconclusive for identifying the samples, so we undertook ultraviolet-visible and Fourier-transform infrared spectroscopy, but these were also inconclusive. EDXRF chemical analysis of both samples showed major amounts of Al, Si, Mn, Ca and Na with traces of Fe, Mg, Ti, Ba and Sr. Such a composition (except for Na) could be expected for

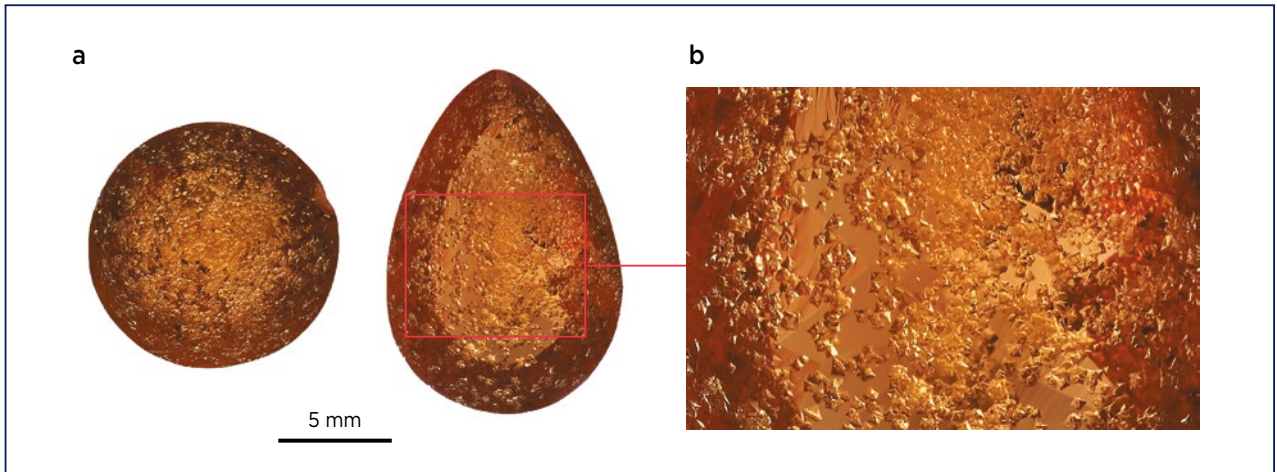


Figure 29: (a) These brownish orange round (1.38 ct) and pear-shaped (1.76 ct) samples were submitted to AGL for analysis. They proved to consist of manufactured glass, and (b) contained abundant inclusions that were identified as eulytine. Photos by Alex Mercado, AGL.

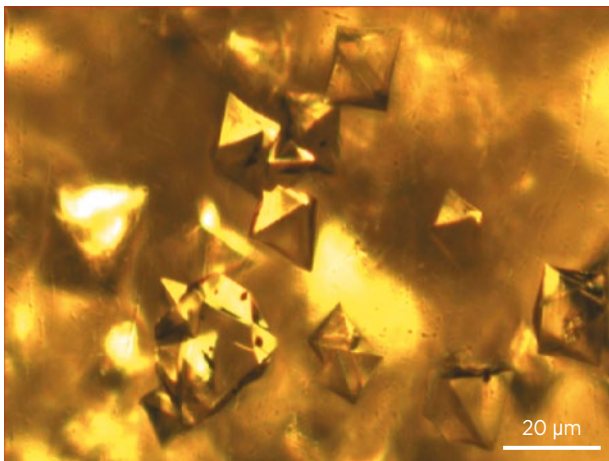


Figure 30: Magnification of the eulytine inclusions reveals their bipyramidal shape. Photomicrograph by R. Zellagui, transmitted light.

grossular-spessartine. However, since the other properties differed from the garnet family, further investigation was necessary to identify these samples.

Raman microspectroscopy of the matrix material of both samples presented intense broad bands at around 800–1100 cm^{-1} and another band in the 400–600 cm^{-1} region (Figure 31), which are characteristic of manufactured glass (White & Minser 1984). Furthermore, Raman analysis of the (surface-reaching) inclusions revealed they were eulytine ($\text{Bi}_4\text{Si}_3\text{O}_{12}$; Figure 32).

The only reference we could find for a host matrix containing eulytine inclusions was for bismuth-germanium oxide crystals ($\text{Bi}_4\text{Ge}_3\text{O}_{12}$, also called BGO; see Piekarczyk *et al.* 1978). Single crystals of BGO are grown for their exceptional electro-optical, electro-mechanical

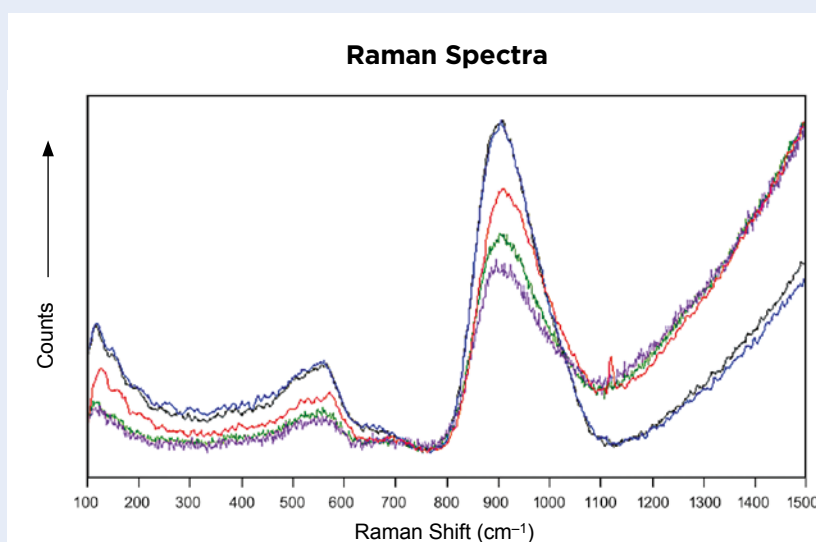


Figure 31: Raman spectra of the matrix of both samples reveal broad features associated with a glass. The different analyses were performed on various areas of both samples.

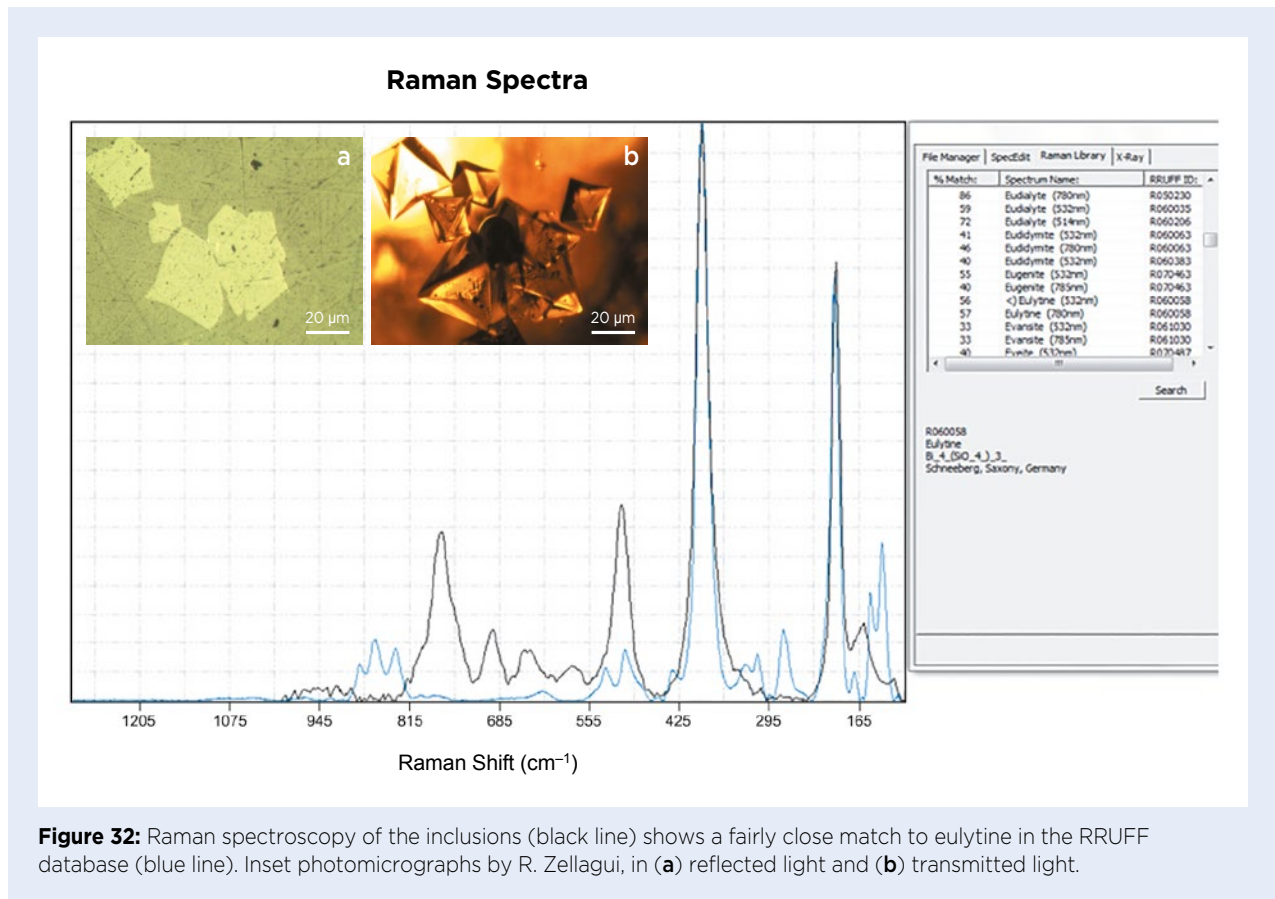


Figure 32: Raman spectroscopy of the inclusions (black line) shows a fairly close match to eulytine in the RRUFF database (blue line). Inset photomicrographs by R. Zellagui, in (a) reflected light and (b) transmitted light.

and luminescence properties (Takagi *et al.* 1981), as scintillometers, for example (Gévy 1987). Various mechanisms of BGO crystal growth are known, but most important is the Czochralski method. With this technique, single crystals of BGO can be produced that sometimes have cloudy inclusions identified as eulytine (Piekarczyk *et al.* 1978). These impurities considerably modify the optical and physical properties of the crystal.

Our hypothesis is that the present glass samples are sub-products or by-products of the production of BGO or a similar material for industrial applications, in which eulytine inclusions precipitated out of a melt. It is presumed that the low transparency of the pieces

led them to be discarded, only to be ‘recycled’ into the gem industry as faceted material. Nevertheless, EDXRF analyses performed on various locations of both samples did not reveal Bi or Ge (as would be expected for a BGO material; also Bi from the eulytine inclusions), and the reason for this is unknown. The presence of the eulytine inclusions in a glass is witness of its manufactured nature.

Lwizahira Vasquez and
Dr Riadh Zellagui (riadh@aglgemlab.com)
American Gemological Laboratories Inc.
New York, New York, USA

References

- Gévy, G. 1987. Growth and characterization of Bi₄Ge₃O₁₂ single crystals. *Progress in Crystal Growth and Characterization*, **15**(3–4), 145–186, [http://doi.org/10.1016/0146-3535\(87\)90010-4](http://doi.org/10.1016/0146-3535(87)90010-4).
- Piekarczyk, W., Świrkowicz, M. & Gazda, S. 1978. The Czochralski growth of bismuth-germanium oxide single crystals. *Materials Research Bulletin*, **13**(9), 889–894, [http://doi.org/10.1016/0025-5408\(78\)90099-5](http://doi.org/10.1016/0025-5408(78)90099-5).
- Takagi, K., Oi, T., Fukazawa, T., Ishii, M. & Akiyama, S. 1981. Improvement in the scintillation conversion efficiency of Bi₄Ge₃O₁₂ single crystals. *Journal of Crystal Growth*, **52**, 584–587, [http://doi.org/10.1016/0022-0248\(81\)90345-6](http://doi.org/10.1016/0022-0248(81)90345-6).
- White, W.B. & Minser, D.G. 1984. Raman spectra and structure of natural glasses. *Journal of Non-Crystalline Solids*, **67**(1–3), 45–59, [http://doi.org/10.1016/0022-3093\(84\)90140-6](http://doi.org/10.1016/0022-3093(84)90140-6).

Opal Doublets from Slovakia

The most famous gem material from Slovakia is play-of-colour opal (also known as precious opal). The deposits occur in the eastern part of the Western Carpathians, in the Libanka and Šimonka mountains of eastern Slovakia, near Dubník, Prešov District, between Zlatá Baňa and Červenica. The stones are commonly called ‘Hungarian’ opals because this region was part of Hungary until the end of World War I (Rondeau *et al.* 2004; Caucia *et al.* 2013). Historically, these deposits were the only source of gem opal in Europe, and represented the largest and most significant play-of-colour opal deposits from Roman times to the 19th century. They dominated the world opal market until the discovery of play-of-colour opal in Australia (Caucia *et al.* 2013), resulting in the closure of the Dubník mines in 1922–1923.

The modern history of Dubník opals began in the 1990s after a new geological survey of the area indicated the deposit appeared to be economically profitable (Semrád 2015). However, administrative problems delayed the start of opal mining. Then, starting in 2008, large quantities of play-of-colour opal from Wollo (or Welo/Wello), Ethiopia, entered the market, so the project to renew opal mining near Dubník was abandoned (Semrád 2015). At present it is possible to find only small quantities of mostly low-quality rough opal from Dubník at regional mineral shows in Slovakia or the Czech Republic. This recent production comes from local collectors who dig the opal from old tailings piles.

The Dubník material has been found as pure masses of opal, as well as boulder and matrix varieties. It has a white to very pale milky grey body colour, and the play-of-colour is mostly limited to blue and violet (although not as bright as Mexican or Australian opal), with bright red spots being rare.

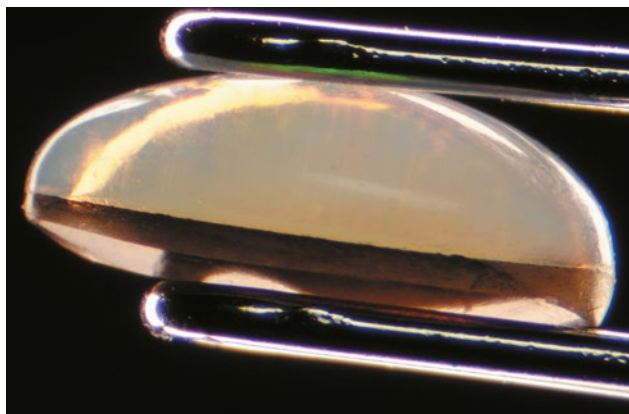


Figure 33: These doublets (0.38–2.08 ct) are formed by a top portion of play-of-colour opal from Dubník (Slovakia) cemented to a base of Slovakian obsidian. Photo by J. Štubňa.

Doublets and triplets made from Dubník opal were not known historically because such composites were first developed only towards the end of the 19th century (Semrád 2015). Recently, however, we encountered opal doublets with a Slovakian gem dealer at a local mineral show in Bratislava (Figure 33). According to the dealer and the authors’ own investigations, the doublets consist of Dubník opal that has been cemented to a base formed by another local material: obsidian from the Tokaj Mountains of Slovakia (Štubňa *et al.* 2019). So far, only six pieces have been produced experimentally, in round, oval and pear shapes that ranged from 5.52×3.56 mm (0.38 ct) to 8.60×8.60 mm (2.08 ct). Viewed from the side, their assembled nature is clearly seen (Figure 34). The obsidian portion is semi-transparent and exhibits inclusions and a banded texture

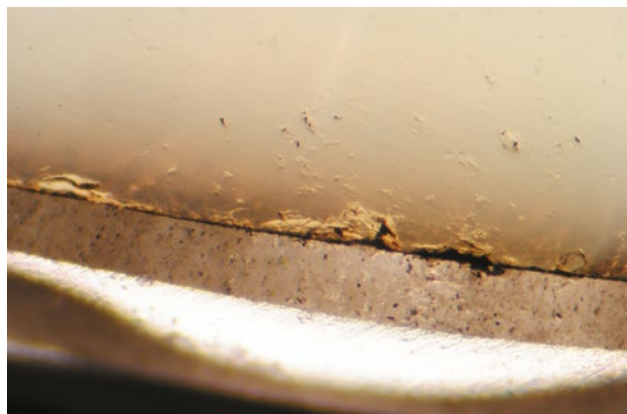


Figure 34: (a) Viewed from the side, the composite nature of this opal-obsidian doublet is obvious. (b) Higher magnification reveals dark-coloured cement at the interface between the opal and obsidian. Photomicrographs by J. Štubňa; magnified 7.5× (a) and 20× (b).

that are typical of this material (cf. Štubňa *et al.* 2019; Figure 35). The overall dark appearance of some of these doublets is due to the dark colour of the obsidian and the cement used to assemble these composites, causing them to resemble black opal. Therefore their face-up appearance may be confused with doublets of play-of-colour opal from Australia.

*Drs Ján Štubňa (janstubna@gmail.com)
and Ludmila Illášová
Gemmological Institute, Constantine the
Philosopher University, Nitra, Slovakia*

*Drs Jana Fridrichová and Peter Bačík
Comenius University, Bratislava, Slovakia*

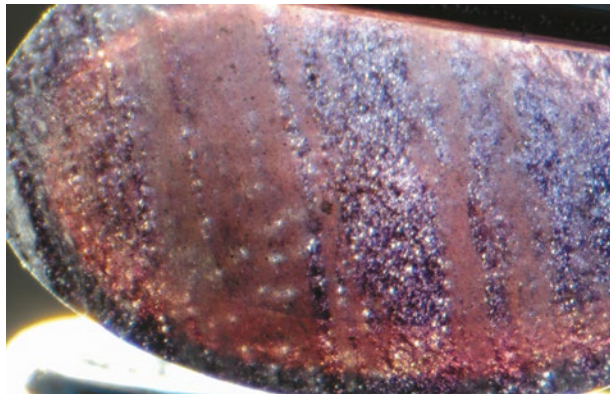


Figure 35: The base of this doublet shows a banded texture within the semi-transparent obsidian. Photomicrograph by J. Štubňa; magnified 10×.

References

- Caucia, F., Mrinoni, L., Leone, A. & Adamo, I. 2013. Investigation on the gemological, physical and compositional properties of some opals from Slovakia (“Hungarian” opal). *Periodico di Mineralogia*, **82**(2), 215–261, <http://doi.org/10.2451/2013PM0015>.
- Rondeau, B., Fritsch, E., Guiraud, M. & Renac, C. 2004. Opals from Slovakia (“Hungarian” opals): A re-assessment of the conditions of formation. *European Journal of Mineralogy*, **16**(5), 789–799, <http://doi.org/10.1127/0935-1221/2004/0016-0789>.
- Semrád, P. 2015. European precious opal from Červenica-Dubník – An historical and gemmological summary. *Australian Gemmologist*, **25**(11–12), 372–388.
- Štubňa, J., Illášová, L., Fridrichová, J. & Bačík, P. 2019. Gem Notes: Obsidian from Slovakia. *Journal of Gemmology*, **36**(5), 409–410.

TREATMENTS

Heated Sapphires with Unstable Colour Centres

Recently there has been a renewed focus on certain sapphire varieties that may exhibit a colour shift (or tenebrescence) as a result of unstable colour centres (Krzemnicki *et al.* 2018; American Gemological Laboratories [AGL] 2019; Krzemnicki & Cartier 2019). Over the past year, AGL has been collecting data on gem corundum that may display unstable colouration, specifically pink, padparadscha, orange and yellow sapphires.

The potentially unstable colour centre causing the colour shift is a trapped-hole centre related to Mg²⁺. This is a naturally occurring phenomenon and is generally stable. However, in certain circumstances, trapped-hole centres are unstable for reasons that are not yet fully understood. When stable, the Mg²⁺-related trapped-hole centre is active and responsible for the yellow colour in the vast majority of yellow sapphires (see, e.g., Emmett & Douthit 1993). Moreover, it is also an essential contributing chromophore in orange sapphires and in the orangey colour component of padparadscha sapphires. However, when the trapped-hole centres are

not stable, there are two states: (1) the colour centre is inactive and therefore does not contribute to a stone’s colour appearance, and (2) the colour centre is activated by exposure to UV radiation and then contributes to the observed colour. The trapped-hole colour centre can be returned to its relaxed (inactive) state by exposing the stone to the heat of a lamp (or otherwise warming it) for a brief period.

At the time of the April 2019 AGL press release, our data had shown that such changes in colour can occur in both unheated sapphires and in those that had been heated at relatively low temperatures. That release further indicated that the colour shifts had thus far not been observed in stones heated at relatively higher temperatures.

Recently, however, AGL examined five sapphires that displayed unexpected results when subjected to colour stability testing. They ranged from colourless to very pale blue and light yellow when they were first examined (Figure 36a). After exposure to short-wave UV radiation for 10 minutes, all five stones exhibited a distinctly stronger yellow colouration (Figure 36b). What was unexpected was that all five sapphires revealed clear evidence of having been heated at relatively high temperatures. This



Figure 36: (a) These heat-treated sapphires (2.63–4.19 ct) ranged from colourless to near-colourless (pale blue) and pale to light yellow when they were initially examined at AGL. (b) Exposing them to short-wave UV radiation for a period of 10 minutes activated unstable colour centres and caused a distinctly stronger yellow colouration. For each case, the stones are shown table-up (left) and from the side (right). Photos by Alex Mercado and Bilal Mahmood, AGL.

was apparent from the presence of heavily altered mineral inclusions, as well as thermally induced and altered stress fractures and partially healed fissures (Figure 37).

Previously it was thought that the heating process stabilised these colour centres, meaning that a colour shift would no longer be observed. The present discovery proves this is not always the case, which has direct implications for gemmological laboratories and the trade at large. Until now, colour-stability tests have been largely relegated to unheated sapphires. The more recent observations that unstable colour centres may be present in sapphires heated at relatively low temperatures—and now at relatively high temperatures—indicate that virtually all sapphires in the colour range of pink through padparadscha and orange to yellow, as well as colourless to near-colourless, should be tested for their colour stability regardless of their unheated or heated condition.

It remains unclear as to why a colour shift was not

observed previously in sapphires heated at relatively high temperatures. However, one factor might be the kinds of sapphires that are typically submitted for laboratory testing, which consist of strongly coloured stones. Therefore, the potential influence of trapped-hole centre absorption may be minimised or reduced. Furthermore, the total trace-element composition (relative to Mg content) of more strongly coloured sapphires may provide a better environment to stabilise the trapped-hole centres than lighter stones with a reduced total trace element composition (again relative to Mg; see, e.g., Emmett *et al.* 2003).

*Christopher P. Smith FGA (chsmith@aglgemlab.com),
Monruedee Chaipaksa, Adrian Perlmutter,
Lwizahira Vasquez, Dr Riadh Zelligui
and Sasitorn Chen
American Gemological Laboratories Inc.*

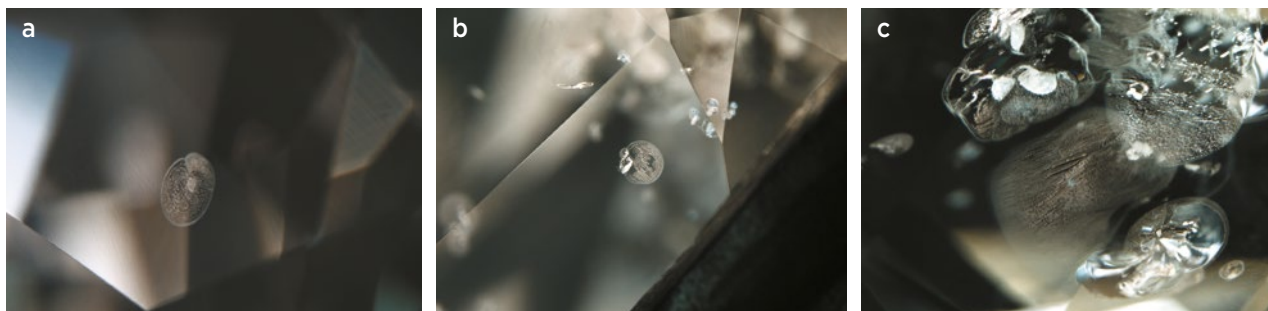


Figure 37: Each of the five sapphires with an unstable colour revealed clear evidence of relatively high-temperature heat treatment, including heavily altered mineral inclusions surrounded by tension fractures, thermally altered and induced stress fractures, and partially healed fissures. Photomicrographs by C. P. Smith; magnified 60× (a), 52× (b) and 48× (c).

References

- American Gemological Laboratories 2019. AGL clarifies its policy on color stability testing of sapphires. <http://aglgemlab.com/news/2019/4/25/agl-clarifies-its-policy-on-color-stability-testing-of-sapphires-1>, 25 April, accessed 5 August 2019.
- Emmett, J.L. & Douthit, T.R. 1993. Heat treating the sapphires of Rock Creek, Montana. *Gems & Gemology*, **29**(4), 250–272, <https://doi.org/10.5741/gems.29.4.250>.
- Emmett, J.L., Scarratt, K., McClure, S.F., Moses, T., Douthit, T.R., Hughes, R., Novak, S., Shigley, J.E., Wang, W., Bordelon, O. & Kane, R.E. 2003. Beryllium diffusion of ruby and sapphire. *Gems & Gemology*, **39**(2), 84–135, <https://doi.org/10.5741/gems.39.2.84>.
- Krzemnicki, M.S. & Cartier, L.E. 2019. Padparadscha-like fancy sapphires with unstable colors: Coloration mechanisms and disclosure. *InColor*, No. 41, 92–94.
- Krzemnicki, M.S., Klumb, A. & Braun, J. 2018. Unstable colouration of padparadscha-like sapphires. *Journal of Gemmology*, **36**(4), 346–354, <http://doi.org/10.15506/JoG.2018.36.4.346>.

MISCELLANEOUS

2019 Rough Stone Sales in Myanmar

Kachin State in northern Myanmar has an area of more than 89,000 km², and is bounded on the north and east by China, and partially on the north-west by India. It hosts a portion of Myanmar's important jadeite deposits (i.e. near Hpakan). The Kachin people, with great effort and enthusiasm, formed the Kachin State Gems and Jewellery Entrepreneurs Association in Myitkyina Township, and organised the second rough jade emporium there on 14–18 May 2019 (Figure 38). The chairman of the association opened the emporium, in the presence of a large crowd, at the association's facility in the industrial zone of Sitapur Quarter. Attendees consisted of parliamentary members, gem merchants and departmental officers. Total jade sales at the emporium amounted to 6,573.98 million kyats, representing 384 lots sold out of 492 lots offered. Panhoke Duwa Co. paid the highest price for a single lot: 4,637.77 million kyats for lot 93, weighing 53,354 kg.

On 8–13 June 2019, Myanmar Gems Enterprise held its seventh sale (in kyats) for local merchants of gem and jade rough material in Nay Pyi Taw. Attendees included 1,140 jade merchants and 53 gem dealers. Total sales were 60,891.97 million kyats, obtained from 3,011 jade lots (60,529.88 million kyats) and 45 gem lots (362.09 million kyats). The highest price was paid for jade lot no. 2983 containing four pieces weighing 8,330 kg, which sold for 520.09 million kyats. The gem emporium included 127 ruby and 63 sapphire lots, but only 10



Figure 38: In May 2019, a rough jade emporium was held in Myitkyina, northern Myanmar. Photo courtesy of T. Hlaing.

ruby lots (eight of which were from Mong Hsu) and 26 sapphire lots were sold. Other sales included peridot and topaz, but none of the lots were sold of amber, amethyst, aquamarine, garnet, goshenite, moonstone, quartz, rubellite and zircon. Overall, proceeds from this year's emporium were higher than at the previous rough stone sale that took place in November 2018 (Table II).

Table II: Total sales at the 2018 and 2019 rough stone emporiums in Nay Pyi Taw.

Date	Lots shown	Lots sold	Total sales (million kyats*)
November 2018	3,435	3,235	49,093.39
June 2019	3,368	3,060	60,891.97

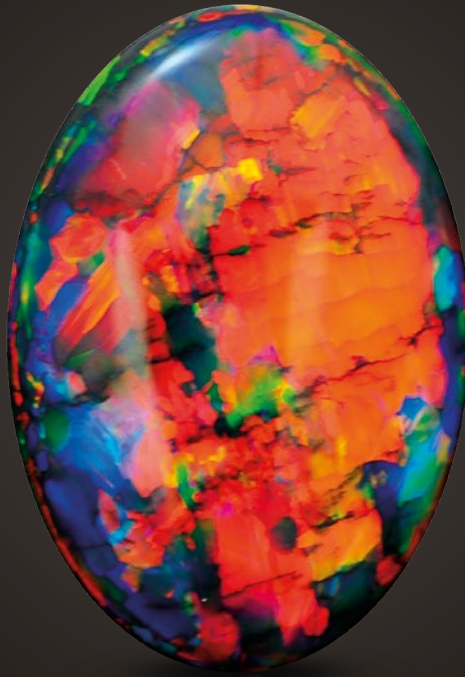
* 1 kyat = 0.00055 British pound or 0.00067 U.S. dollar.

*Dr U Tin Hlaing (p.tinhlaing@gmail.com)
Dept. of Geology (retired)
Panglong University, Myanmar*

The Fire Within

“For in them you shall see the living fire of the ruby, the glorious purple of the amethyst, the sea-green of the emerald, all glittering together in an incredible mixture of light.”

- Roman Elder Pliny, 1st Century AD



BLACK OPAL 15.7 CARATS

Suppliers of Australia's finest opals to the world's gem trade.

CODY  OPAL

LEVEL 1 - 119 SWANSTON STREET MELBOURNE AUSTRALIA

T. +61 3 9654 5533 E. INFO@CODYOPAL.COM

WWW.CODYOPAL.COM


INTERNATIONAL
COLORED GEMSTONE
ASSOCIATION
MEMBER

Selecting a Diamond Verification Instrument Based on the Results of the Assure Program: An Initial Analysis

Harold Dupuy and Jon C. Phillips

ABSTRACT: Recently, the rapid growth in synthetic diamond production—particularly in melee sizes—and the salting of melee parcels with synthetics have generated a commensurate increase in the need for diamond verification instruments (DVIs). Ongoing independent third-party testing of these instruments is being done through the Assure Program. DVI performance is tested in a UL laboratory using carefully developed testing standards and sample sets (i.e. natural diamonds and as-grown and treated synthetics, as well as simulants as appropriate). The initial phase of testing was performed during latter 2018 and the first part of 2019, and as of July 2019 results for 16 widely available devices from 12 DVI manufacturers were published online in the Assure Directory (<https://diamondproducers.com/assure/assure-directory>). From these test results, the authors have evaluated several important parameters that will help users select the best instrument for their needs. Performance results from several additional DVIs are expected to be released in the near future, and further testing and publication of the data will occur as new instruments are introduced and existing ones are updated.

The Journal of Gemmology, 36(7), 2019, pp. 606–619, <http://doi.org/10.15506/JoG.2019.36.7.606>
© 2019 Gem-A (The Gemmological Association of Great Britain)

Conversations within the gem and jewellery trade on how to separate natural from synthetic diamonds have been ongoing for decades. General Electric succeeded in growing synthetic diamonds in the mid-1950s (Bruton 1978), but several decades passed before such products became commercially available in sizes and qualities suitable for gems (i.e. in the mid-1980s from Sumitomo Electric Industries in Japan; Shigley *et al.* 1986). Today, synthetic diamonds are readily available for gem and jewellery use, both legitimately—when they are sold and identified as such—and nefariously, when they are intentionally represented as natural or the customer is allowed to infer that they are natural without proper disclosure from the seller (Rapaport 2013). Large quantities of small-sized synthetics (especially

<0.05 ct) produced using high-pressure, high-temperature (HPHT) growth methods are readily available in variable clarities and in the D–N colour range, particularly from Chinese manufacturers (Eaton-Magaña *et al.* 2017). Chinese factories produce approximately 200,000 carats of HPHT-grown melee per month (Shigley 2017), and production capacity continues to increase. In addition, synthetic diamonds grown by chemical vapour deposition (CVD) are improving in quality and are undergoing limited commercial production for the gem industry (Eaton-Magaña & Shigley 2016). At the same time, reports have been circulating of melee diamond parcels (e.g. Figure 1) and jewellery being salted with synthetics (e.g. Poon *et al.* 2016; Bhoir *et al.* 2017; Ambalathveetil *et al.* 2018), causing concern in the trade. Stories on the Internet and in other consumer

Figure 1: There is growing concern in the gem and jewellery industry over the presence of synthetics and simulants in diamond parcels, particularly for melee-sized goods such as those shown here. Photo courtesy of De Beers Group Industry Services.



media have also highlighted problems surrounding undisclosed synthetics and simulants, and the average jeweller must contend with the fact that they could unknowingly be dealing in these products.

An experienced gemmologist who remains current on the growth technology and properties of the synthetics (both HPHT and CVD grown) can, in some cases, distinguish between natural and laboratory-grown diamonds through the use of classical gemmological tools. However, this is impractical for situations in which numerous stones (often melee-sized) must be quickly and cost-effectively tested on a regular basis. While several gem-testing laboratories offer melee screening services (e.g. Figure 2), it can be expensive and impractical to send quantities of diamonds to labs, and the cost and lost time make it desirable in some cases to have access to in-house instrumentation.

Numerous diamond verification instruments (DVI) are currently on the market for diamond testing, and as of this writing the authors have identified 49 devices from 24 manufacturers (Table I). Some DVIs have been available for more than two decades (e.g. Welbourn *et al.* 1996), but many have only recently been released. Manufacturers claim their instruments can separate colourless to near-colourless natural from synthetic diamonds and from some simulants or, at a minimum, refer those in question for further testing. These instruments range from relatively inexpensive to very costly, and present a diverse array of marketing

claims and features (Drucker & Phillips 2018). Hundreds of businesses in the supply chain have acquired these instruments and base their hard-earned reputations on the results they produce. However, until recently, there was no independent means to verify the accuracy and reliability of such testing and screening devices.

In 2017, the Diamond Producers Association (DPA) proactively sought to address this problem by creating an initiative named Project Assure (Freedman 2017), which was subsequently renamed the Assure Program. This initiative is managed by DPA with support from Signet Jewelers (Akron, Ohio, USA). As of July 2019, the results

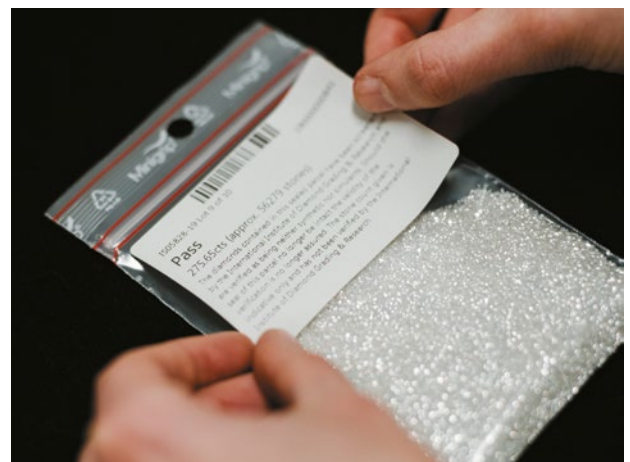


Figure 2: Melee screening services are offered by several gem-testing laboratories. The diamonds in this parcel were identified as natural by the International Institute of Diamond Grading & Research. Photo courtesy of De Beers Group Industry Services.

Table I: Assure-tested and untested diamond verification instruments.^a

Instrument	Manufacturer	Website
Assure tested		
AMS2	De Beers Group Industry Services (UK)	www.debeersgroupservices.com/instruments/automated-melee-testing
ASDI	SATT Gems (Switzerland)	www.sattgems.ch/asdi
DiamondDect 3	Taidiam Technology (Zhengzhou) Co. Ltd (China)	http://en.taidiam.com/product/11.html
DiamondDect 5	Taidiam Technology (Zhengzhou) Co. Ltd (China)	http://en.taidiam.com/product/11.html
DiamondSure	De Beers Group Industry Services (UK)	www.debeersgroupservices.com/instruments/diamondsure
DiamondView	De Beers Group Industry Services (UK)	www.debeersgroupservices.com/instruments/diamondview
G-Certain	Massive Tech Lab (India)	www.massivetechlab.com/g-certain
GemPen	Gemometrics (Sweden)	https://gemometrics.com/product/gempen
GIA iD100	Gemological Institute of America (USA)	www.gia.edu/id100
GV5000	National Gemstone Testing Center (China)	www.ngtc.com.cn/index.php?m=Article&a=show&id=485
J-Certain	Massive Tech Lab (India)	www.massivetechlab.com/j-certain-a-synthetic-diamond-detector-for-studded-jewellery
Leo ^b	Gemlogis (Hong Kong)	www.gemlogis.com/product-details/leo
M-Screen+ ^c	HRD Antwerp (Belgium)	http://hrdantwerp.com/en/equipment/detail/m-screen
Sherlock Holmes ^d	Yehuda Diamond Co. (USA)	www.yehuda.com/shop/hphtmachine
SYNTHdetect	De Beers Group Industry Services (UK)	www.debeersgroupservices.com/instruments/synthdetect
Synthetic Diamond Screener II	Presidium (Singapore)	https://presidium.com.sg/psdproduct/synthetic-diamond-screener-ii-sds-ii

from 16 tested instruments (see Table I and Figure 3) have been published in the Assure Directory (<https://diamondproducers.com/assure/assure-directory>), both as summary web pages and as more detailed downloadable PDF files. The results are complicated and somewhat confusing to interpret due to the wide variety of parameters, as well as the range of DVI features and capabilities. For example, it is necessary to simultaneously consider whether an instrument is designed for screening or testing, can take loose and/or mounted stones, can test for simulants, and will provide results that are automated or require the user’s interpretation, as well as several other variables (speed, cost and reliability). These choices and considerations can be overwhelming, and until now the results of the testing done so far and their implications have only been briefly discussed (e.g. Freedman 2019).

This article describes the Assure Program’s initiative of rigorously evaluating the performance of several commercially available DVIs (as of July 2019). The authors summarise the testing procedures, sample sets and results of instrument performance, and consider implications for selecting an appropriate DVI from those tested so far.

BACKGROUND

Both authors work in the diamond and jewellery wholesale business and have considerable experience with testing diamond parcels using various DVIs. Neither author is associated with the Assure Program or its affiliates, nor were they involved in the testing of the DVIs. During the preparation of this article, the authors obtained information from Lisa Levinson, DPA’s strategic project manager, and Thomas Gelb, a technical consultant to the Assure Program who assisted with the development of testing standards but did not take part in the actual DVI evaluation process.

For the initial phase of testing, DPA reached out to DVI manufacturers representing the most widely available devices in the market. Many responded, but not all. Those DVI manufacturers that chose to participate paid a fee directly to the testing organisation (UL, described below) to cover the cost of the testing process. In 2018, final arrangements were made with 11 manufacturers to test 18 DVIs, and as of July 2019 the results obtained for 16 of them (see Table II) were published in the Assure Directory. After undergoing the

Table I: (continued)

Instrument	Manufacturer	Website
Not Assure tested		
Alpha Diamond Analyzer	HRD Antwerp (Belgium)	https://hrdantwerp.com/en/equipment/detail/alpha-diamond-analyzer
Alrosa Diamond Inspector	Alrosa Technology (Russia)	https://alrosa-inspector.com
D-Guard	Sparrow Technologies (India)	http://sparrowdg.com
D-Screen ^e	HRD Antwerp (Belgium)	https://hrdantwerp.com
D•Secure+	DRC Techno (India)	https://drctechno.com/products/gemological/d-secure-plus
D-Tect	HRD Antwerp (Belgium)	https://hrdantwerp.com/en/equipment/detail/d-tect
DFI Mid-UV Laser+	GGTL Laboratories (Liechtenstein and Switzerland)	www.ggtl-lab.org/products.html
DiamondPlus	De Beers Group Industry Services (UK)	www.debeersgroupservices.com/instruments/diamondplus
Diasure	Maruti Enterprises (India)	www.diatech.co.in
DiaTrue CL	OGI Systems Ltd (Israel)	www.ogisystems.com/diatruexl.html
DiaTrue CM	OGI Systems Ltd (Israel)	www.ogisystems.com/diatrue.html
DiaTrue CS	OGI Systems Ltd (Israel)	www.ogisystems.com/diatruecs.html
DiaTrue Mobile	OGI Systems Ltd (Israel)	www.ogisystems.com/diatruemobile.html
DS2000	Nanjing Baoguang Testing Technology (China)	www.bgyq.cn/spe/spe.html
DS5000	National Gemstone Testing Center/Nanjing Baoguang Testing Technology Co. Ltd (China)	www.ngtc.com.cn/index.php?m=Article&a=show&id=486
GEM-3000 Jewelry Detector	Guangzhou Biaoqi Optoelectronics Technology Development Co. Ltd (China)	www.gzbiaoqi.com/ProductShowen.asp?ArticleID=9
GEM-Smart Portable Jewelry Detector	Guangzhou Biaoqi Optoelectronics Technology Development Co. Ltd (China)	www.gzbiaoqi.com/ProductShow.asp?ArticleID=387
GIA DiamondCheck	Gemological Institute of America (USA)	https://store.gia.edu/DiamondCheck-p/215000.htm
GLIS-3000	Guangzhou Biaoqi Optoelectronics Technology Development Co. Ltd (China)	www.gzbiaoqi.com/ProductShowen.asp?ArticleID=66
J•Detect 9000	DRC Techno (India)	https://drctechno.com/products/gemological/j-detect-9000
J•Mini	DRC Techno (India)	https://drctechno.com/products/gemological/j-mini
J-Screen (formerly EXA by Magilabs)	HRD Antwerp (Belgium)	https://hrdantwerp.com/en/equipment/detail/j-screen
J•Smart Pro	DRC Techno (India)	https://drctechno.com/products/gemological/j-smart-pro
Jewellery Inspector	Gemetrix Pty Ltd (Australia)	www.gemetrix.com.au/JewelleryInspector.html
Melee Inspector	Gemetrix Pty Ltd (Australia)	www.gemetrix.com.au/melee.html
NDC-415 Natural Diamonds Chooser	Guangzhou Biaoqi Optoelectronics Technology Development Co. Ltd (China)	www.gzbiaoqi.com/ProductShow.asp?ArticleID=388
PL-3000	Guangzhou Biaoqi Optoelectronics Technology Development Co. Ltd (China)	www.gzbiaoqi.com/ProductShowen.asp?ArticleID=67
PL5000	National Gemstone Testing Center (China)	www.ngtc.com.cn/index.php?m=Article&a=show&id=487
PL-Inspector	Gemetrix Pty Ltd (Australia)	www.gemetrix.com.au/PLInspector.html
Q-Chk++	Gemological Institute of India and Arotek Scientific Instruments (India)	https://giionline.com/q-chk-adc
Screen-I	SmartPro (Thailand)	www.smartproinstrument.com/event-2/screen-1
SSEF Diamond Spotter	Swiss Gemmological Institute SSEF (Switzerland)	www.ssef.ch/instruments-books
Vista	Gemlogis	www.gemlogisusa.com/gemlogis-vista.html

^a To the authors' knowledge, this list was current as of 1 July 2019, and is subject to change as instruments are updated, newly released and/or discontinued.

^b Leo has been discontinued. The tested device was acquired on the open market, so Gemlogis is not an Assure Partner.

^c Succeeded by M-Screen 4.0.

^d Succeeded by Sherlock Holmes 2.0.

^e According to HRD Antwerp, the D-Screen was still available at press time, although it is no longer being produced and is not shown on their website.



Figure 3: As of July 2019, the Assure Program had tested 16 diamond verification instruments. From left to right, these are: (top row) AMS2, ASDI, DiamondDect 3 and DiamondDect 5; (second row) DiamondSure, DiamondView, G-Certain and GemPen; (third row) GIA iD100, GV5000, J-Certain and Leo; (bottom row) M-Screen+, Sherlock Holmes, SYNTHdetect and Synthetic Diamond Screener II. These photos were supplied to the Assure Program by the instrument manufacturers.

testing, the instruments were returned to the submitting manufacturers.

The Assure Tested Certification Mark (Figure 4) is made available only to Assure Partners, that is, manufacturers that have agreed to submit their instruments for testing by the Assure Program. The certification mark simply indicates that a particular DVI has been tested by the Assure Program, and does not indicate any performance criteria or results. Therefore it is important to look beyond the certification mark and evaluate the actual test results.

Figure 4: The Assure Tested certification mark may be used only by DVI manufacturers that submit their instruments for testing in the Assure Program.



Table II: Specifications of the Assure-tested instruments.^a

Instrument	Portability	Dimensions (W × D × H, in cm)	Weight (kg)	Operation category ^b	Detects or refers synthetics	Sample size range (ct)	'Small Sample' tested
AMS2	Desktop	31.5 × 40 × 55	25	3	Detects	0.0033-0.20	Yes
ASDI	Floor	170 × 90 × 160	350	2	Refers	0.002-0.20	Yes
DiamondDect 3	Portable	22 × 20 × 12	3	1	Detects	0.005-10	Yes
DiamondDect 5	Desktop	20 × 23 × 29	7	1	Refers	0.005-10	Yes
DiamondSure	Portable	17 × 26 × 10	3.5	1	Refers	0.005-10	No
DiamondView	Desktop	20 × 40 × 25	13	1	Detects	0.01-10	No
G-Certain	Desktop	30 × 30 × 37	12	1	Detects	0.001-10	Yes
GemPen	Portable	24 × 3.6 × 3.2	1	1	Detects	Any	Yes
GIA iD100	Portable	16.5 × 20 × 8	1	2	Refers	0.005+	Yes
GV5000	Desktop	50 × 25 × 61	17	3	Detects	0.002-20	Yes
J-Certain	Desktop	43 × 34 × 52	22	1	Detects	0.002-10	Yes
Leof ^f	Portable	20.3 × 14 × 11.4	0.73	3	Refers	0.01-12	No
M-Screen+	Desktop	45 × 30 × 55	45	2	Refers	0.005-0.20	Yes
Sherlock Holmes	Portable	15 × 24 × 15	2.2	1	Detects	Any	Yes
SYNTHdetect	Desktop	31 × 34 × 45.8	30	2	Refers	0.001-100	Yes
Synthetic Diamond Screener II	Portable	13 × 10 × 6.5	0.2	1	Refers	0.02-10	No

Instrument	Colour range	Shapes allowed	Single or multiple samples ^c	Mounted jewellery	Auto-feed and dispense	Operator skill level ^d	Cost (USD, Feb. 2019)
AMS2	D-J	All	Multiple	No	Automatic	Novice	45,000
ASDI	D-J	Round	Multiple	No	Automatic	Novice	Not listed
DiamondDect 3	D-J	All	Single	Yes	Manual	Novice	5,730
DiamondDect 5	D-J	All	Multiple	Yes	Manual	Novice	5,730
DiamondSure	D-J	All	Single	Yes	Manual	Novice	18,200
DiamondView	All	All	Single	Yes	Manual	Expert	35,000
G-Certain	D-Z	All	Multiple	Yes	Manual	Novice	9,999
GemPen	D-Z ^e	All	Multiple	Yes	Manual	Expert	2,300
GIA iD100	D-J	All	Single	Yes	Manual	Novice	4,995
GV5000	D-N	All	Multiple	Yes	Manual	Expert	43,200
J-Certain	D-Z	All	Multiple	Yes	Manual	Novice	13,999
Leof ^f	D-M	All	Single	Yes ^g	Manual	Novice	499
M-Screen+	D-J	Round	Multiple	No	Automatic	Novice	63,000
Sherlock Holmes	D-K	All	Multiple	Yes	Manual	Expert	6,495
SYNTHdetect	D-J	All	Multiple	Yes	Manual	Expert	17,000
Synthetic Diamond Screener II	D-J	All	Single	Yes ^g	Manual	Novice	599

^a Sample size range, colour range and shapes allowed are as reported by the manufacturer.

^b Operation category is illustrated in Figure 5.

^c Single = tests one sample at a time; multiple = tests more than one sample at a time.

^d Interpretation of results: novice = instrument automatically displays results (or auto-sorts the samples, as for AMS2,

ASDI and M-Screen+); expert = user interprets luminescence (and growth structure when using DiamondView) to obtain results.

^e Not designed for Fancy yellows.

^f Device dimensions and weight obtained from Gemlogis website.

^g Only handles open-back settings.

INSTRUMENT CATEGORIES

Thirteen of the 16 instruments are *screeners*, for which the results indicate either a natural diamond or that a sample should be ‘referred’ for further testing. The latter samples could consist of natural diamonds (typically type IIa), synthetic diamonds (HPHT- or CVD-grown) or simulants (e.g. cubic zirconia, synthetic moissanite, etc.). High referral rates generate extra work and expense, either in house or by sending samples to a laboratory to obtain conclusive results.

Three of the 16 instruments are *testers*, which give a conclusion as to the identity of a stone. Testers are designed to identify samples as either natural diamonds, synthetic diamonds (CVD or HPHT) or simulants. However, such instruments sometimes may ‘refer’ more challenging samples.

DVIs are grouped by the Assure Program into three categories based on their claimed capabilities to identify simulants and differentiate synthetics from simulants (Figure 5).

Category 1

Manufacturers of Category 1 devices state that they can correctly separate natural from synthetic diamonds in most cases. However, they cannot identify diamond

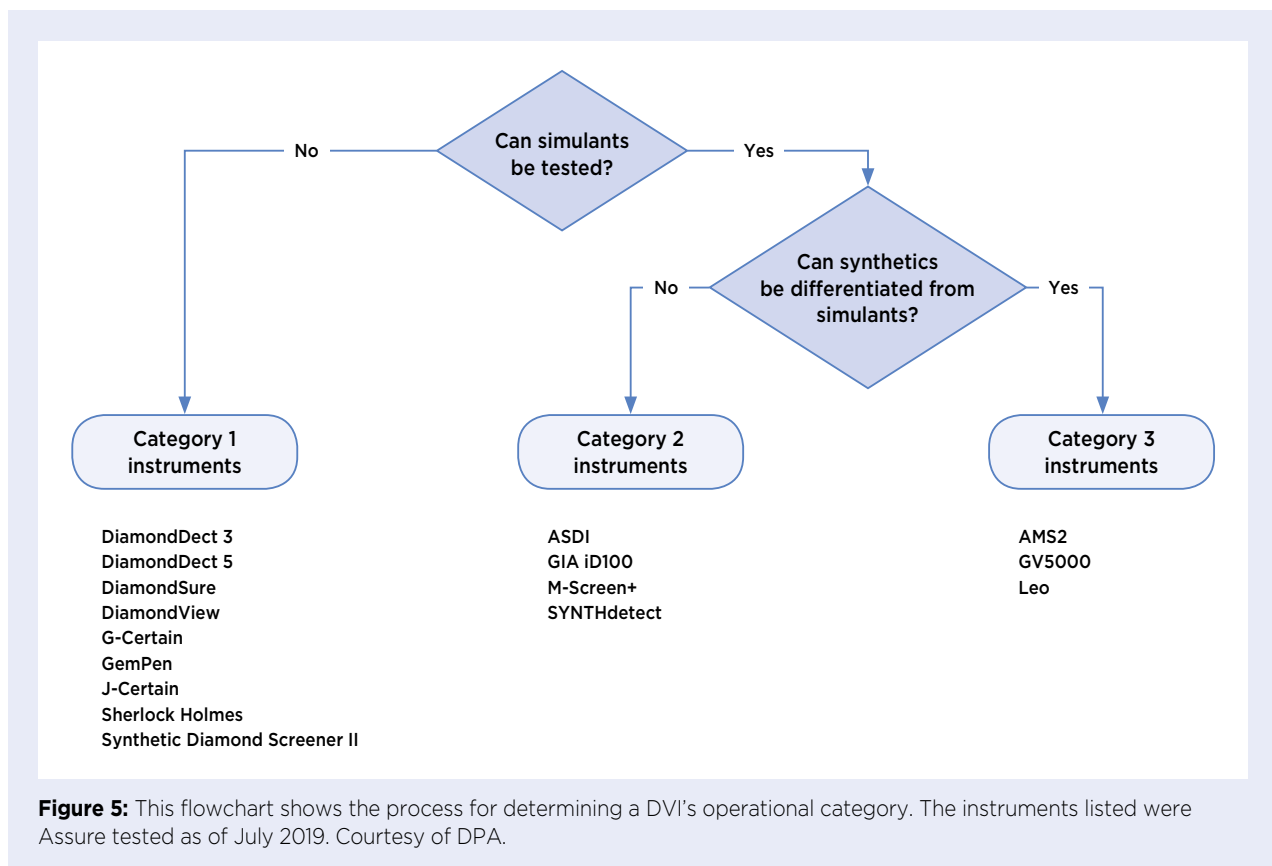
simulants. They also cannot identify the specific type of synthetic diamond (HPHT or CVD). Therefore, users of Category 1 DVIs must pre-screen all samples to ensure that no simulants are present. If knowledge of the type of synthetic diamond is required, such samples will need further testing. Category 1 includes the majority (nine of 16) of the DVIs tested so far.

Category 2

Manufacturers of Category 2 instruments state that they can correctly separate natural from synthetic diamonds and simulants. Unlike Category 1, the Category 2 DVIs can recognise that synthetic diamonds and simulants are ‘non-natural diamonds’ and group them together under that description. They cannot tell the difference between a synthetic diamond and a simulant, just that it is not a natural diamond. Thus, samples identified by Category 2 DVIs as ‘non-natural diamond’ need further testing to determine whether they are synthetic diamonds or simulants. Category 2 includes four of the 16 DVIs tested so far.

Category 3

Manufacturers of Category 3 devices state that they can correctly identify and separate natural and synthetic diamonds and simulants. However, samples identified



as other than natural diamond probably will need further testing to determine the specific type of synthetic diamond or simulant. Category 3 is the most robust testing category and includes only three of the 16 DVIs tested so far.

TESTING STANDARD

The methodology by which instruments are tested by the Assure Program is called the DVI Standard, which is used to evaluate device performance in testing/screening for synthetic diamonds and/or diamond simulants. The DVI Standard was developed and applied in collaboration with UL, a well-known global standards testing company headquartered in the USA. According to the company website (www.ul.com/media-center/company-information), since 1894 UL has helped to set more than 1,600 standards defining safety, security, quality and sustainability, and the company operates in more than 143 countries and across more than 20 industries. The DVI testing was done at a UL laboratory in Canton, Massachusetts, USA, in a controlled environment with the goal of giving accurate and quantifiable testing information on the instruments.

Development of the DVI Standard was supported by the manufacturers, who collaboratively shared basic information about how their instruments operate. Efforts

by the authors to obtain information from DVI manufacturers pertaining to their instruments' technology were met with limited success (see Table III), which is expected considering the desire to avoid disclosing proprietary information and perhaps also the status of pending patent applications. In any case, such technical details are beyond the scope of the present article.

The first draft of the DVI Standard was developed in early 2018 and subjected to an initial testing phase using three different instruments to ensure practical applicability. Throughout the development of the DVI Standard, expertise was provided by a technical committee of leading scientists, academics and gemmological laboratory personnel from around the world. Contributors included De Beers Group Industry Services (UK), the Federal State Budgetary Institution of the Technological Institute for Superhard and Novel Carbon Materials (Russia), Gemmological Institute of India, Gemological Institute of America, National Gemstone Testing Center (China), Scientific and Technical Research Center for Diamond (Wetenschappelijk en Technisch OnderzoeksCentrum voor Diamant or WTOCD; Belgium) and Swiss Gemmological Institute SSEF (Switzerland). All DVIs were tested using the same sample set(s) and conditions (see below) to ensure the performance results are comparable.

Table III: Instrument technology for Assure-tested DVIs, as provided by the manufacturers.

Instrument	Technology
AMS2	Time-resolved photoluminescence using short-wave UV radiation to view fluorescence and short- and long-lived phosphorescence; also takes an additional photoluminescence measurement
ASDI	Raman spectroscopy and short-wave UV transparency
DiamondDect 3	(Manufacturer did not respond)
DiamondDect 5	(Manufacturer did not respond)
DiamondSure	Visible-range absorption spectroscopy
DiamondView	Luminescence imaging of fluorescence or long-lived phosphorescence using ultra-short-wave UV radiation
G-Certain	(Manufacturer did not respond)
GemPen	'Ultra Spectrum Optical Filtering' technology that uses unique combinations of UV wavelengths and filtering to provoke variable fluorescence and phosphorescence
GIA iD100	Fluorescence spectroscopy
GV5000	(Manufacturer did not respond)
J-Certain	(Manufacturer did not respond)
Leo	(Manufacturer did not respond)
M-Screen+	(Manufacturer did not respond)
Sherlock Holmes	(Manufacturer would not disclose)
SYNTHdetect	Time-resolved photoluminescence using short-wave UV radiation to view fluorescence and short- and long-lived phosphorescence
Synthetic Diamond Screener II	Short-wave UV transparency vs. short-wave UV opacity

DPA has made the DVI Standard available exclusively to Assure Partners to create an incentive for them to submit their instruments for testing. It gives manufacturers an opportunity to do in-house testing for internal research-and-development purposes in accordance with the Standard, even in the absence of using the Assure Program's sample sets.

Testing Environment

The DVI Standard specifies particular conditions for lighting, room temperature and humidity, and no manufacturer asked to have their instrument tested outside of those parameters. Other conditions, such as the ideal power supply (i.e. operating voltage and amperage requirements), were set in accordance with the device operating manuals. These factors are important to consider because an instrument's test environment was not necessarily designed to replicate the ordinary commercial setting in which DVIs might be used. Therefore, the Assure Program specifies that the 'test results are not necessarily an indicator of how effectively the instrument would perform in normal commercial operating conditions' (Diamond Producers Association 2019). For commercial settings, DVI users should read the operating manual to learn important information about achieving optimal performance and understanding the limitations of the screening/testing instrumentation.

Sample Sets

Two main sample sets were developed by the Assure Program. The Core Sample was used for testing every instrument, while the Smalls Sample was utilised only for those instruments that could handle melee-sized stones

(i.e. ≤ 2.0 mm diameter; see Table II). The Core Sample (e.g. Figure 6) included 1,000 natural diamonds, 200 synthetic diamonds and, when applicable, 200 diamond simulants. The Smalls Sample had a similar composition and number of specimens as the Core Sample. The very high proportion of synthetic diamonds (20%), as compared to what might be encountered in the marketplace (~2%), enabled the instruments to be tested on a broad range of synthetic diamond material. The Core Sample also included challenging custom-made synthetic diamonds that are not currently commercially available, as they are too difficult to produce and/or prohibitively costly for commercial purposes. The Assure Program used these outliers for two reasons: (1) to 'future-proof' the sample set (in anticipation of the next generations of synthetics) and (2) to help UL differentiate effectively and fairly among the instruments. Consequently, an instrument's performance in a commercial setting is likely to be better than under the test conditions (but only if the manufacturer's optimum operating conditions are adhered to).

Some further details of the sample sets are as follows:

- Core Sample: round brilliant cuts with >2.0 mm girdle diameter (~0.03–0.20 ct), D–J colour (with hints of either yellow or brown), and SI₂ or better clarity.
- Smalls Sample: round brilliant cuts with 1.0–2.0 mm girdle diameter (~0.005–0.03 ct), D–J colour (with hints of either yellow or brown), and SI₂ or better clarity. (Note that five DVIs are claimed to be able to test diamonds below 1.0 mm in diameter—AMS2, ASDI, GV5000, J-Certain and Sherlock Holmes—but the Smalls Sample did not test this range.)



Figure 6: These photos show some of the natural diamonds (left) and simulants (colourless sapphires; right) in the Assure Core Sample. Photos courtesy of DPA.

- The natural diamonds in both sets have a consistent distribution of type Ia/IIa stones.
- The synthetic diamonds include both HPHT- and CVD-grown samples, and some of them were treated (e.g. irradiated or HPHT processed after CVD growth to improve their colour).
- The simulants include cubic zirconia, synthetic moissanite, foil-backed glass and colourless synthetic corundum.

Additional sample sets were developed specifically to include lower colour grades (K–Z) and mounted jewellery (see Table IV). These sets were only used for testing those instruments described by manufacturers as having the capability to handle such samples. The results of this additional testing are included for applicable DVIs in the Assure Directory, but they are not evaluated in this article.

TEST RESULTS

Table V summarises the performance testing results for the Core and Smalls sample sets according to three parameters (listed in order of importance, as determined by the authors): false positive rate, accuracy and referral rate. The results for each of these performance metrics are expressed as percentages, and are reported separately for natural diamonds, synthetic diamonds and simulants (if applicable). The percentages may be calculated differently depending on the DVI category (1, 2 or 3), and examples illustrating the calculations for each of these cases can be downloaded from the Assure Project website at <https://diamondproducers.com/app/uploads/2019/05/5.1.-ASSURE-Performance-Metrics-Infographic-20190523.pdf>.

Diamond false positive rate is the most important—and most complicated—of the three performance metrics, and refers to the percentage of synthetic diamonds (and diamond simulants, if applicable) erroneously classified

as natural diamond out of the total number of synthetic diamonds (and simulants) in the sample set. The optimal diamond false positive rate is 0%, meaning the instrument classified no synthetic diamonds or simulants as natural diamonds. By analogy, the *synthetic diamond false positive rate* refers to the percentage of natural diamonds (and simulants, if applicable) erroneously classified as ‘synthetic diamond’ out of the total number of natural diamonds (and diamond simulants, if applicable) in the sample set. The *simulant false positive rate* refers to the percentage of natural and synthetic diamonds erroneously classified as simulants out of the total number of natural and synthetic diamonds in the sample set.

Diamond accuracy is the percentage of natural diamonds that are correctly categorised as natural out of the total number of natural diamonds. The optimal diamond accuracy is 100%, in which all natural diamonds are correctly classified as natural. *Synthetic diamond accuracy* and *simulant accuracy* are defined as the fraction of test samples correctly classified by the DVI as synthetic diamonds and simulants, respectively.

Diamond referral rate is the percentage of natural diamonds that are referred for further testing out of the total number of natural diamonds in the sample set. Referred samples are unable to be classified by the DVI as natural or synthetic (and, where capable, synthetic or simulant), and require further testing to determine their identity. The lower the referral rate, the better. *Synthetic diamond referral rate* and *simulant referral rate* are the fractions of synthetic diamonds and simulants, respectively, which are referred by the DVI for further testing.

Novice or Expert Operator

The results in Table V are based on the ‘Operator skill level’ given in Table II, which indicates whether a novice or expert performed the testing of a particular DVI. A novice operator received an introductory level of training, which may have included reading the device’s operating manual, watching video tutorials and receiving

Table IV: Additional sample sets developed by the Assure Program.

Sample set	Description
Sample B	>2.0 mm girdle diameter, K–Z colour, round brilliant cuts, mixed clarity
Sample D	1.0–2.0 mm girdle diameter, K–Z colour, round brilliant cuts, mixed clarity
Simple Jewellery	Open-back jewellery set with D–J colour, round brilliant cuts, mixed clarity
Intricate Jewellery	Closed-back jewellery set with D–J colour, round brilliant cuts, mixed clarity
Melee Jewellery	Open-back jewellery set with D–J colour, round brilliant cuts, mixed clarity

Table V: Summary of Assure Program test results for 16 diamond verification instruments.^a

Instrument	Operation category	Core Sample test results (>2.0 mm)								
		Diamond			Synthetic diamond			Simulant		
		False positive rate	Accuracy	Referral rate	False positive rate	Accuracy	Referral rate ^b	False positive rate	Accuracy	Referral rate ^b
AMS2	3	0%	99.1%	0.7%	0.1%	70.9%	29.1%	0.1%	99.0%	1.0%
ASDI	2	0%	93.6%	6.4%	0%		100%	0%		100%
DiamondDect 3	1	0%	96.4%	0.6%	3.0%	99.5%	0.5%			
DiamondDect 5 ^c	1	22.6%	91.6%	8.4%	0%		77.4%			
DiamondSure	1	0%	95.3%	4.7%	0%		100%			
DiamondView	1	0%	100%	0%	0%	100%	0%			
G-Certain	1	17.6%	99.7%	0.2%	0.1%	69.3%	13.1%			
GemPen	1	15.1%	98.7%		1.3%	84.9%				
GLA iD100	2	0%	96.7%	3.3%	0%		100%	0%		100%
GV5000	3	1.0%	98.5%		1.1%	97.5%		0.6%	98.0%	
J-Certain	1	19.6%	99.7%	0.2%	0.1%	67.3%	13.1%			
Leo	3	4.6%	51.6%	3.7%	0%		52.3%	45.2%	91.3%	0%
M-Screen+	2	0%	95.9%	4.1%	0%		100%	0%		100%
Sherlock Holmes	1	0%	97.5%		2.5%	100%				
SYNTHdetect	2	0%	99.3%	0.7%	0%		100%	0%		100%
Synthetic Diamond Screener II	1	0%	84.5%	15.5%	0%		100%			

^a Includes results released as of 1 July 2019. Shaded areas indicate 'not applicable' (i.e. beyond the device's testing capability or the way it classifies samples; see the detailed test summary report PDFs in the Assure Directory).

in-person basic training as indicated by the manufacturer. The results obtained by a novice operator are to be expected for someone who has recently purchased and just begun using the device. Conversely, an expert operator is a representative from the DVI manufacturer or a UL technician trained by the manufacturer so that they are deemed an expert at operating the instrument. The results obtained by an expert operator are expected to be consistent with someone who is very familiar with using a specific instrument.

Instruments tested by an expert operator are also tested by a novice user for comparison, and the results for both types of operators can be found in the detailed reports available in the Assure Directory. As expected, better results overall were obtained for these DVIs when operated by an expert rather than a novice (e.g. Table VI).

SELECTING A DVI

To select the most appropriate DVI, users should first assess their needs to help match their business requirements to the capabilities of the instruments (e.g. Table VII). For example, is speed important? Are simulants to be pre-screened? Will the testing be limited to loose

diamonds? If so, as principal centre stones or as batches of melee? In what colour range? Will finished jewellery be tested? If an expert operator is required, is one currently on staff? Is automation needed for volume processing, or is manual operation sufficient? Does the instrument need to be portable? And, of course, instrument cost is another important criterion.

Screening (eliminating any non-natural diamonds) is distinctly different from detection (positive identification of a synthetic diamond or a simulant). Therefore, it may be helpful to start with identifying an appropriate DVI category (again, see Figure 5). If it is necessary to simply separate synthetics from natural diamonds, then a DVI of at least Category 1 is sufficient, and the user can consider

Table VI: Example of test results for novice and expert operators of the same instrument (here, SYNTHdetect).

Parameter	Novice	Expert
Diamond false positive rate	0%	0%
Diamond accuracy	98.6%	99.3%
Diamond referral rate	1.4%	0.7%
Speed (stones/hour)	225	583

Table V: (continued)

Smalls Sample test results (1.0–2.0 mm)									Average speed (samples tested/hour)	Instrument
Diamond			Synthetic diamond			Simulant				
False positive rate	Accuracy	Referral rate	False positive rate	Accuracy	Referral rate ^b	False positive rate	Accuracy	Referral rate ^b		
0%	98.9%	0.7%	0.1%	87.4%	12.6%	0.3%	99.5%	0.5%	2,677	AMS2
0%	93.2%	6.8%	0%		100%	0%		100%	6,511	ASDI
1.0%	90.6%	4.0%	5.5%	99.0%	0%				289	DiamondDect 3
9.4%	97.8%	2.2%	0%		90.6%				557	DiamondDect 5 ^c
									193	DiamondSure
									112	DiamondView
4.7%	99.3%	0.6%	0.1%	95.3%	0%				908	G-Certain
4.7%	99.5%		0.5%	95.3%					813	GemPen
0%	95.8%	4.2%	0%		100%	0%		100%	440	GIA iD100
0.3%	97.5%		1.4%	95.3%		1.4%	100%		296	GV5000
5.8%	99.3%	0.3%	0.4%	93.7%	0.5%				792	J-Certain
									219	Leo
0%	90.9%	9.1%	0%		100%	0%		100%	12,317	M-Screen+
0%	97.8%		2.2%	100%					530	Sherlock Holmes
0%	98.1%	1.9%	0%		100%				583	SYNTHdetect
									240	Synthetic Diamond Screener II

^b Referral rates for synthetic diamonds and simulants vary widely depending on the way each DVI categorises these sample types.

^c Although the DiamondDect 5 can only handle HPHT-grown synthetics, the Assure sample sets contain both HPHT- and CVD-grown samples.

Table VII: Assure-tested DVIs listed according to various requirements.^a

Requirement	Capable instruments
Identifies diamond simulants	AMS2, ASDI, GIA iD100, GV5000, Leo, M-Screen+, SYNTHdetect
Tests multiple stones at once	AMS2, ASDI, DiamondDect 5, G-Certain, GemPen, GV5000, J-Certain, M-Screen+, Sherlock Holmes, SYNTHdetect
Auto-feed and dispense	AMS2, ASDI, M-Screen+
Size <0.01 ct	AMS2, ASDI, DiamondDect 3, DiamondDect 5, DiamondSure, G-Certain, GemPen, GIA iD100, GV5000, J-Certain, M-Screen+, Sherlock Holmes, SYNTHdetect
Fancy shapes	AMS2, DiamondDect 3, DiamondDect 5, DiamondSure, DiamondView, G-Certain GemPen, GIA iD100, GV5000, J-Certain, Leo, Sherlock Holmes, SYNTHdetect, Synthetic Diamond Screener II
Mounted jewellery	DiamondDect 3, DiamondDect 5, DiamondSure, DiamondView, G-Certain, GemPen, GIA iD100, GV5000, J-Certain, Leo ^b , Sherlock Holmes, SYNTHdetect, Synthetic Diamond Screener II ^b
Automatic interpretation of results	AMS2, ASDI, DiamondDect 3, DiamondDect 5, DiamondSure, G-Certain, GIA iD100, J-Certain, Leo, M-Screen+, Synthetic Diamond Screener II
Portable	DiamondDect 3, DiamondSure, GemPen, GIA iD100, Leo, Sherlock Holmes, Synthetic Diamond Screener II
Cost <USD10,000	DiamondDect 3, DiamondDect 5, G-Certain, GemPen, GIA iD100, Leo, Sherlock Holmes, Synthetic Diamond Screener II

^a Instruments are listed in alphabetical order (see Table V for the performance results for each device). Leo has been discontinued, M-Screen+ has been succeeded by M-Screen 4.0 and Sherlock Holmes has been succeeded by Sherlock Holmes 2.0.

^b Only handles open-back settings.

the full array of 16 DVIs (as of writing this article) in the Assure Program’s test set. If simulant detection is required, then DVIs of at least Category 2 are appropriate, for which seven choices have been Assure tested. If Category 3

capabilities are needed—separating natural from synthetic diamonds, natural diamonds from simulants and synthetic diamonds from simulants—then currently there are three Assure-tested instruments with this capability.

Next, the authors suggest focusing on the most important performance metric in the test results: the diamond false positive rate (i.e. identifying a synthetic or simulant as a natural diamond). Ten of the 16 DVIs tested produced zero diamond false positive results for the Core Sample set (>2.0 mm diameter): AMS2, ASDI, DiamondDect 3, DiamondSure, DiamondView, GIA iD100, M-Screen+, Sherlock Holmes, SYNTHdetect and Synthetic Diamond Screener II. Furthermore, six of the 12 DVIs tested with the Smalls Sample set (1.0–2.0 mm) produced zero diamond false positive results: AMS2, ASDI, GIA iD100, M-Screen+, Sherlock Holmes and SYNTHdetect. In addition to diamond false positives, diamond accuracy and, finally, diamond referral rate should be considered. Across all three metrics, only one DVI scored perfectly in the Assure testing: the DiamondView at a cost of USD35,000 and requiring an expert operator.

Synthetic diamond dealers may also benefit from using a DVI, as they seek to protect their inventory from mixing with natural diamonds. For larger-sized samples (>2.0 mm) nine DVIs provided zero false positive results for synthetic diamonds (ASDI, DiamondDect 5, Diamond-Sure, DiamondView, GIA iD100, Leo, M-Screen+, SYNTHdetect and Synthetic Diamond Screener II). For smaller samples (1.0–2.0 mm), five DVIs had zero false positive results for synthetic diamonds (ASDI, DiamondDect 5, GIA iD100, M-Screen+ and SYNTHdetect).

When shopping for a DVI, the buyer should ask the seller ‘What is the best use of this instrument?’ Even more importantly, ‘What are the limitations of this instrument?’ In other words, what can’t it do? An informed buying decision would also include questions relating to the skillset required to properly operate the instrument and any training that is offered, as well as warranty details and any service requirements/arrangements.

In the end, it is possible that more than one DVI may

be required to meet one’s business needs, since, for example, testing parcels of diamond melee and larger individual samples (or loose stones and jewellery) might not be practical with a single instrument.

CONCLUSIONS

Diamonds (e.g. Figure 7) are a critical component of the global gem and jewellery industry, and it is imperative to correctly separate natural stones from synthetics and simulants. Beyond statutory requirements, consumer confidence is the bedrock of the jewellery business worldwide. A single incidence of an undisclosed synthetic diamond sold as natural can cause reputational harm and even legal consequences for the seller. Furthermore, such instances may quickly reverberate across social media and potentially have far-reaching ramifications for the industry. While a false-positive result (identifying a synthetic diamond as a natural diamond) is perhaps the most egregious error, a false negative (calling a natural diamond a synthetic diamond) can also damage one’s reputation.

To address such concerns, particularly for melee-sized goods, DVIs are now being sought by many segments of the jewellery supply chain (manufacturers, brokers, wholesalers and retailers). Until recently, however, there was no way to verify a DVI manufacturer’s claims regarding the effectiveness of their device for screening or identifying natural and synthetic diamonds and simulants. The authors applaud the Assure Project for addressing this need, and we look forward to the release of future testing results for additional/updated DVIs as they are published in the Assure Directory.

The testing results released for the DVIs tested so far show an overall wide range of performance, and prove that not all devices are equally effective at identifying or

Figure 7: To maintain consumer confidence in diamonds, it is important to reliably separate natural, as-mined diamonds (such as the ~0.70 ct stones from Canada shown here) from synthetic diamonds or simulants. The use of one or more DVIs that have received high marks from the Assure Program can help with this endeavour. Photo courtesy of Dominion Diamonds.



screening synthetics and/or simulants. DVIs are evolving quickly, and some initially-released models have already been discontinued or replaced by second-generation units that have undergone technical and ergonomic improvements. The authors expect this ‘upgrading’ trend to continue as detection technology improves and stays current with advances in synthetic diamond growth technology. We therefore urge future device purchasers to check the Assure Directory for updates.

The diversity of DVI features and capabilities, combined with the testing results from the Assure Program, requires that several factors be considered when choosing an instrument. During the decision-making process, users should first determine their needs and requirements, and then consider the instrument categories and review the

published Assure Program test results. In some cases, more than one DVI may be necessary to fulfil a company’s business needs. Whatever instrument is used, it is critical for the operator to understand at least some of the fundamental operating science employed by it, as well as its limitations, to prevent lapsing into a ‘black box’ mentality of pressing a button and always expecting a correct answer. The topic is not that simple and never will be.

The synthetic diamond industry is developing rapidly and DVI manufacturers are following, not leading, the technology. As growth techniques evolve, DVIs will have to keep pace. Products such as CVD-coated simulants and ‘composite diamonds’ (natural diamonds with CVD synthetic overgrowths) will further challenge some of the existing instruments.

REFERENCES

- Ambalathveetil, A.N., Al Muhari, N. & Singbamroong, S. 2018. Gem News International: Single HPHT synthetic diamond mixed in natural diamond ring. *Gems & Gemology*, **54**(4), 456–457.
- Bhoir, M., Dhawale, P. & D’Haenens-Johansson, U. 2017. Lab Notes: Melee diamond parcel containing nearly one-third CVD synthetics. *Gems & Gemology*, **53**(2), 236–237.
- Bruton, E. 1978. *Diamonds*. Chilton Book Co., Radnor, Pennsylvania, USA, 532 pp.
- Diamond Producers Association 2019. ASSURE Test Process. <https://diamondproducers.com/assure/assure-test-process>, accessed 20 July 2019.
- Drucker, R.B. & Phillips, J.C. 2018. Diamond screeners/testers. *GemGuide*, **37**(5), 1–5.
- Eaton-Magaña, S. & Shigley, J.E. 2016. Observations on CVD-grown synthetic diamonds: A review. *Gems & Gemology*, **52**(3), 222–245, <http://doi.org/10.5741/gems.52.3.222>.
- Eaton-Magaña, S., Shigley, J.E. & Breeding, C.M. 2017. Observations on HPHT-grown synthetic diamonds: A review. *Gems & Gemology*, **53**(3), 262–284, <http://doi.org/10.5741/gems.53.3.262>.
- Freedman, J. 2017. DPA, Signet, De Beers working on ‘Project Assure’. Rapaport, www.diamonds.net/News/NewsItem.aspx?ArticleID=58776, 9 April, accessed 20 June 2019.
- Freedman, J. 2019. What makes a good synthetics detector? Rapaport, www.diamonds.net/News/NewsItem.aspx?ArticleID=63460, 12 March, accessed 20 June 2019.
- Poon, T., Lo, C. & Law, B. 2016. Lab Notes: Mixing of natural diamonds with HPHT synthetic melee. *Gems & Gemology*, **52**(4), 416–417.
- Rapaport, M. 2013. Synthetics. *Rapaport*, **36**(12), 36–41.
- Shigley, J.E. 2017. The latest on synthetic diamonds. Gemological Institute of America, www.gia.edu/UK-EN/gia-news-research-latest-on-synthetic-diamonds-video-presentation, accessed 20 July 2019.
- Shigley, J.E., Fritsch, E., Stockton, C.M., Koivula, J.I., Fryer, C.W. & Kane, R.E. 1986. The gemological properties of the Sumitomo gem-quality synthetic yellow diamonds. *Gems & Gemology*, **22**(4), 192–208, <http://doi.org/10.5741/gems.22.4.192>.
- Welbourn, C.M., Cooper, M. & Spear, P.M. 1996. De Beers natural versus synthetic diamond verification instruments. *Gems & Gemology*, **32**(3), 156–169, <https://doi.org/10.5741/gems.32.3.156>.

The Authors

Harold Dupuy FGA

Stuller Inc., 302 Rue Louis XIV, Lafayette,
Louisiana 70503 USA
Email: harold_dupuy@stuller.com

Jon C. Phillips

Corona Jewellery Co. Ltd, 16 Ripley Ave., Toronto,
Ontario M6S 3N9 Canada
Email: phillips1957@hotmail.com

Acknowledgements

The authors thank the following for their assistance: Thomas Gelb (Diamond Durability Laboratory, New York, New York, USA), Lisa Levinson (Diamond Producers Association, Antwerp, Belgium), Nellie Barnett (Gemological Institute of America, Carlsbad, California, USA), Alvina Schlotterbeck (De Beers Group Industry Services, London), and Bear and Cara Williams (Stone Group Laboratories, Jefferson City, Missouri, USA).

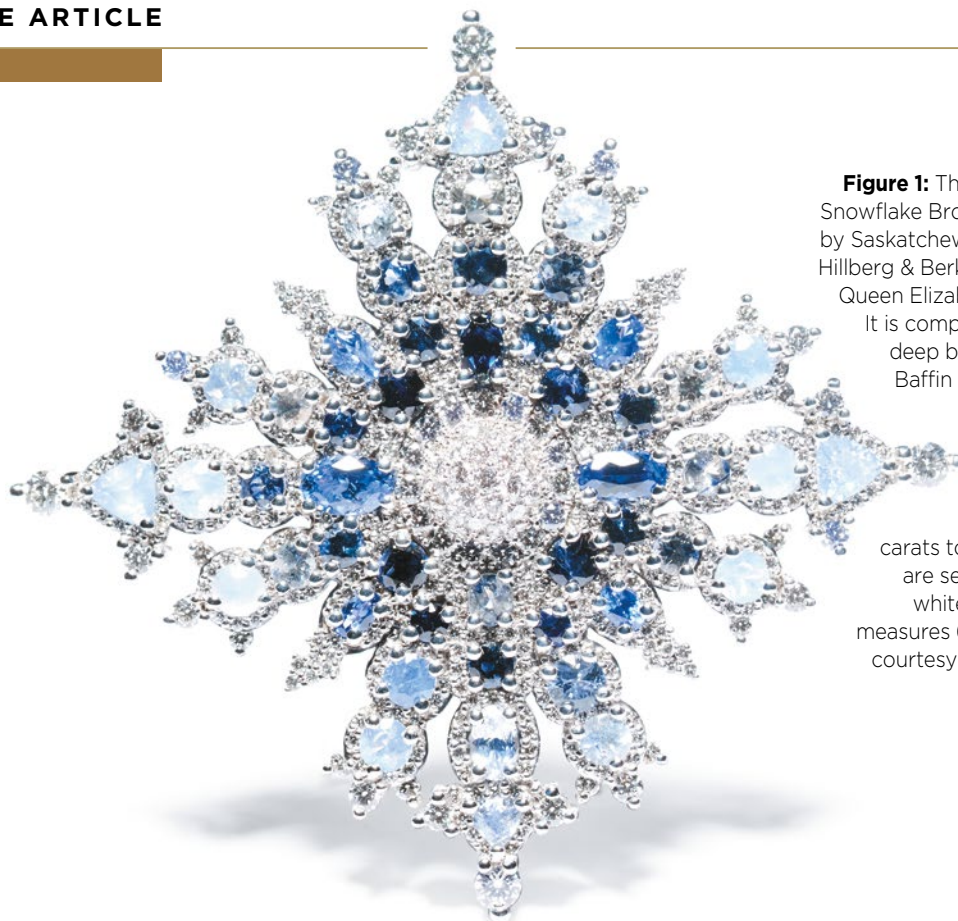


Figure 1: The Sapphire Jubilee Snowflake Brooch was designed by Saskatchewan-based jeweller Hillberg & Berk and presented to Queen Elizabeth II in July 2017. It is composed of 48 pale to deep blue sapphires from Baffin Island (10.19 carats total weight), together with more than 400 Canadian diamonds (4.39 carats total weight), which are set in 18 ct Canadian white gold. The brooch measures 6.1 × 6.6 cm. Photo courtesy of Hillberg & Berk.

Adding Logic to Luck: Recent Advances in Coloured Stone Exploration in Canada

Lee A. Groat

ABSTRACT: Canada exhibits many of the challenges involved with exploring for coloured stones in countries with very low population densities, temperate-to-arctic climates and a lack of infrastructure hindering access to most prospective areas. Despite this, a number of discoveries have occurred, mainly during the past two decades. These include emeralds from Northwest Territories (1997) and Yukon (1998); sapphire (2002) and spinel (from 1982)—including cobalt-blue stones—from Baffin Island in Nunavut; and ruby and pink sapphire (2002) from British Columbia. Such discoveries can be assisted by undertaking scientific research into gem formation, as well as by applying exploration criteria developed elsewhere to uncharted territory. Future exploration in Canada and other countries facing similar challenges will likely benefit from additional geological studies to identify prospective areas and features; innovative means of transportation, such as boats instead of aircraft; drones for exploring rugged terrain; hyperspectral imaging for mineral sensing; surveying with UV lamps to identify minerals associated with gem mineralisation; and careful prospecting (including field mapping and collecting heavy mineral concentrates) by experienced individuals.

The Journal of Gemmology, 36(7), 2019, pp. 620–633, <http://doi.org/10.15506/JoG.2019.36.7.620>
© 2019 Gem-A (The Gemmological Association of Great Britain)

Most coloured stone deposits are discovered by accident, and new finds are more likely to occur in countries with moderate-to-high population density, tropical-to-temperate climates and reasonable access to the land mass. Some gem discoveries are made while exploring for other resources, but most explorationists are unfamiliar with the geology of coloured stone deposits—and furthermore their surface exposures may be quite small—which makes them difficult to find even when they occur in areas being explored for other materials. New gem deposit discoveries are particularly challenging in Canada, with its very low population density (approximately four people per square kilometre, one of the lowest densities in the world), a challenging climate which restricts exploration and poor access to most of the land mass such that many areas can only be explored by air (usually by helicopter).

Canada is a major producer of diamonds, but apart

from ammolite in Alberta and jade in British Columbia and Yukon, the country is not a significant producer of coloured stones. Nevertheless, sapphires from Baffin Island in Nunavut made headlines in July 2017 when they were included in the Sapphire Jubilee Snowflake Brooch which celebrated the 65th anniversary of Queen Elizabeth II's reign (Figure 1). Additional coloured stone discoveries—some in remote Arctic terranes—have provided encouragement for further exploration and suggest that additional deposits are awaiting discovery. Although beyond the scope of the present article on Canadian gems, the recent opening of the Arctic's first economic ruby deposit in Greenland at Aappaluttoq is also an important milestone in gem exploration and mining in this part of the world (e.g. Turner *et al.* 2019).

The goal of this article is to review the geology and discovery of various coloured stone deposits in Canada (Figure 2), and to examine how scientific study can



Figure 2: This map shows the main coloured stone deposits in Canada that are reviewed in this article.

inform exploration strategies and techniques that could be used for locating additional gem-producing areas. It is hoped that these insights will provide inspiration for future exploration activities in Canada and in other countries that share similar challenges to finding new coloured stone deposits.

EMERALD IN NORTH-WESTERN CANADA

Tsa da Glisza, Yukon

In 1998, William Wengzynowski of Archer Cathro & Associates (1981) Ltd. (Vancouver, British Columbia, Canada) was exploring for volcanogenic massive sulphide deposits in talus on the north side of a ridge in south-central Yukon, when he found green crystals that, on closer inspection, revealed a hexagonal outline. He was confident that they were emerald, and his identification was later confirmed by powder X-ray diffraction at the University of British Columbia.

At this locality, subsequently named Tsa da Glisza ('green stone' in the Kaska language), the emerald occurrence is underlain by a granite pluton containing 9.8 to 13.2 ppm Be. The mineralisation is associated with quartz–tourmaline veins and aplite dykes that intruded chlorite–plagioclase schist containing on average 960 ppm Cr (Groat *et al.* 2002). Emeralds occur most commonly at the margins of the quartz veins, but are also found within the veins themselves and in alteration zones surrounding them. The granite is inferred as the source of Be for several reasons, including its close proximity to the deposit, the consistent correlation of Be with Sn, W and Bi in whole-rock and soil geochemical data, and the boron isotopic composition of the

tourmaline that is consistent with a granitic source of B (Galbraith *et al.* 2009). The Cr chromophore in the emerald is most likely derived from the schist (Groat *et al.* 2002).

Emerald mineralisation occurred synchronous with regional deformation and metamorphism related to intrusion of the 112 million-year-old (Ma) granite pluton (Neufeld *et al.* 2004). In particular, mineralisation was syn- to late-tectonic, coinciding with the waning stages of granite emplacement, and took place at temperatures of 365–498°C (Marshall *et al.* 2003). There appears to be a genetic link between (1) the granite intrusion, aplite and pegmatite bodies, and (2) the beryl-bearing quartz veins, which is supported by the presence of beryl in at least two of the aplite dikes (Neufeld *et al.* 2003, 2004; Neufeld 2004). Chromium entered the fluid system and interacted with the Be-bearing fluids by either (1) mixing with hydrothermal fluids that had interacted with the host schist and extracted Cr, or (2) via element exchange during metasomatic alteration (in which the composition of the rock changes as the result of the introduction or removal of chemical constituents adjacent to the vein by the mineralising fluids). The geology suggests that, in the recent classification scheme of Giuliani *et al.* (2019), Tsa da Glisza is a type I (tectonic-magmatic related), subtype A (hosted in mafic-ultramafic rocks) deposit.

True North Gems Inc. (Vancouver, British Columbia, Canada) built an all-season mining camp near the deposit (Figure 3) and spent the better part of a decade and several million dollars evaluating the deposit using geochemical prospecting, geological mapping, trenching, core drilling and underground work via an adit (see Rohtert & Montgomery 2002; Davison 2005,

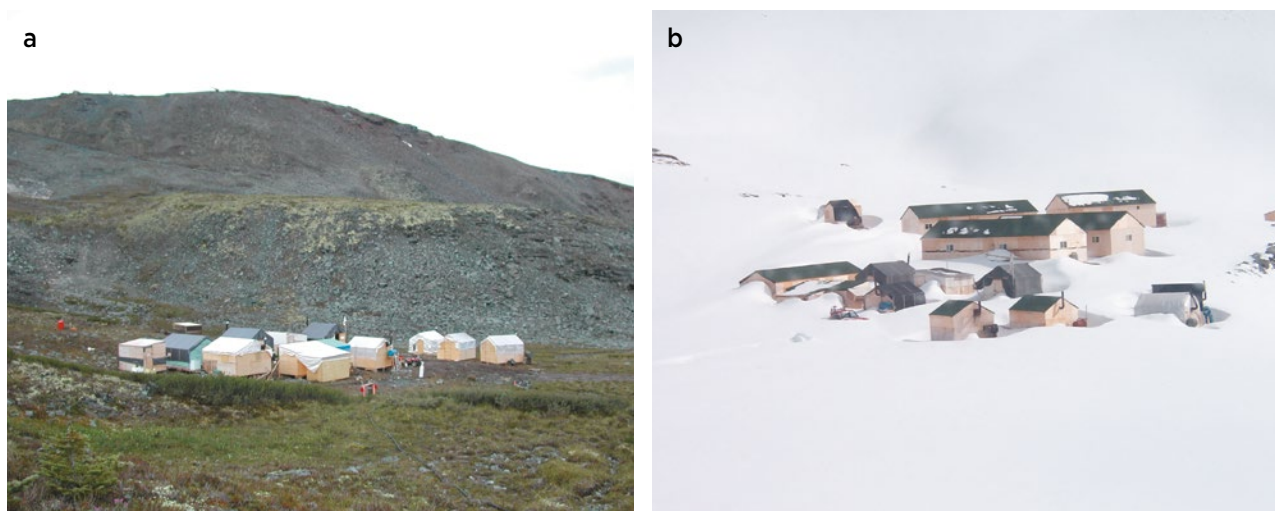


Figure 3: The mining camp at the Tsa da Glisza emerald deposit is shown here in (a) summer 2002 and (b) winter 2004. Photos by (a) L. A. Groat and (b) courtesy of True North Gems Inc.

2006; Figure 4). The results showed that although there is much emerald material showing good colour, the majority of the crystals have been affected by post-crystallisation deformation and therefore could only yield rather small cut stones (Figure 5a). Although some gems up to approximately 2.5 ct were cut, they were quite rare. After limited sales of loose stones and experiments with setting the emeralds in melee jewellery (Figure 5b), the company concluded that mining would not be economic, and the deposit was abandoned after environmental rehabilitation in 2013.

Lened, Northwest Territories

In 1997, prospector Ron Berdahl discovered emeralds at Lened in western Northwest Territories (Figure 6), approximately 160 km north-east of the Tsa da Glisza deposit. The emeralds are hosted by quartz veins that cut skarn and older strata proximal to the ~100 Ma Lened pluton. Approximately half of the 26 outcropping quartz veins contain opaque-to-translucent beryl crystals, which range from colourless to yellowish green to bluish green. Almost all of the crystals are euhedral, but less than 5% of the beryl is transparent and bluish green (and therefore can be considered pale emerald; Figure 7). The crystals are typically <0.5 cm wide and may attain a length of up to 5 cm; only a few stones have been cut from this material.

Lake *et al.* (2017) used field relationships, geochronology, whole-rock geochemistry, stable isotopes and

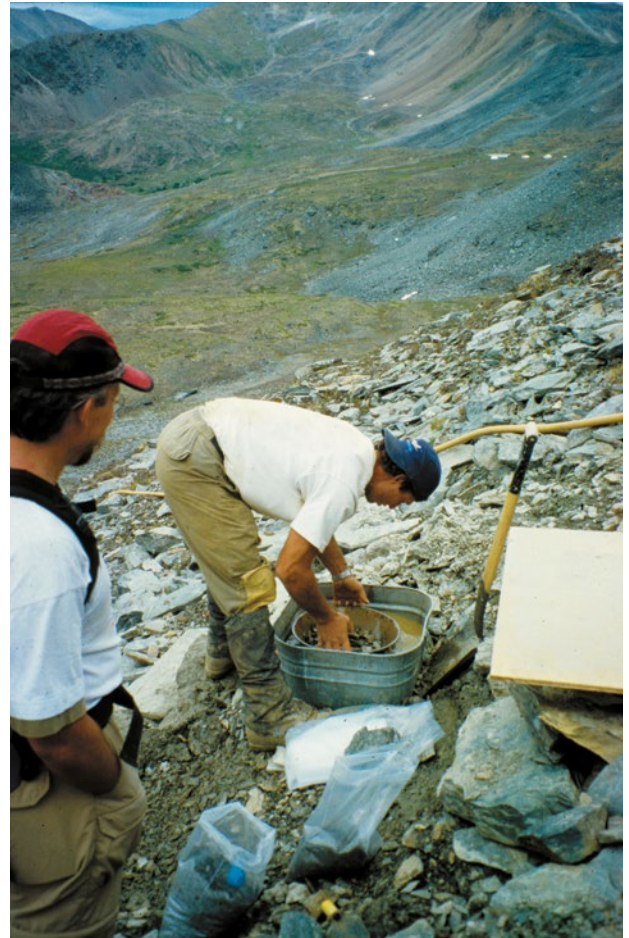


Figure 4: William Wengzynowski washes material sampled from Tsa da Glisza in 1999, a year after his discovery of emeralds there. Photo by L. A. Groat.



Figure 5: Faceted emeralds from Tsa da Glisza show attractive colour but are typically small. (a) These three stones were assessed at USD1,500 per carat but weigh only ~0.1 ct each (up to ~3 mm in longest dimension). Stones courtesy of Bradley S. Wilson; photo composite by Tom Fa/Panotora. (b) Melee-size emeralds are featured in these pendants set in gold (left) and silver (right). Photo courtesy of True North Gems Inc.



Figure 6: At the Lened occurrence in Northwest Territories, emeralds occur in quartz veins cutting a skarn (white area in top-centre, in front of black mudstones). An old cabin is seen in the foreground and a tent used during prospecting in 2002 is shown in the background. Photo by L. A. Groat.



Figure 7: The Lened deposit is the source of these pale emerald specimens, which include a euhedral crystal on quartz and a 0.17 ct faceted stone (inset). Photos by Donald J. Lake and Tom Fa/Panotora (inset; specimen courtesy of Bradley S. Wilson).

mineral chemistry to assess the sources of the emerald-forming fluids and chromophores. The results showed that the emerald occurrence is related to the proximal pluton and can be classified as a type I (tectonic-magmatic related), subtype B (hosted in metasedimentary rocks) deposit (Giuliani *et al.* 2019). Beryllium and other incompatible elements (i.e. W, Sn, Li, B and F) in the emerald, vein minerals and surrounding skarn were introduced during the terminal stages of crystallisation of the Lened pluton. Decarbonation during pyroxene-garnet

skarn formation in the host carbonate rocks probably caused local overpressuring and fracturing that allowed ingress of magmatic-derived fluids and formation of quartz-calcite-beryl-scheelite-tourmaline-pyrite veins. The chromophoric elements (V>Cr) were mobilised by metasomatism of metasedimentary rocks that underlie the emerald occurrence (Lake *et al.* 2017).

Emerald Exploration 2003–2004

The Tsa da Glisza and Lened discoveries, as well as reports of numerous beryl occurrences in north-western Canada, suggested that emerald-focused exploration could result in more discoveries. In mid-2002 the author approached True North Gems Inc. with a proposal for an emerald exploration programme. Archer Cathro & Associates (1981) Ltd. was hired to develop targets using publicly available data—primarily regional geochemical surveys (mostly of silt samples) and assessment reports filed by companies—and their own extensive database of traverse reports, geochemical data and geological maps. The target development involved four steps, the first of which was to search the databases for occurrences of beryl, other Be-bearing minerals such as chrysoberyl and potential accessory minerals such as tourmaline. The second step was to consider geochemical reservoirs as suggested by Murphy *et al.* (2002), who plotted potential Be sources (plutonic rocks) and Cr and V reservoirs (ultramafic rocks, volcanic rocks and the Earn Group black shale) in Yukon, and suggested looking for emeralds where these elements come together. The third step was to consider the reservoirs in more detail as suggested by Lewis *et al.* (2003), who noted that all known beryl occurrences in Yukon are intrusion-related, but for an intrusion to become enriched enough to reach beryllium saturation to form beryl it must be ‘ultra-fractionated’. Numerous lithological and geochemical features (e.g. accessory mineralogy, Rb/Sr ratio from whole-rock analyses, K/Rb ratio in K-feldspar and others) can help pinpoint fractionated pegmatites with elevated gem potential. The fourth step was to search the regional geochemical survey data for enrichment in the chromophores Cr and V. This task was constrained by the fact that in 2002–2003 these data were only available for portions of Yukon, Northwest Territories and British Columbia.

The result of this four-step programme was a list of approximately 100 targets for type I (tectonic-magmatic related) emerald deposits in Yukon, Northwest Territories and the northern part of British Columbia. During the summer of 2003 a team primarily composed of the author, William Wengzynowski, and students

Heather Neufeld and Dawn Kellet spent approximately four months evaluating 20 of the targets. No emerald was found, but the team did make other discoveries: the True Blue aquamarine prospect (Turner 2006; Turner *et al.* 2007), which produced unusually dark blue crystals that subsequently were used to confirm the cause of the blue colour in aquamarine (Groat *et al.* 2010, Lin *et al.* 2013); the Batea Pb-Zn occurrence (Davison & Skinner 2008); and the Amigo Ni-As-Cu-Pb prospect (Davison 2007). This shows that coloured stone exploration by experienced prospectors can result in the discovery of other commodities. More work was conducted in 2004, but by then interest in emerald exploration was waning because the price of gold, in particular, began to rise.

Mountain River, Northwest Territories

In 2007, a team of geologists from the Northwest Territories Geological Survey discovered green beryl (Figure 8) near Mountain River in western Northwest Territories (Mercier 2008). Although the green colour is due to the chromophores Cr and V (Mercier 2008), the stones are not transparent enough for gem use, and are therefore referred to here as green beryl rather than emerald. The beryl is hosted by extensional quartz-carbonate veins cutting Neoproterozoic sandstone and siltstone within the hanging wall of a thrust fault that emplaced these strata above Paleozoic rocks (Hewton *et al.* 2013). The occurrence was studied in detail by Hewton *et al.* (2013), who showed that the isotopic composition of water extracted from the beryl is typical of evolved sedimentary sulphate brines. The inferred temperature of vein formation is 380–415°C. Calculations based on mineral



Figure 8: These samples of green beryl are from the Mountain River occurrence. The largest piece is approximately 2 × 1 cm. Specimens courtesy of Donald J. Lake; photo by Tom Fa/Panotora.

pair isotope equilibration and the typical geothermal gradient indicate vein formation at depths of 6–11 km. A Re-Os age of 345 ± 20 Ma from pyrite indicates that mineralisation was contemporaneous with estimated ages of some northern Cordilleran Zn-Pb occurrences.

Inorganic thermochemical sulphate reduction via the circulation of warm basinal brines through siliciclastic, carbonate and evaporitic rocks is thought to have liberated the elements necessary to form beryl (Hewton *et al.* 2013). The Mountain River green beryl occurrence thus represents a variant of the type II (tectonic-metamorphic related), subtype B (hosted in sedimentary rocks: black shales) emerald deposit in the classification scheme of Giuliani *et al.* (2019).

Such emerald deposits are unusual because there is no evidence for associated magmatic activity. The best (and until the Mountain River discovery, the only) examples of this type are in Colombia, where more than 200 emerald mines and occurrences produce the world's highest-quality emeralds. Colombian emeralds are hosted by extensional carbonate-silicate-pyrite veins, pockets and breccias in a black shale-limestone succession, and they are thought to have formed as a result of hydrothermal growth associated with tectonic activity (Ottaway *et al.* 1994; Giuliani *et al.* 1995; Cheillett & Giuliani 1996; Branquet *et al.* 1999a, b). The parent fluids are inferred to have formed at depth from meteoric and formational water interacting with evaporitic sequences (Escobar & Mariano 1981; Giuliani *et al.* 2000). The occurrence of a variant of this type of deposit at Mountain River suggests the potential for Colombian-type emerald mineralisation in north-western Canada.

Colombian Emerald Exploration Criteria Applied to North-Western Canada

Both the Lened and Mountain River occurrences are hosted in rocks of the Selwyn Basin which were deposited on the passive margin of Laurentia (ancestral North America). However, unlike in the Cordillera Oriental of Colombia, where there are no significant occurrences of igneous rocks, the Paleozoic black shales and mudstones of the Selwyn Basin are commonly intruded by Cretaceous felsic stocks of the Selwyn and Tombstone plutonic suites. (Nevertheless, the closest intrusion to the Mountain River occurrence is at least 150 km away.)

Lake (2017) applied criteria for emerald exploration in Colombia to Canada's Yukon and Northwest Territories. These criteria include: (1) the Na content of stream sediments (Beus 1979); (2) the Li, Na and Pb content of soil samples from altered tectonic blocks

(Ringsrud 1986); (3) the presence of gypsum and anhydrite deposits, which provide evidence for evaporite sequences (Cheilletz & Giuliani 1996); (4) favourable structures such as thrust faults (Branquet *et al.* 1999a, b); and (5) the presence of cogenetic minerals such as fluorite, fluorapatite, parisite-(Ce) and florencite-(Ce) in heavy mineral concentrates (HMCs; Lake *et al.* 2017).

Lake (2017) applied the first criterion to stream-sediment geochemical data made publicly available by the Yukon and Northwest Territories geological surveys (the latter without Be). The criterion had to be adjusted for a number of factors, including the absence of Be data in Northwest Territories and elevated Na due to plutonic alkali feldspar weathering into black shale drainages. Lake (2017) also noted that Colombian-type emerald deposits have relatively small footprints, and regional-scale geochemical surveys with data points located 5–10 km apart might not be sufficient to show an emerald occurrence. In fact, the Mountain River deposit was not predicted by this analysis. Therefore, Lake (2017) was unsure of the usefulness of this technique with the existing data density.

Despite these constraints, Lake (2017) used multiple criteria to identify several regions of interest (Figure 9). Similar to emerald localities in Colombia, the anomalous areas within black shale units are also in the vicinity of important thrust zones (the Dawson, Tombstone and

Robert Service thrusts, and the Mackenzie fold-and-thrust belt). Lake (2017) also noted that florencite-(Ce) occurs in the Rusty Shale Formation in the Mackenzie Mountains (Pouliot & Hofmann 1981) and has been recovered in HMCs from the Selwyn Range west of Lened (Falck *et al.* 2015). Lake (2017) mentioned several targets in need of follow up, but evaluating them has been constrained by available time and funds, and it is obvious that there is ample scope for additional fieldwork.

SAPPHIRE AND SPINEL ON BAFFIN ISLAND, NUNAVUT

Sapphire

In the summer of 2002, brothers Seemeega and Nowdluk Aqqik were hunting south of Kimmirut on Baffin Island when they saw a barrel-shaped blue crystal protruding from an outcrop. The brothers took the crystal back to Kimmirut, where district geologist Paul ‘Jethro’ Gertzbein identified it as a sapphire. True North Gems Inc. acquired the property soon after and discovered more occurrences of sapphire (colourless and yellow, as well as blue; see Figures 1 and 10) and Co-bearing spinel (see below). The company’s activities were described by Rohtert & Pemberton (2005) and Rohtert (2006).

The sapphires occur in scapolite-rich calc-silicate rock hosted in marble of the Lake Harbour Group

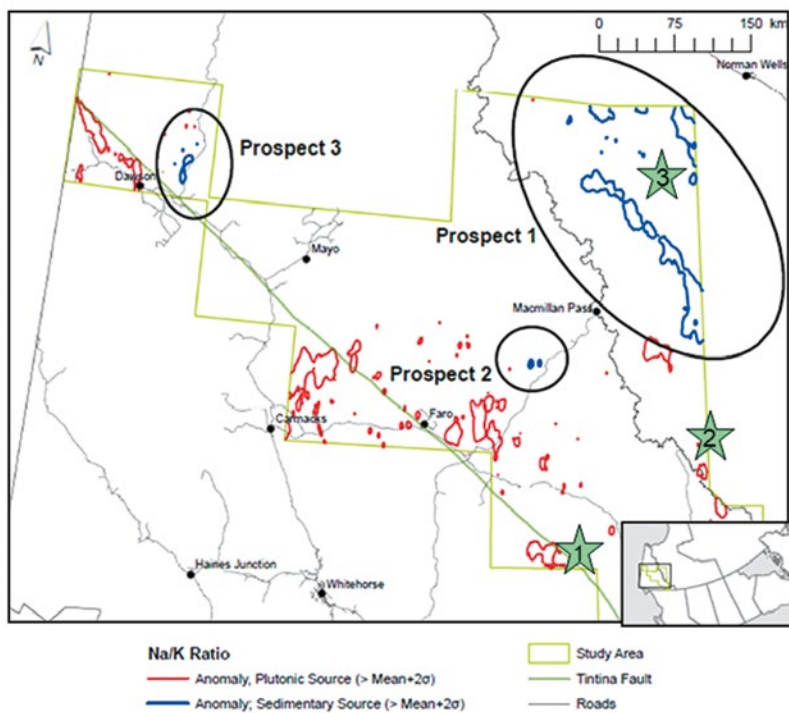


Figure 9: Areas defined by Lake (2017) as being prospective for type I (tectonic-magmatic related, shown in red) and type II (tectonic-metamorphic related, shown in blue) emerald deposits were determined using regional geochemical survey data and, in the case of the type II deposits, by applying exploration criteria developed in Colombia. Green stars indicate known occurrences (1 = Tsa da Glisza, 2 = Lened and 3 = Mountain River), and black ovals outline areas for additional exploration for type II emerald deposits, which will be a focus of future work by the author’s team.



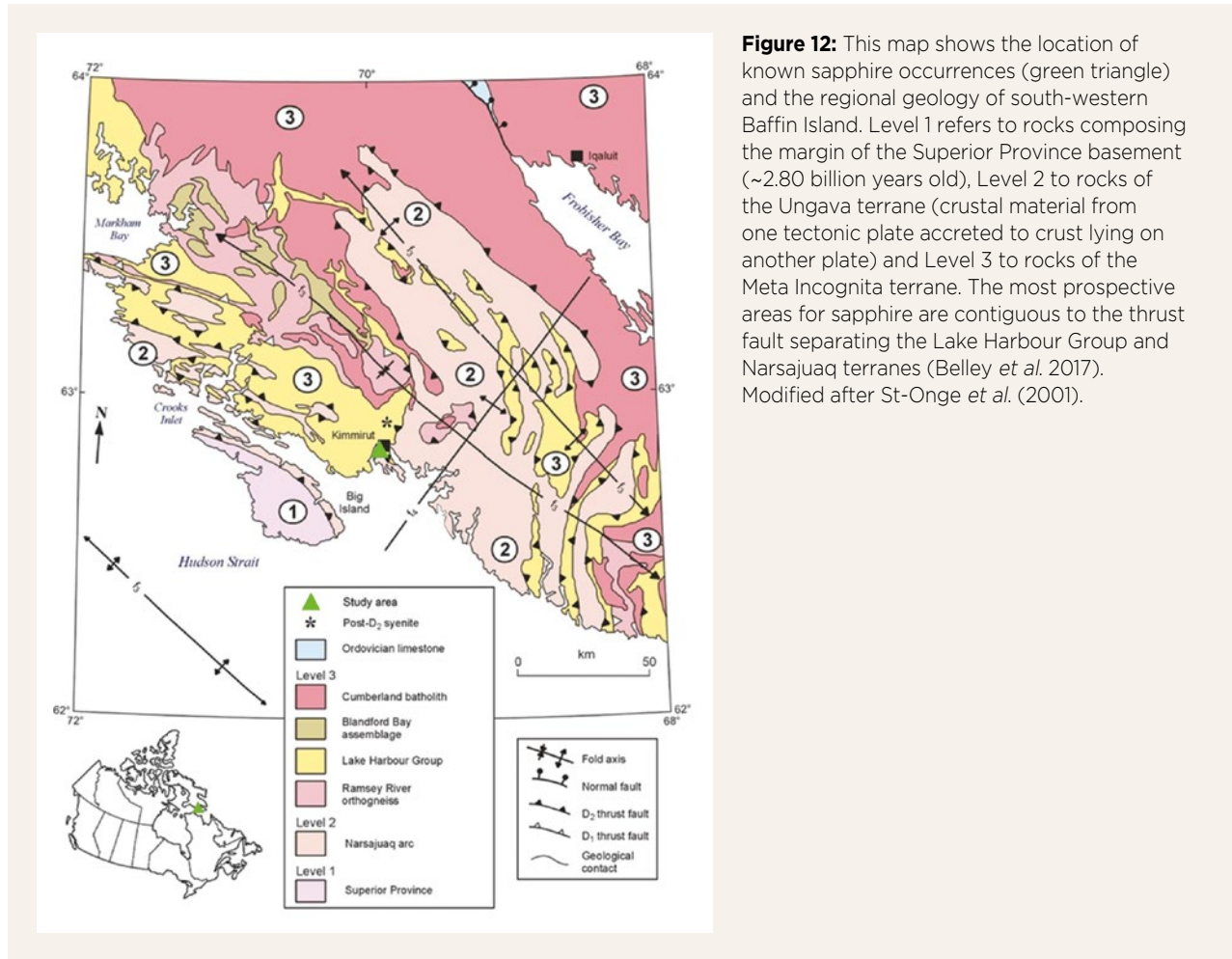
Figure 10: These sapphires are from the Kimmirut occurrences on Baffin Island. Clockwise from upper left: 1.47 ct yellow from Beluga South, 2.50 ct colourless from Aqvik, 0.58 ct blue from Beluga and 1.17 ct deep blue from Beluga. All of the gems are unheated. Stones courtesy of Bradley S. Wilson; photos by Tom Fa/Panotora.

(Figures 11 and 12). Belley *et al.* (2017) compared the Beluga occurrence of blue-to-colourless sapphires to a similar calc-silicate pod generally lacking corundum but containing nepheline (Bowhead occurrence) located 170 m south-southwest. They concluded that corundum formation depended on three equally important sequential metamorphic reactions: (1) formation of nepheline, diopside and K-feldspar (inferred) at granulite facies peak-metamorphic conditions; (2) partial retrograde replacement of the peak assemblage by phlogopite, oligoclase, calcite and scapolite (Me_{50} – Me_{67}) as a result of CO_2 - H_2O -Cl-F-bearing fluid influx at $1,782.5 \pm 3.7$ Ma ($720^\circ C$, 6.2 kbar); and (3) retrograde breakdown of

scapolite + nepheline (with CO_2 - and H_2O -bearing fluid) to form albite, muscovite, corundum and calcite. Based on thermodynamic models, the corundum-forming reaction occurred only in a $<100^\circ C$ temperature window, with the upper limit determined by scapolite-nepheline stability and the lower limit determined by the formation of Al-silicate rather than corundum. The protolith was inferred to be dolomitic argillaceous marl (calcareous sediments) with no evidence to suggest the initial presence of evaporites (Belley *et al.* 2017). Belley *et al.* (2017) concluded that in the Baffin Island area, the most prospective areas are contiguous to the thrust fault separating the Lake Harbour Group and Narsajuaq

Figure 11: The Beluga sapphire occurrence is shown here after extraction of a bulk sample. Note the characteristic mottled appearance of the calc-silicate rock within the marble, and also the diamond-bladed chainsaw (at the end of the hose) used for removing pieces of the sapphire-bearing rock. Photo by Bradley S. Wilson.





terrane (Figure 12), where the metamorphic conditions are most favourable for the formation of corundum.

From 2007 to 2010, employees of True North Gems Inc. used headlamps equipped with multiple UV wavelengths to explore for associated scapolite (which is strongly fluorescent) and discovered approximately 15 new sapphire occurrences. Scapolite could be seen fluorescing up to 5 m away, but exploration was constrained by the limited hours of darkness in the Arctic summer (Lepage & Rohtert 2006). Turner *et al.* (2017) studied rock samples from the Baffin Island sapphire occurrence in the laboratory using imaging spectroscopy in the short-wave infrared region (~975–2500 nm). The unique spectral responses they encountered suggest that high spatial-resolution hyperspectral imaging could be used to map and explore for gem corundum targets during regional surveys.

Spinel

Gem spinel is widespread in the Lake Harbour Group on Baffin Island. Wilson (2014) described the following occurrences: (1) violet crystals up to 3 cm in marble near the Soper River lapis lazuli occurrence; (2) blue

and violet crystals up to 3 cm at Waddell Bay; (3) violet crystals up to 4.5 cm in a mica exploration trench at Soper Lake; (4) violet crystals in ‘chondrodite’ at Soper Falls; (5) violet crystals up to 5 cm at Glencoe Island (see also Grice *et al.* 1982); (6) cobalt-blue, mostly opaque pieces up to 1 cm discovered by employees of True North Gems Inc. at the Qila occurrence near Kimmirut (Figure 13); and (7) cobalt-blue, occasionally transparent and heavily fractured crystals up to 2.7 cm, also discovered by employees of True North Gems Inc., at the Trailside occurrence near Kimmirut. Small faceted gemstones (almost all under 0.5 ct) and a 2.14 ct cabochon have been produced from these localities (Wilson 2014).

Belley & Groat (2019) studied spinel from 14 localities in the Lake Harbour Group. Most was blue to violet and not of gem quality, with the exception of the vivid blue, Co-bearing (0.03–0.07 wt. % CoO) stones from the Qila and Trailside localities. The spinel mostly occurs in metasedimentary (*sensu stricto*) deposits, with the exception of two metasomatic occurrences at Markham Bay. All of the spinels occur in marble and calc-silicate/silicate-rich metacarbonate rocks. Minerals occurring

in a stable assemblage with spinel include calcite, dolomite, phlogopite, pargasite, diopside, humite, forsterite, scapolite, anorthite, graphite and pyrrhotite. The spinel formed under peak granulite-facies metamorphic conditions, and at two localities it is partly replaced by retrograde corundum.

Belley & Groat (2019) interpreted the spinel-bearing metacarbonates to have the following protoliths: (1) impure dolomite-bearing and dolomitic limestone, (2) dolomitic marl and (3) evaporitic magnesian marl. They determined that spinel genesis in the metacarbonates is favoured by: (1) the low abundance of Si relative to Al, which is the primary control on whether spinel forms in most calc-silicate rocks; (2) low K activity limiting the formation of phlogopite and thus leaving Al available for spinel formation (this factor is predominant in marbles, but also occurs in calc-silicates); and (3) insufficient quantities of Mg or dolomite reactant in diopsidite, limiting Al incorporation into phlogopite to form spinel.

Belley & Groat (2019) noted that the spatial distribution of Co enrichment at the cobalt-blue spinel occurrences is indicative of highly localised enrichment, with possibly only small-scale (≤ 1 m) diffusion occurring during metamorphism. Cobalt and Ni are expected to have been enriched in the original sediment or during diagenesis (the conversion of sediment to sedimentary rock) or low-grade metamorphism. Concentrations of Co (especially) and Ni are anomalously high (up to 29 ppm, conservatively twice the expected Co concentration in a comparable metasediment), while concentrations of Fe, Mn, V, Cr and Cu are much lower than expected; this is a chemical signature that possibly, with the exception of low Fe and Mn, could be caused by diagenetic processes prior to metamorphism.

Ferrous iron was found to be the most common

chromophore in Lake Harbour Group spinel (with the exception of Co-bearing spinel; Belley & Groat 2019). Too much Fe in spinel leads to overly dark colours. Pyrrhotite strongly partitions Fe relative to spinel, and therefore abundant sulphide is expected to improve the gem quality of spinel by decreasing the amount of Fe available during its crystallisation (Belley & Groat 2019).

Belley & Groat (2019) suggested that marbles containing abundant layers of metamorphosed dolomitic marl (magnesian calc-silicate) offer the best potential for gem spinel discoveries on southern Baffin Island. Small, sometimes localised variations in whole-rock Al/Si and K/Al ratios can correspond to the occurrence of spinel.

RUBY AND PINK SAPPHIRE IN BRITISH COLUMBIA

Bradley S. Wilson discovered a calcite marble-hosted gem corundum locality north-west of Revelstoke in British Columbia in 2002 (Figure 14). Several sapphires and rubies from this locality have been faceted, although the largest is under 0.5 ct.

The geology of the property is described by Dzikowski *et al.* (2014). The corundum occurs in thin, folded and stretched layers with green muscovite + Ba-bearing K-feldspar + anorthite \pm phlogopite \pm scapolite. Predominantly pink (locally red or purple) opaque-to-transparent corundum crystals contain elevated Cr_2O_3 (up to 0.21 wt. %), variable amounts of TiO_2 and low Fe_2O_3 (generally < 0.07 wt. %). The associated micas have elevated Cr, V, Ti and Ba contents. Petrography of the silicate layers showed that corundum formed from muscovite at the peak of metamorphism ($\sim 650\text{--}700^\circ\text{C}$ and 8.5–9 kbar). The corundum was preserved because, occurring in an almost pure calcite marble, it did not react with dolomite to



Figure 13: (a) This outcrop at the Qila locality on Baffin Island contains Co-bearing spinel with white carbonate in calc-silicate rock. Photo by L. A. Groat. (b) These Co-bearing spinel gemstones were faceted from Qila material; the largest weighs 0.16 ct. Stones courtesy of Bradley S. Wilson; photo by Tom Fa/Panotora.

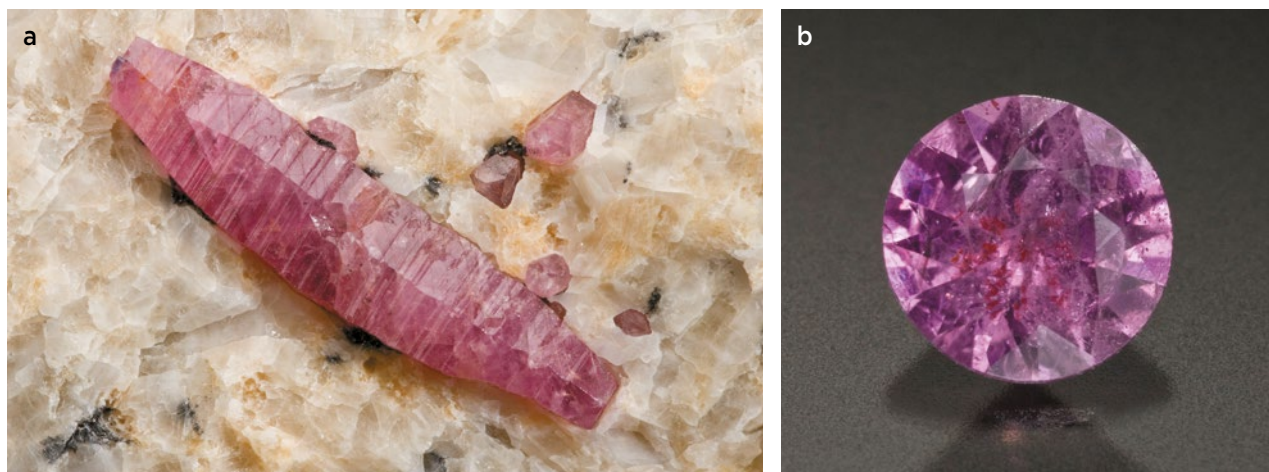


Figure 14: (a) The Revelstoke occurrence in British Columbia is the source of this pink sapphire (2.1 cm long) in marble. (b) The 0.20 ct pink sapphire shown here was faceted from Revelstoke material. Specimens courtesy of Bradley S. Wilson; photos by Michael J. Bainbridge.

form spinel + calcite during decompression. Gem-quality corundum crystals formed especially on the borders of the mica-feldspar layers in an assemblage with calcite.

Whole-rock geochemical data show that the corundum-bearing silicate (mica-feldspar) layers formed by mechanical mixing of carbonate with the host gneiss protolith. High element mobility is supported by the homogenisation of oxygen- and carbon-isotope values in carbonates and silicates within the marble and silicate layers. The silicate layers and the gneiss contain elevated contents of Cr and V due to a volcanoclastic component of their protolith (Dzikowski *et al.* 2014).

There is potential for placer gem corundum in this area, but it has not yet been evaluated. This discovery and reports of sapphire in HMCs from British Columbia, Yukon and Northwest Territories (Falck *et al.* 2015) suggest the potential for additional gem corundum occurrences as both primary and secondary (placer) deposits.

CONCLUSION AND FUTURE EXPLORATION

In addition to the emerald, sapphire and spinel occurrences mentioned in this article, several other gem localities are known in Canada, including amethyst, aquamarine, garnet, iolite, peridot, scapolite, topaz, tourmaline and zircon (see, e.g., Wilson 2014 and Figure 15), and large areas remain to be explored. How do we increase the odds of discovering new gem deposits in large, thinly populated countries such as Canada? A first step is to use geological and geochemical data to define prospective areas. These areas can then be evaluated by experienced prospectors, such as those individuals celebrated as ‘Prospector of the Year’ by the

Prospectors & Developers Association of Canada and the Yukon Prospectors Association. Prospecting is a skill that requires concentration, and for that reason experienced practitioners often work alone and do short traverses (e.g. prospectors working in Yukon will often cover only 7 km per day). They also know that it is important to look where others haven’t, for example, in talus rather than on ridge tops (see Bill Wegzynowski’s discovery of Tsa da Glisza above), and to look for unusual features such as rusty areas around quartz veins (cf. Tsa da Glisza).

A significant number of exploration companies in Canada have been using drones to map claims, among other applications. The author’s students Philip Belley and Donald Lake have employed a drone to explore for peridot in British Columbia. The peridot crystals occur in mantle xenoliths entrained in basaltic lava flows, and the drone was used to rule out unproductive sites by air, accomplishing an estimated two weeks of work in just three days. The drone weighs less than 1 kg and does not require any special licencing.

In the future, the author and his team intend to follow up on the ~80 emerald targets from the 2003–2004 exploration programme, and also to explore the areas highlighted for emerald by Lake (2017), as time, funding and logistics (in particular, the availability of helicopters proximal to the areas of interest) become available. The team also intends to look for sapphires by mapping and exploring the entire Lake Harbour Group on Baffin Island, especially the area contiguous to the thrust fault separating the Lake Harbour Group and Narsajuaq terranes. Given the lack of roads and high cost of helicopters, access to this area might be best accomplished from the sea; the team envisages using a converted fishing boat with drones (perhaps carrying imaging sensors) and all-terrain vehicles (perhaps towing

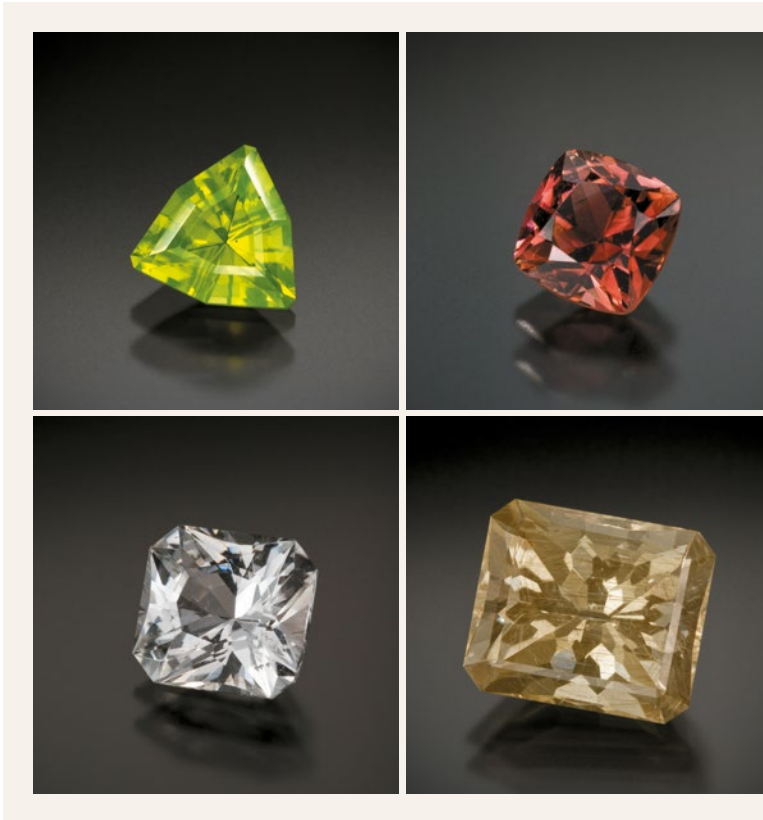


Figure 15: Detailed prospecting has uncovered a variety of gem occurrences in Canada, some of which are illustrated by the following stones (clockwise from upper left): a 0.94 ct peridot from Whitehorse, Yukon; a 0.68 ct elbaite from the Stargazer claim, O'Grady Lake, Northwest Territories; a 5.51 ct scapolite from Kimmirut, Nunavut; and an ~2.25 ct topaz from Mount Foster, British Columbia. Stones courtesy of Bradley S. Wilson; photos by Michael J. Bainbridge.

trailers with imaging sensors and geophysical equipment). It has been suggested that customised filtered glasses would allow us to see scapolite UV fluorescence in daylight (S. Gumpesberger, pers. comm. 2018). Although the team's focus will be on gem materials, it is likely that such an exploration programme would discover occurrences of other commodities, as happened with the emerald exploration programme in 2003–2004.

Other areas that face similar exploration challenges as Canada include Russia and Alaska (USA). Developing successful coloured-stone exploration programmes in

these areas will likely require additional scientific study to identify prospective terranes and features, and also the training of prospectors. Innovative means of transport such as boats or even airships might lower the cost of exploration in distant areas that lack infrastructure. Remote observations using drones will undoubtedly play an increasing role in coloured stone prospecting, as will various types of imaging. The gem discoveries that have been made in Canada (and Greenland) in the past few decades suggest that further prospecting will identify additional coloured-stone occurrences in such areas.

REFERENCES

- Belley, P.M. & Groat, L.A. 2019. Metacarbonate-hosted spinel on Baffin Island, Nunavut, Canada: Insights into the origin of gem spinel and cobalt-blue spinel. *Canadian Mineralogist*, **57**(2), 147–200, <http://doi.org/10.3749/canmin.1800060>.
- Belley, P.M., Dzikowski, T.J., Fagan, A., Cempirek, J., Groat, L.A., Mortensen, J.K., Fayek, M., Giuliani, G., Fallick, A.E. & Gertzbein, P. 2017. Origin of scapolite-hosted sapphire (corundum) near Kimmirut, Baffin Island, Nunavut, Canada. *Canadian Mineralogist*, **55**(4), 669–699, <http://doi.org/10.3749/canmin.1700018>.
- Beus, A.A. 1979. Sodium – A geochemical indicator of emerald mineralization in the Cordillera Oriental, Colombia. *Journal of Geochemical Exploration*, **11**(2), 195–208, [http://doi.org/10.1016/0375-6742\(79\)90023-2](http://doi.org/10.1016/0375-6742(79)90023-2).
- Branquet, Y., Cheilletz, A., Giuliani, G., Laumonier, B. & Blanco, O. 1999a. Fluidized hydrothermal breccia in dilatant faults during thrusting: The Colombian emerald deposits. *Geological Society, London, Special Publications*, **155**(1), 183–195, <http://doi.org/10.1144/gsl.Sp.1999.155.01.14>.
- Branquet, Y., Laumonier, B., Cheilletz, A. & Giuliani, G. 1999b. Emeralds in the Eastern Cordillera of Colombia: Two tectonic settings for one mineralization. *Geology*, **27**(7), 597–600, [http://doi.org/10.1130/0091-7613\(1999\)027<0597:Eiteco>2.3.Co;2](http://doi.org/10.1130/0091-7613(1999)027<0597:Eiteco>2.3.Co;2).
- Cheilletz, A. & Giuliani, G. 1996. The genesis of Colombian emeralds: A restatement. *Mineralium Deposita*, **31**(5), 359–364, <http://doi.org/10.1007/bf00189183>.

- Davison, J.G. 2005. *2004–2005 Report of Activities on the Goal and RS Claims, the Tsa da Glisza Project, Finlayson Lake Area, Yukon Territory, Canada*. True North Gems Inc., Vancouver, British Columbia, Canada, 202 pp., www.sedar.com/GetFile.do?lang=EN&docClass=13&issuerNo=00018399&issuerType=03&projectNo=00799558&docId=1511533.
- Davison, J.G. 2006. *43-101 Report of 2005–2006 Activities on the Goal and RS Claims, the Tsa da Glisza Project, Finlayson Lake Area, Yukon Territory, Canada*. True North Gems Inc., Vancouver, British Columbia, Canada, 103 pp., www.sedar.com/GetFile.do?lang=EN&docClass=13&issuerNo=00018399&issuerType=03&projectNo=00955599&docId=1748544.
- Davison, J.G. 2007. *Report of 2006–2007 Activities on the Amigo Claims, the Bandito Project, Toobally Lake Area, Yukon Territory, Canada*. True North Gems Inc., Vancouver, British Columbia, Canada, 149 pp., <http://yma.gov.yk.ca/094621/094621.pdf>.
- Davison, J.G. & Skinner, T. 2008. *2007 Report of Activities, Batea Claims, Yukon Territory, Canada*. True North Gems Inc., Vancouver, British Columbia, Canada, 45 pp., <http://yma.gov.yk.ca/094907.pdf>.
- Dzikowski, T.J., Cempírek, J., Groat, L.A., Dipple, G.M. & Giuliani, G. 2014. Origin of gem corundum in calcite marble: The Revelstoke occurrence in the Canadian Cordillera of British Columbia. *Lithos*, **198**, 281–297, <http://doi.org/10.1016/j.lithos.2014.03.030>.
- Escobar, R. & Mariano, A.N. 1981. On the origin of the Colombian emeralds. *Nuclide Spectra*, **14**, 1025–1081.
- Falck, H., Day, S., Pierce, K.L., Cains, S. & Watson, D. 2015. *Geochemical, Mineralogical and Indicator Mineral Data for Stream Silt Sediment, Heavy Mineral Concentrates and Waters, Flat River Area, Northwest Territories (Part of NTS 95E, 105H and 105I)*. Northwest Territories Geoscience Office, Yellowknife, Canada, 26 pp., www.nwtgeoscience.ca/sites/ntgs/files/final_flat_river_nwt_open_report_2015-002.pdf.
- Galbraith, C.G., Clarke, D.B., Trumbull, R.B. & Wiedenbeck, M. 2009. Assessment of tourmaline compositions as an indicator of emerald mineralization at the Tsa da Glisza prospect, Yukon Territory, Canada. *Economic Geology*, **104**(5), 713–731, <http://doi.org/10.2113/gsecongeo.104.5.713>.
- Giuliani, G., Cheillett, A., Arboleda, C., Carrillo, V., Rueda, F. & Baker, J.H. 1995. An evaporitic origin of the parent brines of Colombian emeralds: Fluid inclusion and sulphur isotope evidence. *European Journal of Mineralogy*, **7**(1), 151–166, <http://doi.org/10.1127/ejm/7/1/0151>.
- Giuliani, G., France-Lanord, C., Cheillett, A., Coget, P., Branquet, Y. & Laumonnier, B. 2000. Sulfate reduction by organic matter in Colombian emerald deposits: Chemical and stable isotope (C, O, H) evidence. *Economic Geology*, **95**(5), 1129–1153, <http://doi.org/10.2113/gsecongeo.95.5.1129>.
- Giuliani, G., Groat, L.A., Marshall, D., Fallick, A.E. & Branquet, Y. 2019. Emerald deposits: A review and enhanced classification. *Minerals*, **9**, article 105 (63 pp.), <http://doi.org/10.3390/min9020105>.
- Grice, J.D., Gault, R.A. & Waller, R. 1982. Spinel from Glencoe Island. *Rocks & Minerals*, **57**(4), 155–157, <http://doi.org/10.1080/00357529.1982.11764558>.
- Groat, L.A., Marshall, D.D., Giuliani, G., Murphy, D.C., Piercey, S.J., Jambor, J.L., Mortensen, J.K., Ercit, T.S., Gault, R.A., Matthey, D.P., Schwarz, D., Maluski, H., Wise, M.A., Wengzynowski, W. & Eaton, D.W. 2002. Mineralogical and geochemical study of the Regal Ridge emerald showing, southeastern Yukon. *Canadian Mineralogist*, **40**(5), 1313–1338, <http://doi.org/10.2113/gscanmin.40.5.1313>.
- Groat, L.A., Rossman, G.R., Dyar, M.D., Turner, D., Piccoli, P.M.B., Schultz, A.J. & Ottolini, L. 2010. Crystal chemistry of dark blue aquamarine from the True Blue showing, Yukon Territory, Canada. *Canadian Mineralogist*, **48**(3), 597–613, <http://doi.org/10.3749/canmin.48.3.597>.
- Hewton, M.L., Marshall, D.D., Ootes, L., Loughrey, L.E., Creaser, R.A. & Hanley, J. 2013. Colombian-style emerald mineralization in the northern Canadian Cordillera: Integration into a regional Paleozoic fluid flow regime. *Canadian Journal of Earth Sciences*, **50**(8), 857–871, <http://doi.org/10.1139/cjes-2012-0128>.
- Lake, D.J. 2017. *Are there Colombian-type emeralds in Canada's northern Cordillera? Insights from regional silt geochemistry, and the genesis of emerald at Lened, NWT*. M.Sc. thesis, University of British Columbia, Vancouver, Canada, 120 pp, <http://doi.org/10.14288/1.0360786>.
- Lake, D.J., Groat, L.A., Falck, H., Mulja, T., Cempírek, J., Kontak, D., Marshall, D., Giuliani, G. & Fayek, M. 2017. Genesis of emerald-bearing quartz veins associated with the Lened W-skarn mineralization, Northwest Territories, Canada. *Canadian Mineralogist*, **55**(4), 561–593, <http://doi.org/10.3749/canmin.1700025>.
- Lepage, L. & Rohtert, W. 2006. Ultraviolet mineral prospecting for sapphire on Baffin Island, Nunavut, Canada. *Gems & Gemology*, **42**(3), 155–156.
- Lewis, L., Hart, C. & Murphy, D. 2003. Roll out the beryl. Poster presentation, *Yukon Geoscience Forum 2003*, Whitehorse, Yukon, Canada, 15–18 November.
- Lin, J., Chen, N., Huang, D. & Pan, Y. 2013. Iron pairs in beryl: New insights from electron paramagnetic resonance, synchrotron X-ray absorption spectroscopy, and *ab initio* calculations. *American Mineralogist*, **98**(10), 1745–1753, <http://doi.org/10.2138/am.2013.4472>.
- Marshall, D., Groat, L., Giuliani, G., Murphy, D., Matthey, D., Ercit, T.S., Wise, M.A., Wengzynowski, W. & Eaton, W.D. 2003. Pressure, temperature and fluid conditions during emerald precipitation, southeastern Yukon, Canada: Fluid inclusion and stable isotope evidence. *Chemical Geology*, **194**(1–3), 187–199, [http://doi.org/10.1016/s0009-2541\(02\)00277-2](http://doi.org/10.1016/s0009-2541(02)00277-2).

- Mercier, M. 2008. *Geology and mineralogy of the Mountain River beryl (variety emerald) showing, Mackenzie Mountains, Northwest Territories, Canada*. B.Sc. thesis, University of Ottawa, Ontario, Canada, 68 pp.
- Murphy, C., Lipovsky, P.S., Stuart, A., Fonseca, A., Piercey, S.J. & Groat, L. 2002. What about those emeralds, eh? Geological setting of emeralds at Regal Ridge (SE Yukon) provides clues to their origin and to other places to explore. *GAC-MAC Annual Meeting 2002*, Saskatoon, Saskatchewan, Canada, 27–28 May, 154.
- Neufeld, H.L.D. 2004. *The Tsa da Glisza (Regal Ridge) emerald occurrence, southeastern Yukon Territory, Canada: Descriptive, genetic, and exploration models*. M.Sc. thesis, University of British Columbia, Vancouver, Canada, 183 pp., <http://doi.org/10.14288/1.0052753>.
- Neufeld, H.L.D., Groat, L.A. & Mortensen, J.K. 2003. Preliminary investigations of emerald mineralization in the Regal Ridge area, Finlayson Lake District, southeastern Yukon. In: Emond, D.S. & Lewis, L.L. (eds) *Yukon Exploration and Geology 2002*, Exploration and Geological Services Division, Yukon Region, Indian and Northern Affairs Canada, Whitehorse, Yukon, Canada, 281–284.
- Neufeld, H.L.D., Israel, S., Groat, L.A. & Mortensen, J.K. 2004. Geology and structural setting of the Regal Ridge emerald property, Finlayson Lake District, southeastern Yukon. In: Emond, D.S. & Lewis, L.L. (eds) *Yukon Exploration and Geology 2003*, Exploration and Geological Services Division, Yukon Region, Indian and Northern Affairs Canada, Whitehorse, Yukon, Canada, 281–288.
- Ottaway, T.L., Wicks, F.J., Bryndzia, L.T., Kyser, T.K. & Spooner, E.T.C. 1994. Formation of the Muzo hydrothermal emerald deposit in Colombia. *Nature*, **369**(6481), 552–554, <http://doi.org/10.1038/369552a0>.
- Pouliot, G. & Hofmann, H.J. 1981. Florencite; a first occurrence in Canada. *Canadian Mineralogist*, **19**(4), 535–540.
- Ringsrud, R. 1986. The Coscuez mine: A major source of Colombian emeralds. *Gems & Gemology*, **22**(2), 67–79, <http://doi.org/10.5741/gems.22.2.67>.
- Rohtert, W.R. 2006. *43-101 Report 2005 Report on Field Activities for the Beluga Sapphire Project, Nunavut, Canada*. True North Gems Inc., Vancouver, British Columbia, Canada, 40 pp., www.sedar.com/GetFile.do?lang=EN&docClass=13&issuerNo=00018399&issuerType=03&projectNo=00018399&docId=1725393.
- Rohtert, W.R. & Montgomery, J.H. 2002. *Qualifying Report: 2001 Report on Field Activities for the Regal Ridge Emerald Project, Yukon Territory, Canada*. True North Gems Inc., Vancouver, British Columbia, Canada, 71 pp., www.sedar.com/GetFile.do?lang=EN&docClass=13&issuerNo=00018399&issuerType=03&projectNo=00482433&docId=955813.
- Rohtert, W.R. & Pemberton, B.C. 2005. *43-101 Report: 2004 Report on Field Activities for the Beluga Sapphire Project, Nunavut Territory, Canada*. True North Gems Inc., Vancouver, British Columbia, Canada, 41 pp., www.sedar.com/GetFile.do?lang=EN&docClass=13&issuerNo=00018399&issuerType=03&projectNo=00786786&docId=1490769.
- St-Onge, M.R., Scott, D.J. & Wodicka, N. 2001. *Geology, Meta Incognita Peninsula, Baffin Island, Nunavut*. Geological Survey of Canada, “A” Series Map 2009A, Natural Resources Canada, Ottawa, Ontario, <http://doi.org/10.4095/212621>.
- Turner, D.J. 2006. *Mineralogical and geochemical study of the True Blue aquamarine showing, southern Yukon*. M.Sc. thesis, University of British Columbia, Vancouver, Canada, 147 pp., <http://doi.org/10.14288/1.0052583>.
- Turner, D., Groat, L.A., Hart, C.J.R., Mortensen, J.K., Linnen, R.L., Giuliani, G. & Wengzynowski, W. 2007. Mineralogical and geochemical study of the True Blue aquamarine showing, southern Yukon. *Canadian Mineralogist*, **45**(2), 203–227, <http://doi.org/10.2113/gscanmin.45.2.203>.
- Turner, D., Groat, L.A., Rivard, B. & Belley, P.M. 2017. Reflectance spectroscopy and hyperspectral imaging of sapphire-bearing marble from the Beluga occurrence, Baffin Island, Nunavut. *Canadian Mineralogist*, **55**(4), 787–797, <http://doi.org/10.3749/canmin.1700023>.
- Turner, D., Rohtert, W., Ritchie, M. & Wilson, B. 2019. Modern discovery of Aappaluttoq. *Gems&Jewellery*, **28**(2), 14–17.
- Wilson, B.S. 2014. Coloured gemstones from Canada. In: Groat, L.A. (ed) *Geology of Gem Deposits*, 2nd ed., Mineralogical Association of Canada Short Course Vol. 44, Québec, Canada, 375–405.

The Author

Dr Lee A. Groat

Department of Earth, Ocean and Atmospheric Sciences, University of British Columbia, Vancouver, Canada
Email: groat@mail.ubc.ca

Acknowledgements

Bradley S. Wilson (Alpine Gems, Kingston, Ontario, Canada) is thanked for loaning stones for photography. Michael J. Bainbridge (Bainbridge Photography, Minden, Ontario, Canada) is thanked for supplying specimen photos for this article. Sylvia Gumpesberger provided helpful information on filters for observing UV fluorescence in the field. Three anonymous reviewers are thanked for their constructive reviews.

An Update on Mineral Inclusions and Their Composition in Ruby from the Bo Rai Gem Field in Trat Province, Eastern Thailand

Supparat Promwongnan and Chakkaphan Sutthirat

ABSTRACT: The Bo Rai alluvial gem field in Trat Province, eastern Thailand, was a major mining site for Thai ruby during the early 1980s, and this material continues to circulate in the gem market worldwide. For this study, approximately 1,000 Bo Rai ruby samples were examined and pre-screened for mineral inclusions. The rough stones usually formed platy, waterworn, tabular crystals with etched or resorbed surfaces. UV-Vis-NIR spectroscopy indicated a relatively high Fe content, which was confirmed by trace-element analysis. Solid inclusions typically consisted of Al-rich pyroxene, plagioclase and pyrope with subordinate sillimanite and spinel (both of which are reported here for the first time), as well as sulphides and silicate melt inclusions. The inclusion assemblage of pyroxene, plagioclase, pyrope and spinel closely resembles the mineralogy of mafic granulite xenoliths in alkali basalt associated with the Bo Rai gem field, which supports ruby formation in mafic granulite prior to being transported to the earth's surface via basaltic eruptions.

The Journal of Gemmology, 36(7), 2019, pp. 634–645, <http://doi.org/10.15506/JoG.2019.36.7.634>

© 2019 Gem-A (The Gemmological Association of Great Britain)

For decades, Thai ruby has been well known for its attractive purplish red colour, which can be heat treated to deep red (Figure 1). The stones typically occur in alluvial deposits associated with Cenozoic intraplate basalts (Vichit 1992; Sutthirat *et al.* 1994). During the early 1980s (Keller 1982), the Bo Rai gem field—located in Trat Province, eastern Thailand, close to Cambodia—was the main source of Thai ruby, and associated minerals in the alluvium include garnet, magnetite, pyroxene and ilmenite (Vichit *et al.* 1978; Vichit 1992). Some other significant mining areas for Thai rubies include Na Wong and Nong Bon in Trat Province and Pong Nam Ron and Bo Welu in Chanthaburi Province. In addition, minor Thai ruby occurrences are known in Ubon Ratchathani and Si Sa Ket Provinces in the north-eastern part of the country (Vichit 1992;

Pattamalai 2015). Although there is currently very little production of Thai ruby, the material continues to circulate in the global gem market.

Several authors have previously described the properties of Thai ruby (e.g. Gübelin 1971; Intasopa *et al.* 1999; Saminpanya *et al.* 2003; Saminpanya & Sutherland 2011; Sangsawong *et al.* 2017). Moreover, various types of mineral inclusions in Thai corundum (both ruby and sapphire) have been investigated (Gübelin 1940). Optical microscopy, Raman spectroscopy and powder X-ray diffraction have been used to identify the mineral inclusions in Thai corundum (e.g. Gübelin & Koivula 1986; Koivula & Fryer 1987; Intasopa *et al.* 1999; Hughes 2017; Saeseaw *et al.* 2017; Sangsawong *et al.* 2017), whereas the chemical composition of these minerals has been investigated using electron probe

Figure 1: This collection shows the deep red appearance of high-quality Thai rubies (here, 0.87–2.86 ct). They have been heat treated to improve their colour. Stones courtesy of Thai Lapidary International Co. Ltd; photo by S. Promwongnan.



micro-analysis (EPMA; e.g. Gübelin 1971; Guo *et al.* 1994; Sutherland *et al.* 1998a; Sutthirat *et al.* 2001; Khamloet *et al.* 2014), proton microprobe analysis (Guo *et al.* 1994) and scanning electron microscopy with energy-dispersive X-ray spectroscopy (Saminpanya & Sutherland 2011).

Sutherland *et al.* (1998b) separated the mineral inclusions in basaltic-type gem corundum into two groups: metamorphic origin (e.g. Mg-rich spinel, sapphirine, 'fassaite' [pyroxene with a low Fe content] and garnet) and magmatic origin (e.g. plagioclase, zircon, Fe-Ti oxides, Nb-Ta oxides, U-Th oxides and rare-earth phosphates). Typical inclusions in Thai rubies have been reported by various researchers as pyrrhotite, apatite, garnet, diopside, sapphirine and plagioclase (Gübelin 1971; Intasopa *et al.* 1999; Sutthirat *et al.* 2001; Saminpanya & Sutherland 2011), and some of these authors

also suggested that Thai ruby possibly crystallised from high-grade metamorphosed mafic rocks. Recently, Sutthirat *et al.* (2018) documented ruby-bearing mafic granulite xenoliths from the Bo Rai deposit, which provide the most significant direct evidence for the primary metamorphic formation of Thai ruby.

In this study, approximately 1,000 unheated Bo Rai rubies were pre-screened to select samples for examination of mineral inclusions. (These included some purple sapphires, although the sample collection is here classified as 'ruby' since during heat treatment the purple stones are usually transformed into the colour range of ruby.) Our examination of the inclusions particularly focused on mineral chemistry, which is the primary aim of this project. In addition, the samples' gemmological properties, optical and spectroscopic characteristics and trace-element compositions were investigated.

MATERIALS AND METHODS

Using a gemmological microscope, we selected 88 samples (containing 141 mineral inclusions) for examination from the approximately 1,000 unheated rough Bo Rai rubies. The samples were carefully cut and polished with a Facetron faceting machine to expose their mineral inclusions at the surface for analysis. After polishing, they ranged from 0.006 to 0.17 g.

Standard gemmological properties (i.e. colour, diaphaneity, RIs and fluorescence reactions to long- and short-wave UV radiation) were recorded for all 88 samples. (Specific gravity was not measured due to their small size.) Internal and external features were observed with a gemmological microscope, and an attached Canon EOS 7D camera was used for photomicrography.

Mid-infrared spectra ($4000\text{--}400\text{ cm}^{-1}$) were obtained in transmittance mode for all 88 samples (resolution of 4.0 cm^{-1} and 128 scans) using a Thermo-Nicolet 6700 Fourier-transform infrared (FTIR) spectrometer. Ultraviolet-visible-near infrared (UV-Vis-NIR) absorption spectra were obtained for all samples using a PerkinElmer Lambda 950 spectrophotometer in the range 250–800 nm with a 3.0 nm sampling interval and 441 nm/minute scan speed. Good-quality trace-element analyses were obtained for 78 of the samples by energy-dispersive X-ray fluorescence (EDXRF) spectroscopy with an Eagle III system; semi-quantitative results for Al, Cr, Fe, Ti, V and Ga were subsequently normalised and reported as oxides. Preliminary identification of the mineral inclusions in all samples was performed with a Renishaw inVia Raman microspectroscopy system utilising 532 nm excitation from an Nd:YAG laser. The

magnification of the objective lens was $50\times$. All of the analyses mentioned above were done at the Gem Testing Laboratory of the Gem and Jewelry Institute of Thailand (Public Organization) in Bangkok.

Mineral inclusions in 41 of the rubies were selected for major- and minor-element analysis by EPMA. The samples were mounted in epoxy resin and polished prior to carbon coating and analysis with a JEOL JXA-8100 instrument based at the Geology Department, Faculty of Science, Chulalongkorn University, Bangkok. Operating conditions included an accelerating voltage of 15.0 kV and a sample current of $\sim 25.0\text{ nA}$, with a focused beam of $<1\text{ }\mu\text{m}$ in diameter. Measurement times for each element were set at 30 seconds for peak counts and 10 seconds for background counts. The analytical results were then subjected to automated ZAF correction and reported as weight percent oxides. The ferrous and ferric iron contents of some minerals (e.g. pyroxene, garnet and spinel) were calculated using the methodology of Droop (1987).

RESULTS

Gemmological Properties

The samples typically formed platy waterworn crystals that were semi-transparent to transparent. Their colouration (see, e.g., Figure 2) can be summarised as follows: moderate to slightly purplish red (pR, $\sim 2\%$ of the collection), purple-red to red-purple (PR-RP, $\sim 79\%$), reddish purple (rP, $\sim 17\%$) and purple (P, $\sim 2\%$). They had RIs of 1.760–1.771 and birefringence values of 0.008–0.010. They showed inert-to-moderate red fluorescence to long-wave UV radiation and were inert to short-wave UV.

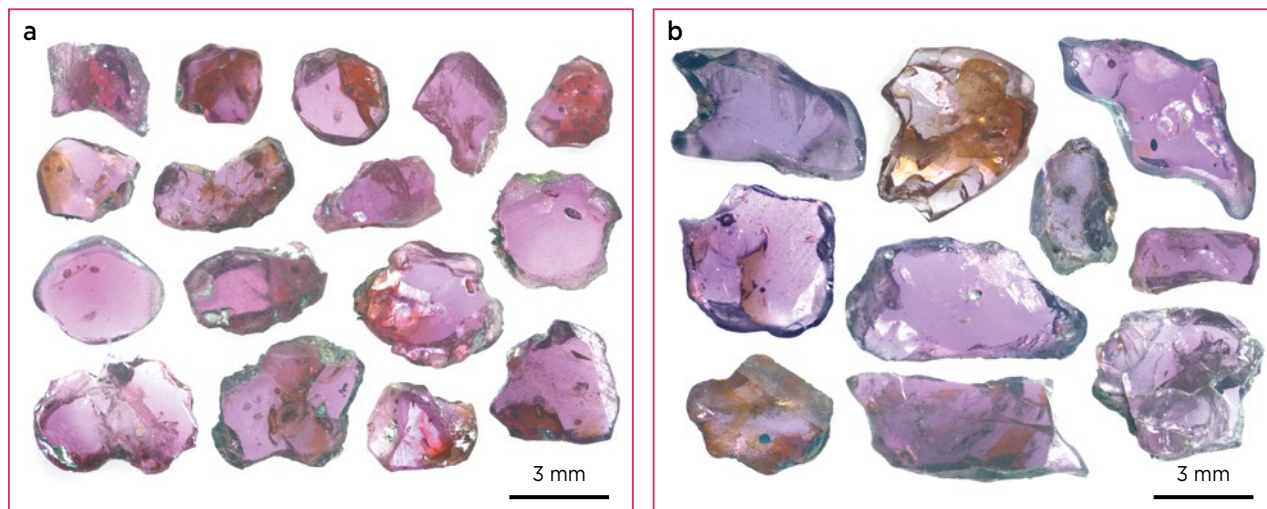


Figure 2: Representative rough pieces of Bo Rai gem corundum show a range of colour: (a) moderate to slightly purplish red to red-purple, and (b) reddish purple to purple. Most of the samples have been polished on both sides to expose mineral inclusions on their surfaces. Photos by S. Promwongnan.

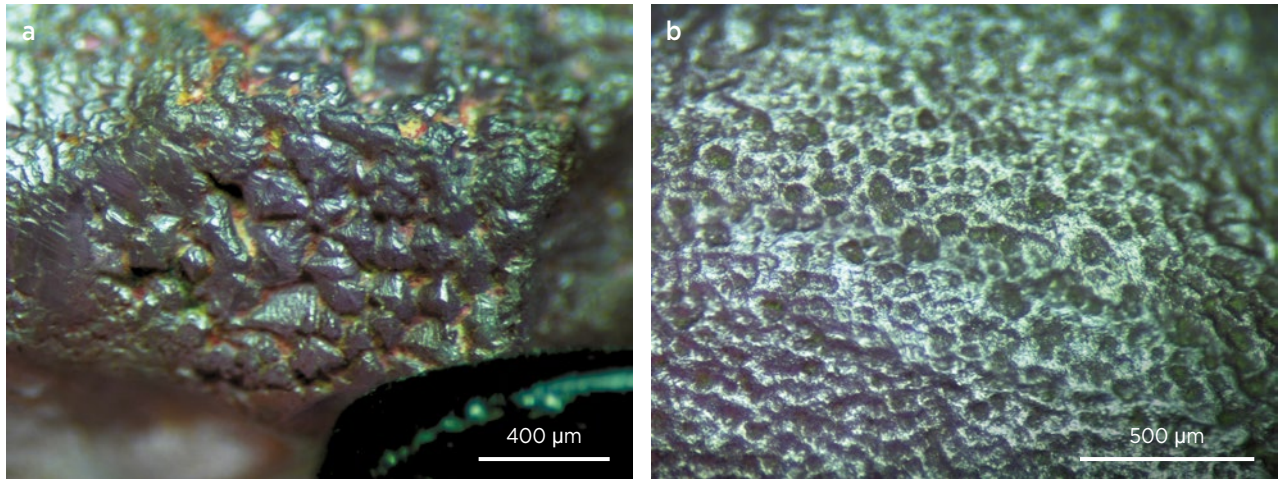


Figure 3: These photomicrographs show etched and dissolved features on the surfaces of two rough rubies from Bo Rai. Photomicrographs by S. Promwongnan in reflected light.

Before being polished into plates for inclusion examination, some of the samples presented etched or dissolved surfaces (Figure 3).

Spectroscopic Features

The FTIR spectra of the rubies showed similar patterns for all the samples, including bands at approximately 2363 and 2342 cm^{-1} due to CO_2 , and at 2924 and 2852 cm^{-1} due to C-H stretching (Figure 4; cf. Beran & Rossman 2006). Some samples (e.g. Figure 4, red spectrum) also presented a shoulder at about 3170 cm^{-1} and a series of sharp bands at 3697, 3669, 3652 and 3620 cm^{-1} that relate to the hydrous component of a

kaolinite-group mineral (cf. Beran & Rossman 2006; Schwarz *et al.* 2008).

UV-Vis-NIR spectra showed an absorption at ~ 330 nm related to high Fe content (Figure 5, blue spectrum), and in some samples this absorption was so strong that the spectra presented a cut-off in this region (Figure 5, red spectrum). Most of the pR and PR-RP samples showed distinct Cr-related absorption features at around 410, 560 and 694 nm (Figure 5, blue spectrum), consistent with their dominantly red colour. However, those samples falling in the rP to P colour range clearly showed intense Fe-related absorptions at 387 and 450 nm (Figure 5, red spectrum).

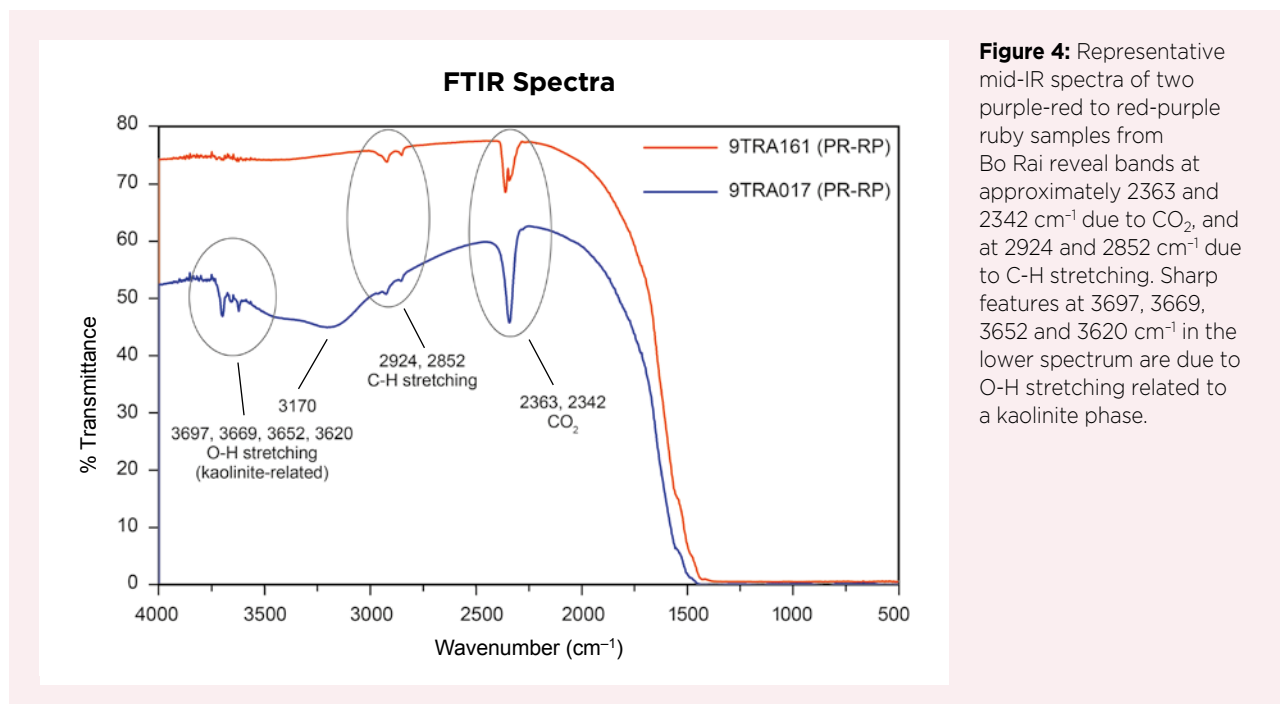


Figure 4: Representative mid-IR spectra of two purple-red to red-purple ruby samples from Bo Rai reveal bands at approximately 2363 and 2342 cm^{-1} due to CO_2 , and at 2924 and 2852 cm^{-1} due to C-H stretching. Sharp features at 3697, 3669, 3652 and 3620 cm^{-1} in the lower spectrum are due to O-H stretching related to a kaolinite phase.

EDXRF Analyses

Semi-quantitative chemical analyses of the Bo Rai samples varied within fairly narrow ranges (e.g. Table I). Overall, Fe and Ti concentrations ranged from ~0.35 to 1.26 wt. % Fe₂O₃ and 0.01 to 0.67 wt. % TiO₂, respectively. Chromium contents fell within the range of 0.06–0.92 wt. % Cr₂O₃. Overall, the rP to P samples contained less Cr than those falling into the pR to PR-RP colour range. About 20% of the samples yielded V contents below the detection limit, and the highest value was only ~0.04 wt. % V₂O₅. Gallium was below the detection limit in some samples, while the greatest amount measured was ~0.03 wt. % Ga₂O₃.

Internal Features

Apart from the mineral inclusions described below, a variety of internal features could be seen in our samples with the microscope. The most typical characteristics were minute crystals (too small to be reliably identified by Raman or microprobe analysis) surrounded by equatorial thin films (Figure 6a). Also present were parallel twin planes, needle-like inclusions (Figure 6b) and partially healed fractures (‘fingerprints’). In addition, some samples hosted inclusions containing multiple fluid/gas phases (Figure 7a) or two-phase assemblages consisting of a solidified silicate melt and a gas phase (possibly CO₂; Figure 7b). The latter

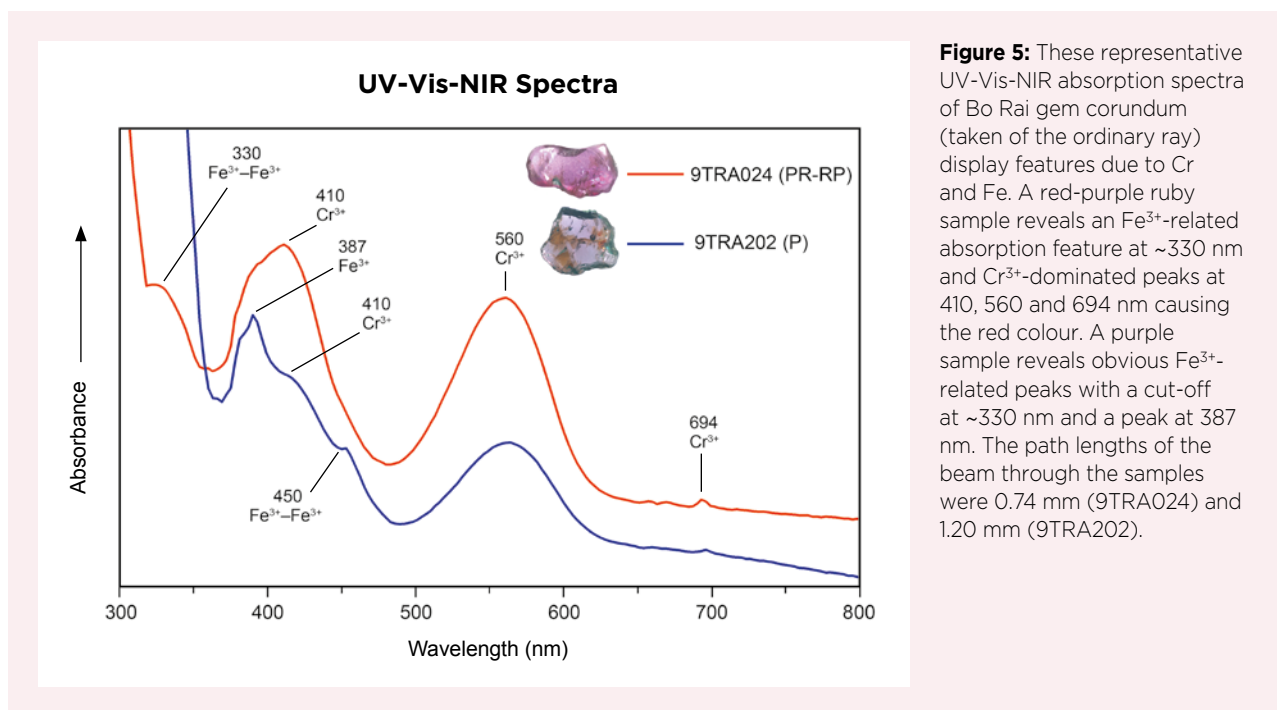


Figure 5: These representative UV-Vis-NIR absorption spectra of Bo Rai gem corundum (taken of the ordinary ray) display features due to Cr and Fe. A red-purple ruby sample reveals an Fe³⁺-related absorption feature at ~330 nm and Cr³⁺-dominated peaks at 410, 560 and 694 nm causing the red colour. A purple sample reveals obvious Fe³⁺-related peaks with a cut-off at ~330 nm and a peak at 387 nm. The path lengths of the beam through the samples were 0.74 mm (9TRA024) and 1.20 mm (9TRA202).

Table I: Representative semi-quantitative EDXRF analyses of the Bo Rai ruby sample set.

Colour range	Purple-red to red-purple						Reddish purple to purple						
Sample no.	9TRA 075	9TRA 045	9TRA 208	9TRA 212	9TRA 124	9TRA 078	9TRA 219	9TRA 217	9TRA 137	9TRA 156	9TRA 228	9TRA 029	9TRA 155
Oxide (wt.%)													
V ₂ O ₅	0.01	nd*	0.01	0.01	0.01	nd	0.01	nd	0.04	0.01	0.01	nd	0.01
TiO ₂	0.44	0.17	0.04	0.06	0.08	0.67	0.04	0.05	0.07	0.08	0.02	0.02	0.08
Al ₂ O ₃	98.16	98.49	99.13	99.09	98.75	97.83	99.07	98.91	98.54	98.95	99.29	99.44	98.83
Cr ₂ O ₃	0.50	0.48	0.27	0.26	0.35	0.45	0.24	0.26	0.31	0.18	0.08	0.06	0.12
Ga ₂ O ₃	nd	0.02	0.01	0.01	0.02	nd	nd	0.01	0.02	nd	0.01	0.01	0.01
Fe ₂ O ₃	0.89	0.84	0.55	0.57	0.79	1.05	0.64	0.77	1.03	0.78	0.60	0.46	0.95
Total	100.00	100.00	100.00	100.00	100.00	100.00	100.00	100.00	100.00	100.00	100.00	100.00	100.00

*Abbreviation: nd = not detected.

commonly formed rounded shapes, and EPMA analyses of the melt inclusions showed major Si, Al and Ca, with minor Fe, Mg, Na and K.

Pyroxene was the most common mineral inclusion identified in this study, with 122 of these crystals observed in 71 of the 88 samples of Bo Rai ruby. It usually formed

rounded crystals with ellipsoidal or columnar shapes (Figure 8). Most were colourless, but some appeared light brown (Figure 8c). Their chemical composition characterised them as Al-rich pyroxene, close to diopside composition (see Table II and Figure 9; cf. Clark & Papike 1968).

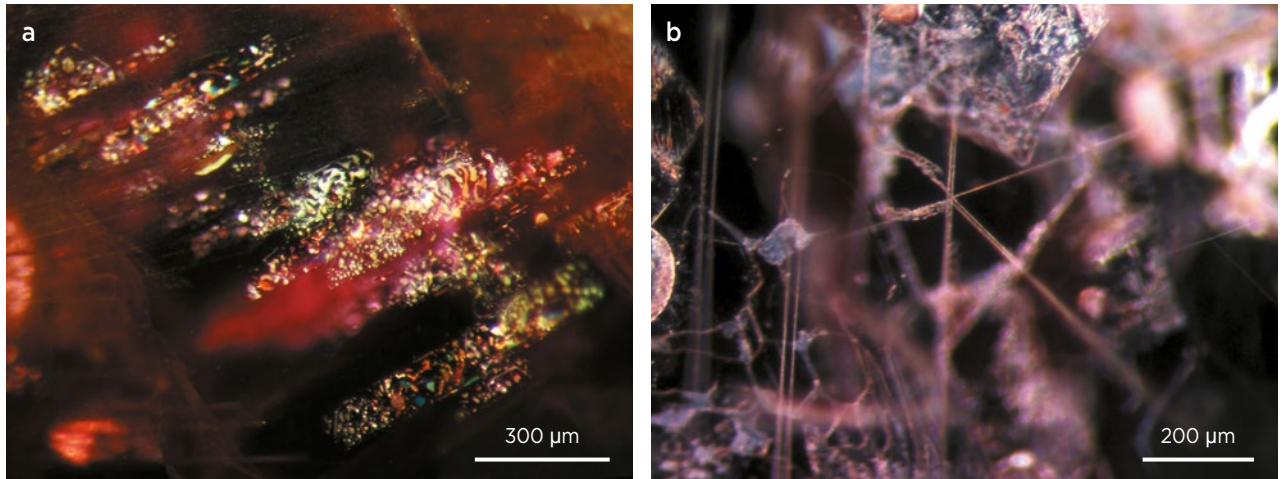


Figure 6: Internal features observed in the Bo Rai ruby samples include: (a) equatorial thin films surrounding minute crystals and (b) needle-like inclusions. Photomicrographs by S. Promwongnan; darkfield illumination with fibre-optic light.

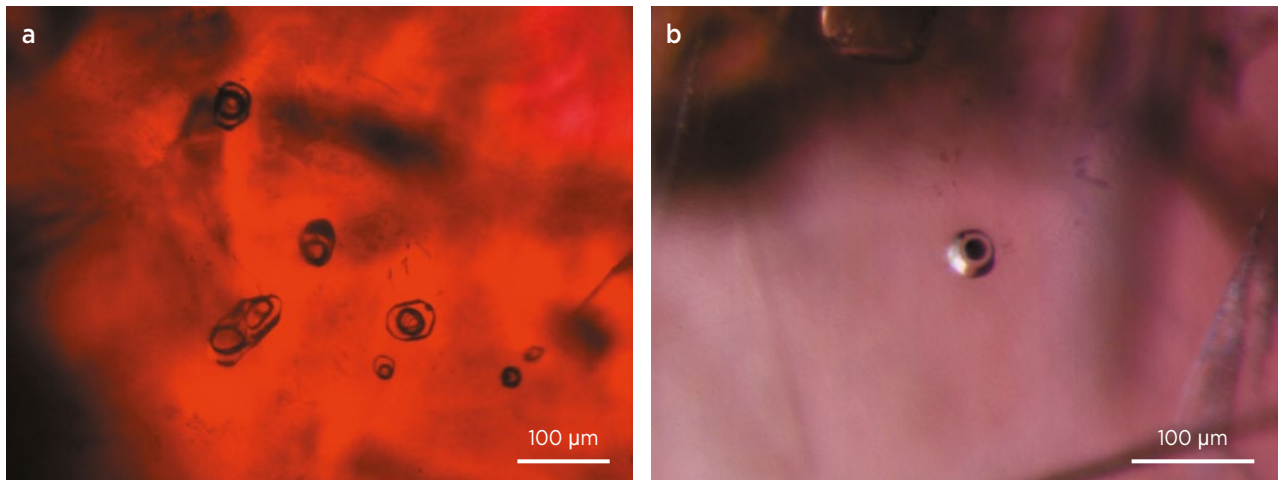


Figure 7: (a) These inclusions in a Bo Rai ruby appear to contain multiple fluid/gas phases. (b) Silicate melt inclusions in the rubies were associated with a gas phase (likely CO₂). Photomicrographs by S. Promwongnan; (a) darkfield illumination and (b) brightfield illumination with fibre-optic light.

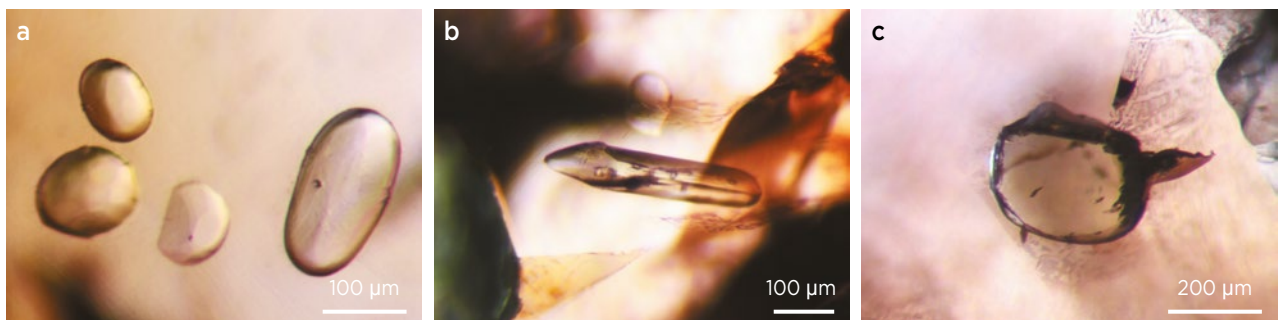


Figure 8: Pyroxene is a common mineral inclusion in Bo Rai ruby and typically forms (a) ellipsoidal or (b) columnar shapes. Most are colourless, but some are light brown (c). Photomicrographs by S. Promwongnan; brightfield illumination with fibre-optic light.

Table II: Representative EPMA analyses of pyroxene inclusions in the Bo Rai ruby sample set.

Sample no.	9TRA 016-1	9TRA 023-1	9TRA 118-2	9TRA 124-1	9TRA 036-1	9TRA 156-1
Oxide (wt.%)						
SiO ₂	46.51	47.10	46.85	46.16	46.55	47.56
TiO ₂	0.14	0.04	0.03	0.08	0.11	0.60
Al ₂ O ₃	14.68	14.69	14.50	15.81	13.88	14.15
Cr ₂ O ₃	0.14	0.08	0.04	0.13	0.04	0.07
FeO _{tot}	2.25	2.25	3.39	2.79	2.67	3.51
MnO	nd*	0.04	0.08	0.02	0.01	0.05
MgO	11.93	11.65	11.97	11.10	13.32	11.01
CaO	22.09	21.76	20.98	22.24	21.34	21.47
Na ₂ O	1.02	1.20	1.44	0.87	0.97	1.41
K ₂ O	0.01	0.01	0.01	0.02	0.01	nd
Total	98.76	98.81	99.29	99.21	98.89	99.81
Formula per 6(O)						
Si	1.705	1.722	1.713	1.687	1.706	1.731
Ti	0.004	0.001	0.001	0.002	0.003	0.016
Al	0.634	0.633	0.625	0.681	0.599	0.607
Cr	0.004	0.002	0.001	0.004	0.001	0.002
Fe ³⁺	0.025	0.005	0.071	0.000	0.077	0.000
Fe ²⁺	0.044	0.063	0.032	0.085	0.005	0.107
Mn	nd	0.001	0.002	0.001	0.000	0.002
Mg	0.652	0.635	0.653	0.605	0.727	0.597
Ca	0.868	0.853	0.822	0.871	0.838	0.837
Na	0.073	0.085	0.102	0.062	0.069	0.099
K	0.000	0.001	0.000	0.001	0.001	nd
Total	4.008	4.002	4.024	3.999	4.026	3.998
% Ca	55.50	55.00	54.55	55.80	53.38	54.32
% Mg	41.69	40.94	43.33	38.76	46.31	38.74
% Fe	2.81	4.06	2.12	5.45	0.32	6.94
Total	100.00	100.00	100.00	100.00	100.00	100.00

*Abbreviation: nd = not detected.

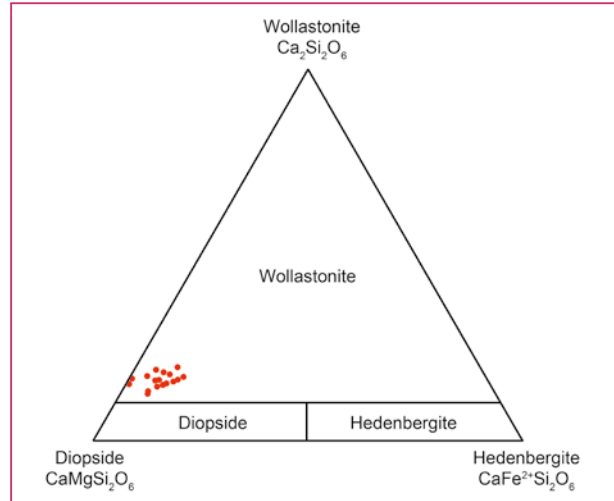


Figure 9: A compositional plot of Al-rich pyroxene inclusions analysed in the Bo Rai rubies shows them to be close to diopside composition. The apparent shift from diopside is caused by substitution from the Ca-Tschermak's component (CaAl₂SiO₆), which is not taken into account by this diagram. (diagram after Morimoto *et al.* 1988).

Garnet commonly formed subhedral crystals that appeared either colourless or pale purplish red (Figure 10a). The garnet inclusion in one sample (9TRA053) was oriented along the trigonal structure of the host ruby (Figure 10b). The dominant composition of the garnet inclusions was pyrope, and most had very low Cr contents (see Table III). This is similar to the composition of garnet inclusions reported previously in Thai ruby (Sutthirat *et al.* 2001; Saminpanya & Sutherland 2011). One elongated garnet inclusion associated with black crystals (probably a sulphide; Figure 10c) in sample 9TRA029 contained higher Fe and slightly lower Mg than most of the garnets analysed in our samples.

Feldspar inclusions were observed in four of the samples. They usually formed rounded to ellipsoidal grains (Figure 11) with chemical compositions that indicate plagioclase (i.e. bytownite: Ab₁₁₋₁₅An₈₅₋₈₉Or_{0.1-0.2}). One

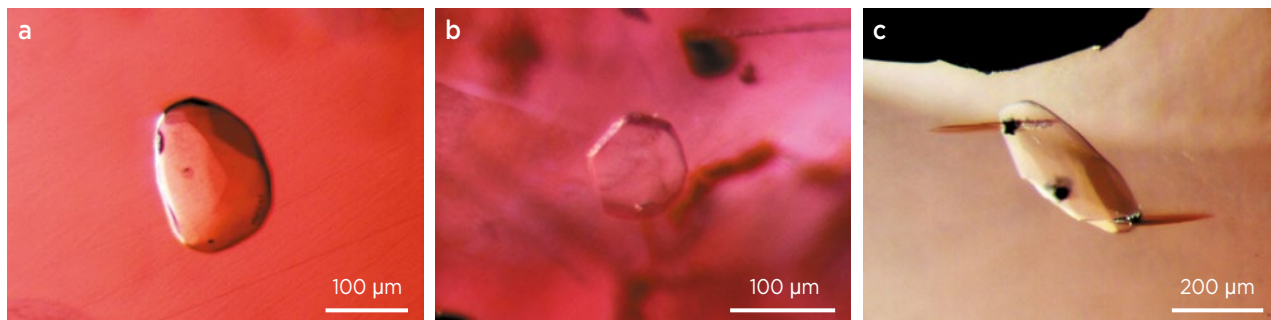


Figure 10: Garnet inclusions in Bo Rai ruby consist of low-Cr pyrope that usually form (a) colourless to pale purplish red crystals. (b) In one sample, a garnet inclusion clearly reflects the trigonal structure of the host ruby. (c) Another ruby sample hosts a garnet inclusion that was shown to contain relatively higher Fe and lower Mg, together with minute black crystals (likely a sulphide). Photomicrographs by S. Promwongnan; brightfield illumination with fibre-optic light.

Table III: Representative EPMA analyses of garnet, sillimanite and spinel inclusions in the Bo Rai ruby sample set.

Mineral	Garnet (pyrope)							Sillimanite		Spinel
Sample no.	9TRA 049-1	9TRA 053-1	9TRA 053-2	9TRA 206-3	9TRA 215-1	9TRA 218-1	9TRA 029-1	9TRA 169-1	9TRA 024-1	9TRA 024-2
Oxide (wt.%)										
SiO ₂	41.77	42.56	41.94	41.88	42.07	41.43	41.45	36.60	36.49	0.09
TiO ₂	0.02	0.01	0.03	0.01	0.05	0.02	0.05	nd*	nd	nd
Al ₂ O ₃	23.01	23.30	23.32	22.65	23.39	24.12	23.09	62.42	62.24	67.59
Cr ₂ O ₃	0.18	0.06	0.10	0.05	0.09	0.10	0.02	0.02	0.21	1.41
FeO _{tot}	6.55	7.09	7.05	7.21	9.27	6.29	11.29	0.39	0.73	8.12
MnO	0.20	0.22	0.16	0.20	0.19	0.12	0.23	nd	0.01	0.03
MgO	18.33	17.97	18.27	17.21	15.69	18.71	15.65	0.07	0.12	22.59
CaO	8.78	8.48	8.35	9.43	9.33	9.90	8.58	0.27	0.16	nd
K ₂ O	nd	nd	nd	nd	nd	nd	0.01	0.18	0.08	0.01
Na ₂ O	0.02	0.02	0.02	nd	nd	nd	nd	0.03	0.03	0.01
Total	98.85	99.70	99.73	100.69	100.07	99.73	100.36	99.98	100.07	99.85
Formula	per 12(O)							per 20(O)		per 4(O)
Si	3.004	3.033	3.005	3.030	3.023	2.933	2.997	3.969	3.960	0.002
Ti	0.001	0.001	0.002	0.001	0.003	0.001	0.003	nd	nd	nd
Al	1.950	1.957	1.969	1.932	1.981	2.012	1.967	7.977	7.960	1.969
Cr	0.010	0.004	0.006	0.003	0.005	0.006	0.001	0.002	0.018	0.028
Fe ³⁺	0.048	0.000	0.023	0.005	0.000	0.169	0.051	0.035	0.066	0.000
Fe ²⁺	0.346	0.422	0.399	0.432	0.557	0.203	0.631	—	—	0.168
Mn	0.012	0.013	0.010	0.012	0.012	0.007	0.014	nd	0.001	0.001
Mg	1.965	1.908	1.951	1.856	1.681	1.974	1.687	0.011	0.019	0.832
Ca	0.677	0.647	0.641	0.731	0.718	0.751	0.665	0.031	0.019	nd
K	nd	nd	nd	nd	nd	nd	0.001	0.025	0.011	0.000
Na	0.003	0.002	0.003	nd	nd	nd	nd	0.006	0.006	0.000
Total	8.016	7.987	8.008	8.002	7.981	8.057	8.017	12.05	12.060	3.000

*Abbreviation: nd = not detected.



Figure 11: Plagioclase forms rounded to ellipsoidal grains in Bo Rai ruby. Photomicrograph by S. Promwongnan; brightfield illumination with fibre-optic light.

inclusion of andesine (Ab₅₆An₃₈Or₆) was also found in sample 9TRA031 (see Table IV and Figure 12).

Sillimanite was hosted by a fluid inclusion in sample 9TRA169 (Figure 13a). Moreover, a composite sillimanite-spinel inclusion was observed in sample 9TRA024 (Figure 13b), and it could be clearly differentiated using backscattered-electron imaging (Figure 13c). This is the first report of both sillimanite and spinel inclusions in Thai ruby. The sillimanite contained traces of Fe and Mg, and the spinel also contained some Fe: (Mg_{0.83}Fe_{0.17})Al₂O₄ (again, see Table III).

Sulphide inclusions formed metallic opaque black crystals with rounded or sub-hexagonal shapes (Figure 14). They were mostly present as tiny rounded grains that were each surrounded by a tension disc. EPMA analyses of the sulphides usually showed low total compositions,

Table IV: Representative EPMA analyses of plagioclase inclusions in the Bo Rai ruby sample set.

Sample no.	9TRA017-1	9TRA031-1	9TRA171-8	9TRA219-2
Mineral	Bytownite	Andesine	Bytownite	Bytownite
Oxide (wt.%)				
SiO ₂	47.20	58.17	45.34	46.31
TiO ₂	nd*	0.08	0.01	nd
Al ₂ O ₃	33.36	24.72	33.87	34.47
CaO	17.52	7.52	18.13	17.02
FeO	0.13	0.46	0.42	0.22
MnO	nd	0.02	0.03	nd
MgO	0.01	0.64	nd	0.07
K ₂ O	0.02	1.05	0.02	0.03
Na ₂ O	1.68	6.02	1.48	1.14
Total	99.92	98.68	99.30	99.26
Formula per 8(O)				
Si	2.171	2.643	2.111	2.139
Ti	nd	0.003	0.000	nd
Al	1.808	1.324	1.858	1.876
Ca	0.863	0.366	0.905	0.842
Fe	0.005	0.017	0.016	0.008
Mn	nd	0.001	0.001	nd
Mg	0.001	0.043	nd	0.005
K	0.001	0.061	0.001	0.002
Na	0.149	0.530	0.134	0.102
Total	4.998	4.988	5.026	4.974
Element (at.%)				
Ca	85.15	38.27	87.02	89.02
Na	14.73	55.40	12.87	10.79
K	0.12	6.34	0.11	0.19

*Abbreviation: nd = not detected.

and apart from Fe and S, Ni and Cu were present as major and minor components in some samples (Table V). The sulphide inclusion in ruby sample 9TRA231 yielded the composition of pyrrhotite (Fe₇S₈). Others were closer to compositions of pentlandite ([Fe,Ni]₉S₈; sample 9TRA055) or digenite (Cu₉S₅; sample 9TRA160).

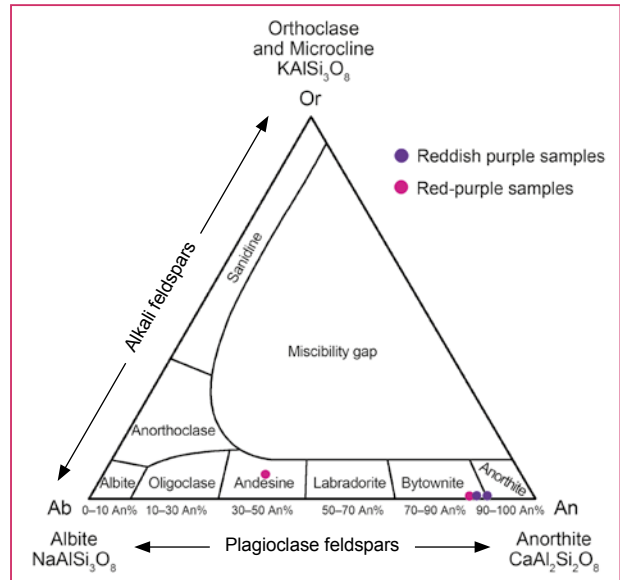


Figure 12: This ternary diagram shows that the feldspar inclusions in our Bo Rai samples fall within the plagioclase range (bytownite and andesine).

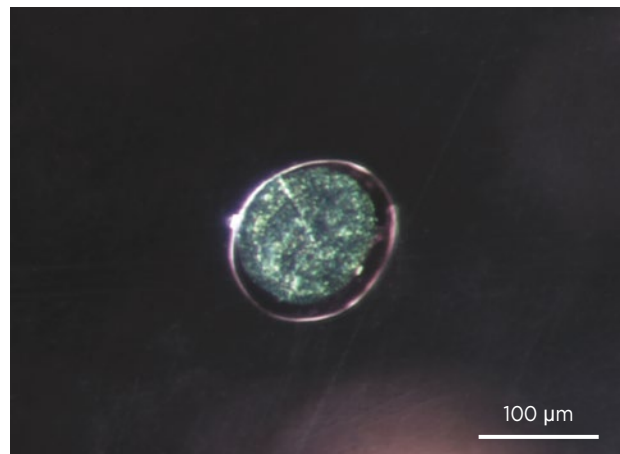


Figure 14: The sulphide inclusions in Bo Rai rubies typically form rounded to sub-hexagonal opaque grains that appear black, although they may show metallic reflections (causing the greenish grey appearance seen here). Photomicrograph by S. Promwongnan; darkfield illumination with fibre-optic light.

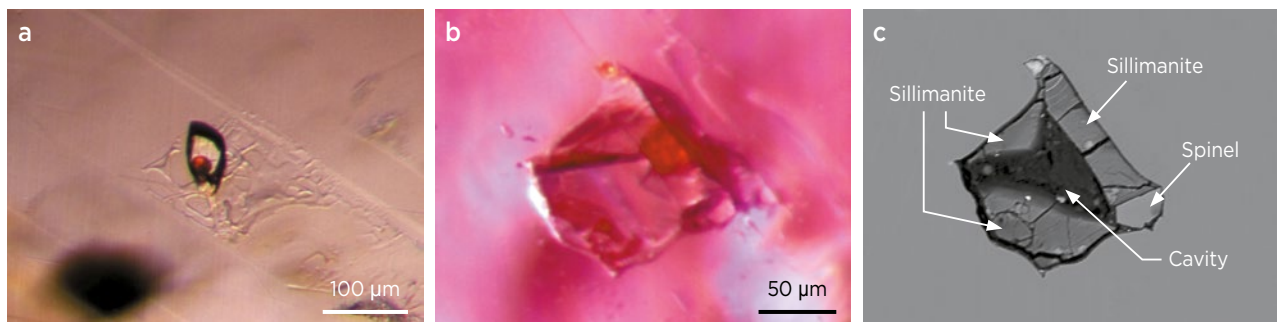


Figure 13: (a) The colourless crystal seen here in a Bo Rai ruby, identified as sillimanite, is hosted by a fluid inclusion and itself contains a rounded area of red material. (b) Sillimanite also forms part of a subhedral composite inclusion along with spinel. (c) The sillimanite and spinel components of the composite inclusion are clearly visible with the use of backscattered-electron imaging. Photomicrographs by S. Promwongnan; brightfield illumination with fibre-optic light (a, b).

Table V: Representative EPMA analyses of sulphide inclusions in the Bo Rai ruby sample set.

Sample no.	9TRA214-1	9TRA160-1	9TRA176-1	9TRA208-1	9TRA055-1	9TRA231-1	9TRA202-1
Element (wt.%)							
Al	0.09	0.04	0.06	0.05	0.04	0.11	0.03
S	18.71	19.35	14.93	22.12	27.72	25.34	26.49
Ti	0.29	nd*	0.04	0.21	0.37	0.18	0.3
Fe	9.39	9.19	9.21	21.61	34.68	42.42	31.21
Ni	0.06	0.06	4.59	0.14	22.63	4.58	11.67
Co	nd	na*	nd	nd	na	na	nd
Cu	62.17	64.39	51.69	42.88	0.03	1.05	18.32
Zn	nd	na	nd	nd	na	na	nd
As	nd	na	nd	nd	na	na	nd
Mo	0.23	0.39	0.43	0.44	0.42	0.44	0.45
In	0.01	nd	nd	0.05	nd	nd	nd
Sn	nd	na	nd	nd	na	na	nd
Ba	0.28	0.35	0.27	0.22	nd	nd	0.11
Pt	nd	nd	nd	nd	0.02	0.14	0.04
Pb	nd						
Total	91.24	93.78	81.22	87.71	85.90	74.25	88.63

*Abbreviations: na = not analysed, nd = not detected.

DISCUSSION

The etched patterns on the surfaces of some samples of Bo Rai ruby were apparently caused by chemical resorption in the magma. Such features are also typically observed on corundum from basaltic terranes elsewhere (Coenraads 1992).

Spectroscopic features within the mid-IR range showed the presence of a kaolinite-group mineral in these untreated rubies, which has been documented previously in basaltic-related corundum (e.g. in sapphires from southern Vietnam: Smith *et al.* 1995). This hydrous phase appears to form in corundum as a secondary product (Smith *et al.* 1995; Beran & Rossman 2006; Schwarz *et al.* 2008) and may be used as an indicator of an unheated stone.

UV-Vis-NIR spectra of the rP to P samples commonly showed iron- and chromium-related absorption features, consistent with their chemical compositions, in particular an Fe₂O₃:Cr₂O₃ ratio that was usually >3.

The most common mineral inclusion observed in our samples from Bo Rai was Al-rich pyroxene, which had compositions similar to those of pyroxenes associated with alluvial rubies from Bo Rai and Pailin (Sutherland *et al.* 1998b; Sutthirat *et al.* 2001), as well as those found in ruby-bearing mafic granulite xenoliths in alkali basalt from Bo Rai (Sutthirat *et al.* 2018). The pyroxene inclusions analysed in this study were also similar to ruby-bearing mafic xenocrysts embedded in alkali basalt from the Nong Bon gem field (Sutthirat *et al.* 2001), located about 20 km west of Bo Rai.

The Cr-poor pyrope inclusions in Bo Rai ruby have compositions that are similar to those of garnet xenocrysts embedded in Nong Bon basalt and to garnet in mafic xenoliths from Bo Welu (located ~30 km northwest of Bo Rai), which were documented by Sutthirat *et al.* (2001) and Saminpanya & Sutherland (2011), respectively. Plagioclase was reported previously as an inclusion in Thai ruby by Gübelin (1971), although the compositions of such inclusions were not documented until now. The spinel inclusions analysed in this study contained greater Mg than that of a pleonastic spinel inclusion found in ruby from western Pailin in Cambodia (Sutherland *et al.* 1998b). The varying composition of the sulphide inclusions in Bo Rai rubies may reflect locally heterogeneous formational environments. Gübelin (1971) documented chalcopyrite (CuFeS₂) in Thai rubies, and additional sulphide minerals have been reported by other researchers.

Overall, the inclusion assemblage in Bo Rai ruby—particularly clinopyroxene, garnet, plagioclase and spinel—closely resembles the minerals composing ruby-bearing mafic granulite xenoliths (plagioclase + clinopyroxene + spinel ± garnet ± corundum) in basalts surrounding the Bo Rai gem field (Promprated *et al.* 2003; Sutthirat *et al.* 2018). The mineral chemistries of these assemblages are also comparable, indicating that the alluvial rubies originally crystallised in mafic granulites prior to being transported to the surface via basaltic eruptions. Weathering of the basalts resulted in the accumulation of gem corundum within the alluvial

deposits. Based on the isotope study of Yui *et al.* (2006), mafic metamorphic rock was suggested to be related to the original formation of Thai ruby. This agrees with corundum formation in mafic granulites, which are high-grade metamorphic rocks.

Palke *et al.* (2018) documented melt inclusions in reddish violet sapphire from Yogo Gulch, Montana, USA, and in rubies from Thailand and Cambodia, with similar compositions of 53.4–60.5% SiO₂, 20.6–24.0% Al₂O₃, 4.9–6.2% CaO and 4.3–5.2% Na₂O with negligible Ti, Mg, Fe and K. These melt compositions were interpreted together with trace elements and oxygen isotopic analyses of their corundum hosts. In their genetic model, Palke *et al.* (2018) suggested that Thai ruby was associated with the transformation of anorthosite to garnet pyroxenite along with a partial melting process. The melt inclusions found in our Bo Rai ruby samples contained approximately 48.5–56.5% SiO₂, 26.4–31.9% Al₂O₃, 9.7–11.1% CaO, 1.6–2.0% FeO_{tot}, 3.0–3.2% MgO and 0.8–1.4% Na₂O, and therefore have lower Si and Na contents and higher

Al, Ca, Fe and Mg contents compared to those reported by Palke *et al.* (2018). These variations in composition could relate to different degrees of partial melting and crystallisation. The presence of sillimanite and silicate melt inclusions in the Bo Rai samples clearly suggests exposure to high temperatures (>500°C), consistent with partial melting, prior to the crystallisation of Thai ruby.

CONCLUSIONS

Bo Rai rubies commonly contain minute mineral inclusions surrounded by equatorial thin films. In addition, various mineral inclusions were identified in this study, particularly pyroxene, pyrope and plagioclase and minor spinel, which is consistent with the inferred original source rock of mafic granulite. Moreover, sillimanite and silicate melt inclusions indicate a high-temperature environment during crystallisation. The presence of sillimanite and spinel inclusions is described here for the first time in Thai ruby.

REFERENCES

- Beran, A. & Rossman, G.R. 2006. OH in naturally occurring corundum. *European Journal of Mineralogy*, **18**(4), 441–447, <http://doi.org/10.1127/0935-1221/2006/0018-0441>.
- Clark, J.R. & Papike, J. 1968. Crystal-chemical characterization of omphacites. *American Mineralogist*, **53**(5–6), 840–868.
- Coenraads, R.R. 1992. Surface features on natural rubies and sapphires derived from volcanic provinces. *Journal of Gemmology*, **23**(3), 151–160, <http://doi.org/10.15506/JoG.1992.23.3.151>.
- Droop, G.T.R. 1987. A general equation for estimating Fe³⁺ concentrations in ferromagnesian silicates and oxides from microprobe analyses, using stoichiometric criteria. *Mineralogical Magazine*, **51**(361), 431–435, <http://doi.org/10.1180/minmag.1987.051.361.10>.
- Gübelin, E. 1940. Differences between Burma and Siam rubies. *Gems & Gemology*, **3**(5), 69–72.
- Gübelin, E. 1971. New analytical results of the inclusions in Siam rubies. *Journal of Gemmology*, **12**(7), 242–252, <http://doi.org/10.15506/JoG.1971.12.7.242>.
- Gübelin, E.J. & Koivula, J.I. 1986. *Photoatlas of Inclusions in Gemstones*. ABC Edition, Zurich, Switzerland, 532 pp.
- Guo, J., Griffin, W.L. & O'Reilly, S.Y. 1994. A cobalt-rich spinel inclusion in a sapphire from Bo Ploi, Thailand. *Mineralogical Magazine*, **58**(391), 247–258, <http://doi.org/10.1180/minmag.1994.058.391.07>.
- Hughes, R.W. 2017. *Ruby & Sapphire: A Gemologist's Guide*. RWH Publishing, Bangkok, Thailand, 816 pp.
- Intasopa, S., Atichat, W., Pisutha-Arnond, V., Sriprasert, B., Narudeesombat, N. & Puttharat, T. 1999. Inclusions in Chanthaburi-Trat corundums: A clue to their genesis. *Symposium on Mineral, Energy and Water Resources of Thailand: Towards the Year 2000*, Bangkok, Thailand, 28–29 October, 471–484 (in Thai).
- Keller, P.C. 1982. The Chanthaburi-Trat gem field, Thailand. *Gems & Gemology*, **18**(2), 186–196, <https://doi.org/10.5741/gems.18.4.186>.
- Khamloet, P., Pisutha-Arnond, V. & Sutthirat, C. 2014. Mineral inclusions in sapphire from the basalt-related deposit in Bo Phloi, Kanchanaburi, western Thailand: Indication of their genesis. *Russian Geology and Geophysics*, **55**(9), 1087–1102, <http://doi.org/10.1016/j.rgg.2014.08.004>.
- Koivula, J.I. & Fryer, C.W. 1987. Sapphirine (not sapphire) in a ruby from Bo Rai, Thailand. *Journal of Gemmology*, **20**(6), 369–370, <http://doi.org/10.15506/JoG.1987.20.6.369>.
- Morimoto, N., Fabries, J., Ferguson, A.K., Ginzburg, I.V., Ross, M., Seifert, F.A., Zussman, J., Aoki, K. & Gottardi, G. 1988. Nomenclature of pyroxenes. *American Mineralogist*, **73**(9–10), 1123–1133.
- Palke, A.C., Wong, J., Verdel, C. & Ávila, J.N. 2018. A common origin for Thai/Cambodian rubies and blue and violet sapphires from Yogo Gulch, Montana, U.S.A.? *American Mineralogist*, **103**(3), 469–479, <http://doi.org/10.2138/am-2018-6164>.
- Pattamalai, K., 2015. Chanthaburi-Trat corundum deposits, eastern Thailand. *Proceedings of the 3rd Lao-Thai Technical Conference on Geology and Mineral Resources*, Bangkok, Thailand, 7–11 July, 219–229.

- Promprated, P., Taylor, L.A. & Neal, C.R. 2003. Petrochemistry of mafic granulite xenoliths from the Chantaburi [*sic*] basaltic field: Implications for the nature of the lower crust beneath Thailand. *International Geology Review*, **45**(5), 383–406, <http://doi.org/10.2747/0020-6814.45.5.383>.
- Saeseaw, S., Sangsawong, S., Vertriest, W., Atikarnsakul, U., Raynaud-Flattot, V.L., Khowpong, C. & Weeramonkhonlert, V. 2017. *A Study of Sapphire from Chanthaburi, Thailand and Its Gemological Characteristics*. Gemological Institute of America, 12 April, 42 pp., www.gia.edu/doc/Blue-sapphires-Chanthaburi-Thailand-finalfinal.pdf.
- Saminpanya, S. & Sutherland, F.L. 2011. Different origins of Thai area sapphire and ruby, derived from mineral inclusions and co-existing minerals. *European Journal of Mineralogy*, **23**(4), 683–694, <http://doi.org/10.1127/0935-1221/2011/0023-2123>.
- Saminpanya, S., Manning, D.A.C., Droop, G.T.R. & Henderson, C.M.B. 2003. Trace elements in Thai gem corundums. *Journal of Gemmology*, **28**(7), 399–416, <http://doi.org/10.15506/JoG.2003.28.7.399>.
- Sangsawong, S., Vertriest, W., Saeseaw, S., Pardieu, V., Muylal, J., Khowpong, C., Atikarnsakul, U. & Weeramonkhonlert, V. 2017. *A Study of Rubies from Cambodia and Thailand*. Gemological Institute of America, July, 37 pp., www.gia.edu/gia-news-research/study-rubies-cambodia-thailand.
- Schwarz, D., Pardieu, V., Saul, J.M., Schmetzer, K., Laurs, B.M., Giuliani, G., Klemm, L., Malsy, A.-K., Erel, E., Hauzenberger, C., Du Toit, G., Fallick, A.E. & Ohnenstetter, D. 2008. Rubies and sapphires from Winza, central Tanzania. *Gems & Gemology*, **44**(4), 322–347, <http://doi.org/10.5741/gems.44.4.322>.
- Smith, C.P., Kammerling, R.C., Keller, A.S., Peretti, A., Scarratt, K.V., Khoa, N.D. & Repetto, S. 1995. Sapphires from southern Vietnam. *Gems & Gemology*, **31**(3), 168–186, <http://doi.org/10.5741/gems.31.3.168>.
- Sutherland, F.L., Hoskin, P.W.O., Fanning, C.M. & Coenraads, R.R. 1998a. Models of corundum origin from alkali basaltic terrains: A reappraisal. *Contributions to Mineralogy and Petrology*, **133**(4), 356–372, <http://doi.org/10.1007/s004100050458>.
- Sutherland, F.L., Schwarz, D., Jobbins, E.A., Coenraads, R.R. & Webb, G. 1998b. Distinctive gem corundum suites from discrete basalt fields: A comparative study of Barrington, Australia, and West Pailin, Cambodia, gemfields. *Journal of Gemmology*, **26**(2), 65–85, <http://doi.org/10.15506/JoG.1998.26.2.65>.
- Sutthirat, C., Charusiri, P., Farrar, E. & Clark, A.H. 1994. New $^{40}\text{Ar}/^{39}\text{Ar}$ geochronology and characteristics of some Cenozoic basalts in Thailand. *Proceedings of the International Symposium on Stratigraphic Correlation of Southeast Asia, 15–20 November 1994, Bangkok, Thailand*. Department of Mineral Resources and IGCP 306, Bangkok, Thailand, 306–321.
- Sutthirat, C., Saminpanya, S., Droop, G.T.R., Henderson, C.M.B. & Manning, D.A.C. 2001. Clinopyroxene-corundum assemblages from alkali basalt and alluvium, eastern Thailand: Constraints on the origin of Thai rubies. *Mineralogical Magazine*, **65**(2), 277–295, <http://doi.org/10.1180/002646101550253>.
- Sutthirat, C., Hauzenberger, C., Chualaowanich, T. & Assawincharoenkij, T. 2018. Mantle and deep crustal xenoliths in basalts from the Bo Rai ruby deposit, eastern Thailand: Original source of basaltic ruby. *Journal of Asian Earth Sciences*, **164**, 366–379, <http://doi.org/10.1016/j.jseaes.2018.07.006>.
- Vichit, P. 1992. Gemstones in Thailand. In: Piencharoen, C. (ed) *Proceedings of a National Conference on Geologic Resources of Thailand—Potential for Future Development: 17–24 November 1992, Bangkok, Thailand*. Department of Mineral Resources, Bangkok, Thailand, 124–150.
- Vichit, P., Vudhichativanich, S. & Hansawek, R. 1978. The distribution and some characteristics of corundum-bearing basalts in Thailand. *Journal of the Geological Society of Thailand*, **3**, M4-1–M4-38.
- Yui, T.-F., Wu, C.-M., Limtrakun, P., Sricharn, W. & Boonsoong, A. 2006. Oxygen isotope studies on placer sapphire and ruby in the Chanthaburi-Trat alkali basaltic gemfield, Thailand. *Lithos*, **86**(3–4), 197–211, <http://doi.org/10.1016/j.lithos.2005.06.002>.

The Authors

Supparat Promwongnan

Geology Department, Faculty of Science, Chulalongkorn University, Bangkok, Thailand, and Gem Testing Laboratory, Gem and Jewelry Institute of Thailand (GIT), Bangkok, Thailand
Email: psupparat@git.or.th

Dr Chakkaphan Sutthirat

Faculty of Science and Environmental Research Institute, Chulalongkorn University, Bangkok, Thailand
Email: chakkaphan.s@chula.ac.th

Acknowledgements

The authors thank Thai Lapidary International Co. Ltd and Prima Gems (Bangkok, Thailand), as well as an anonymous private collector, for loaning stones and jewellery for photography. This research was supported financially by the 90th Anniversary of Chulalongkorn University, Rachadapisek Sompote Fund of Chulalongkorn University. The first author would like to thank Duangkamol Jiambutr (GIT director), Wilawan Atichat, Dr Visut Pisutha-Arnond, Thanong Leelawatanasuk and Dr Sakonvan Chawchai for their suggestions and encouragement throughout her M.Sc. studies. Special thanks also go to Sopit Poompeang for assistance with sample preparation and EPMA analyses.

Doubling and Differential Magnification of Images Seen Through Calcite and Other Uniaxial Materials

Harold Killingback

Although the beauty of diamonds is universally admired and much pleasure is derived from the ostentatious display of them and other precious stones in necklaces and rings, those whose curiosity and desire for understanding is greater than their love of luxury will, I believe, be no less impressed by a transparent crystalline material which has recently come to us from Iceland. Its properties are so wonderful and unusual that it is surely one of nature's most fascinating creations.—Erasmus Bartholinus (Bartholini 1669), referring to the colourless transparent form of calcite called Iceland spar; opening sentence translated from the original Latin by H. Killingback

ABSTRACT: Image doubling can be seen when looking at an object or inscription through a piece of transparent calcite bounded by plane surfaces. As shown in this article, in uniaxial crystals such as calcite, the maximum separation angle between the axes of these images is determined not by the magnitude of either refractive index (RI), nor by the difference between them (the birefringence), but by the ratio of the highest RI to the lowest RI value, regardless of whether the crystal is optically positive or negative. Doubling is not seen when the crystal is viewed either along or at right angles to the optic axis. When the surface of the material is curved rather than planar (thus forming a lens), two images can be seen even when the crystal is viewed at right angles to the optic axis. This effect is not due to ray separation but is ascribed to the different magnifying powers resulting from the two RIs. The author therefore recommends that the term *doubling* be reserved for the effect of ray separation, while the phenomenon associated with surface curvature should be called *differential magnification*. When the curved surface is viewed in directions oblique to the optic axis, the effects of both ray separation and differential magnification can be seen.

The Journal of Gemmology, 36(7), 2019, pp. 646–654, <http://doi.org/10.15506/JoG.2019.36.7.646>
© 2019 Gem-A (The Gemmological Association of Great Britain)

Calcite is the crystalline form of calcium carbonate and, when pure, is commonly colourless and transparent. (The soft, porous form of calcium carbonate is chalk.) Calcite crystals readily cleave on three planes, forming rhombic parallelepipeds (i.e. rhombohedrons or rhombs; Figure 1). These have six faces, all of parallelogram shape, with opposite faces being parallel.

Calcite is uniaxial and doubly refractive (i.e. it has two RI values). The value of the RI for the ordinary ray

is constant at 1.658, but the RI for the extraordinary ray decreases from 1.658 along the optic axis to 1.486 at right angles to the optic axis, so calcite is described as optically negative.

This article examines the images that can be seen when looking through a piece of transparent calcite at an object or an inscription below it. The refraction of the ordinary ray obeys Snell's Law, with the RI value being equal to the sine of the angle of incidence of a light ray into the crystal, divided by the sine of the angle of

refraction within it. Different rules apply to the extraordinary ray. It and the ordinary ray take separate paths except when the crystal is viewed along or at right angles to the optic axis, when there is no separation of the rays.

MATERIALS AND METHODS

This study employed observations of five samples of transparent calcite: (1) a rhomb in the author's collection measuring $26 \times 50 \times 76$ mm; (2) a polished block measuring $35 \times 29 \times 32$ mm, loaned by Marcus McCallum (Hatton Garden, London), that was cut with opposite polished plane faces oriented parallel to the optic axis; (3) a sphere of 40 mm in diameter in the collection of Cornell University, Ithaca, New York, USA; (4) a sphere of 90 mm in diameter displayed at the Natural History Museum (NHM) in London; and (5) a sphere of 31.4 mm in diameter that McCallum had cut for the author for this study.

Photographs of all but the NHM and Cornell samples (which were not directly handled by the author) were taken using a Canon G15 pocket digital camera. The camera was mounted on a tripod and the timer was used for releasing the shutter so that any movement or blur could be eliminated. Focus and exposure were automatic, while the aperture was set to minimum to obtain the maximum depth of field. Photographing the rhomb was challenging because any one face showed portions of adjacent parallel planes. In addition, the view through a small sphere is highly sensitive to position because its surface curvature produces high magnification. The smallest sphere was kept stationary for photography by placing it on a slight depression made by punching a hole through a piece of cardboard that lay under the paper background. A circle was drawn on the paper to be viewed through the calcite sphere. The paper was carefully positioned so that the hole and the circle were concentric. No photographic enhancements were done except for routine cropping, brightness and clarity adjustments.

A London dichroscope was used to visualise the orthogonal polarisation of the refracted rays through the calcite samples.

IMAGES SEEN THROUGH CALCITE

Specimens with Plane Surfaces

The most commonly encountered form of crystalline calcite is the cleavage rhomb. The separation of rays upon entering a transparent calcite crystal can be made visible by the fluorescence caused by the beam of a 405 nm laser pointer (Killingback 2014). Figure 1 shows the rhomb sample standing on its smallest face (26×50 mm) with

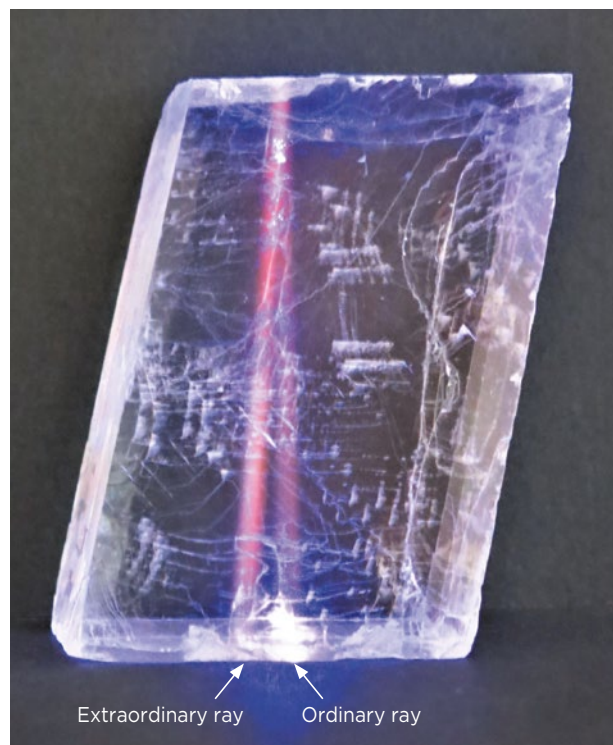


Figure 1: Laser-induced fluorescence makes visible the path of a 405 nm laser beam through a calcite rhomb ($26 \times 50 \times 76$ mm). The beam is normal to the top face. The ordinary ray continues vertically downward, in accordance with Snell's Law. The extraordinary ray proceeds separately and does not obey Snell's Law. Photo by H. Killingback.

a laser aimed vertically downward through the top face. The camera view is normal to its 50×76 mm face. The ordinary ray continues vertically downward, in accordance with Snell's Law. The extraordinary ray is separated from the ordinary one, illustrating that it does not conform to Snell's Law in this orientation of the crystal relative to the incident beam.

Figure 2a shows the view looking perpendicular to the 50×76 mm face (i.e. through the least thickness of the rhomb) as it lies on an X mark. Figure 2b shows the view perpendicular to the 26×50 mm face (i.e. through the greatest thickness of the rhomb). A comparison of these photographs shows that, as the ray paths lengthen, the size of the two X's (and the distance between them) increases, but within each view both images of the X are of the same size. Scaling from the photographs, the separation angle (α) between the two rays is about 5.7° .

Figure 3a shows the view normal to the 26×76 mm face (i.e. through the intermediate thickness of the rhomb). Figure 3b shows the same view, with a London dichroscope aligned over the images so that the border between the two abutting Polaroid sheets (which have their axes of polarisation at right angles to one another) lies over the centre of each image. Only half of each X

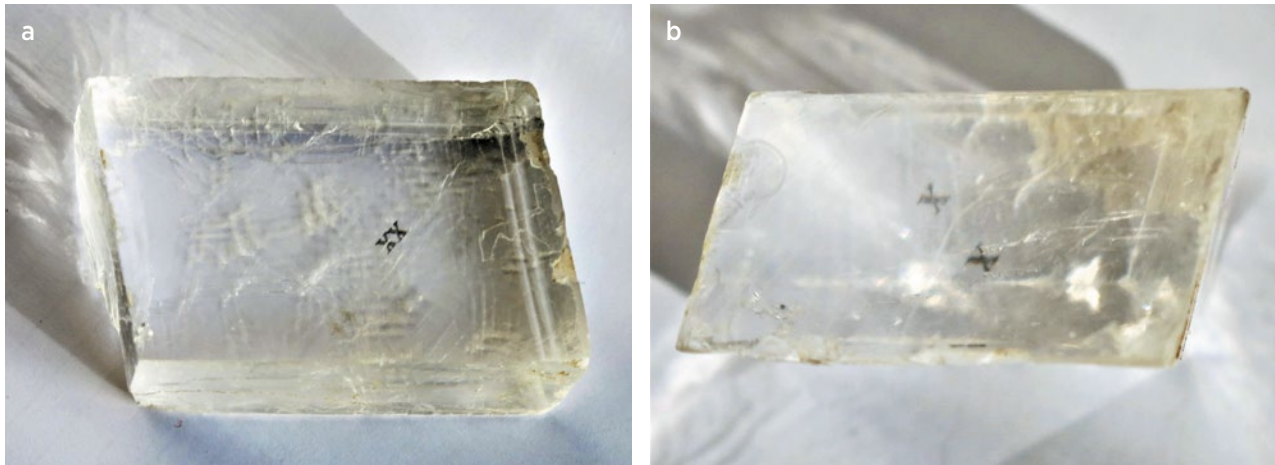


Figure 2: The same calcite rhomb lies on an X mark and is viewed (a) through the 50 × 76 mm face, which is the smallest distance through the specimen, and (b) through the 26 × 50 mm face, showing the greatest distance through the specimen. Photos by H. Killingback.

image can be seen, showing that the rays forming each of the images are orthogonally polarised.

The maximum value of the separation angle, α_{\max} , between the largest and smallest RI values (n_{\max} and n_{\min}) can be calculated using the following formula (Sturman & Back 2002):

$$\tan \alpha_{\max} = (n_{\max}^2 - n_{\min}^2) / 2 \times n_{\max} \times n_{\min}$$

Using Q for the ratio n_{\max}/n_{\min} and rearranging, we get:

$$2 \times \tan \alpha_{\max} = Q - 1/Q$$

Thus, the maximum separation angle depends only on the *ratio* of the refractive indices (Q), not on their individual values nor on their difference (the birefringence). This explains why the maximum separation angle in calcite ($\alpha_{\max} = 6.30^\circ$) is greater than that in

rutile ($\alpha_{\max} = 5.97^\circ$). Although rutile’s RIs are large (2.616 and 2.903), and their difference is high (birefringence = 0.287), their ratio $Q = 1.110$ is a little smaller than that for calcite, for which the RIs are 1.486 and 1.658 (birefringence = 0.172) and $Q = 1.116$.

It can be calculated that the greatest separation of the rays in calcite is seen when the angle between the optic axis and the normal to the cleavage face being viewed is about 42° (Sturman & Back 2002). The angle between the optic axis and the cleavage plane of calcite is just over 44° . Therefore, looking perpendicularly through the face of a calcite cleavage rhomb gives almost the best view of the doubling (Skalwold & Bassett 2015).

Figure 4 shows a plot of α_{\max} vs. Q for various materials. Sodium nitrate, with $Q = 1.186$, is not of interest as a gem because it is soluble in water, but it has been included to

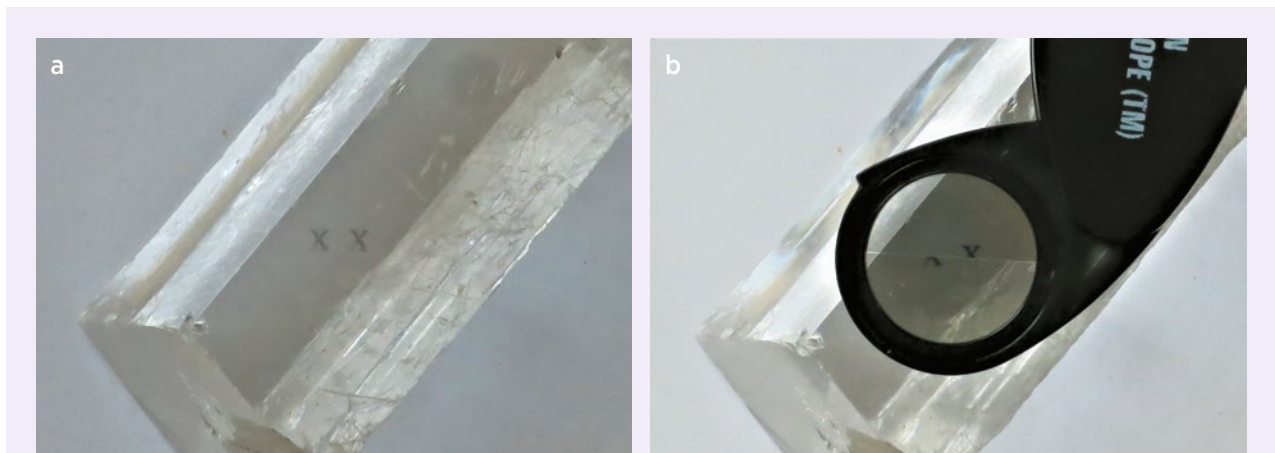


Figure 3: (a) The same calcite rhomb is seen here with the X mark viewed through the 26 × 76 mm face, showing an intermediate distance through the specimen. (b) A London dichroscope is orientated so that the junction between its polarising plates coincides with the centres of the two X images. The images seen through the dichroscope show that the rays are polarised at a right angle to one another. Photos by H. Killingback.

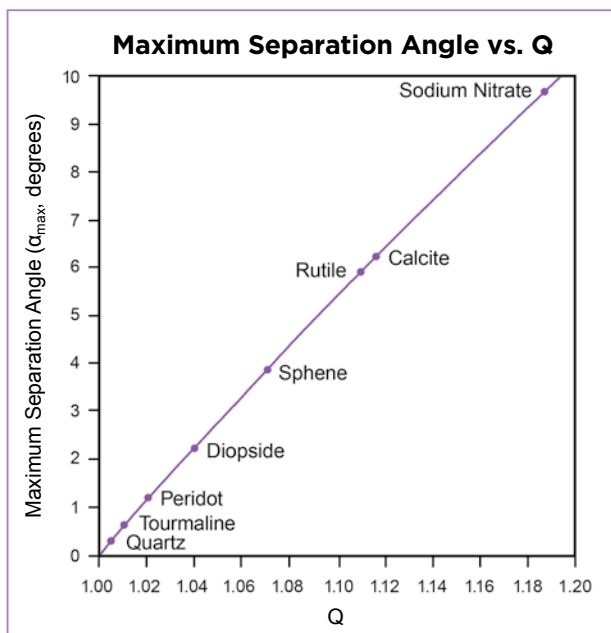


Figure 4: The maximum ray separation angle for various crystals is plotted against Q, the ratio of the highest RI to the lowest RI value.

show that calcite is far from having the highest value of Q. The graph is virtually a straight line. A close approximation to this line is provided by the simple equation:

$$\alpha_{\max} = 56 \times (Q - 1)$$

This equation can be used to provide a quick estimate of the maximum separation angle for any transparent uniaxial substance for which the RIs are known.

Figure 5a shows a block of calcite which has opposite polished plane faces parallel to the optic axis. The block is resting on a circle mark, and the view vertically downward is at a right angle to the optic axis. There is only one image of the circle. This is in accordance with Snell's Law and confirms that only one image can be seen in this direction. Looking obliquely, as in Figure 5b, there are two overlapping images.

Specimens with Curved Surfaces

Because calcite cleaves easily, it is difficult to find a large piece of rough without cracks, let alone to cut a sphere from one. The author was, therefore, very impressed by a 90 mm diameter optically clean calcite sphere displayed at the Natural History Museum in London. In fact, it was this specimen that stimulated his interest in the behaviour of images seen through calcite. He therefore asked if the curator could supply a photograph looking vertically down on the sphere, lying on a 4 mm diameter circle and orientated so that its optic axis was horizontal. The result is shown in Figure 6. A second 4 mm circle is seen to the upper left of the sphere, for comparison. Through the sphere is seen not one image as in Figure 5a, but three: two near the centre and another weaker one near the periphery of the specimen.

At that time, the author was unable to obtain a calcite sphere for himself to confirm what was seen through the NHM sphere, so he made the same photo request to the curator at Cornell University, as he knew there was a 40 mm diameter calcite sphere in their collection. The

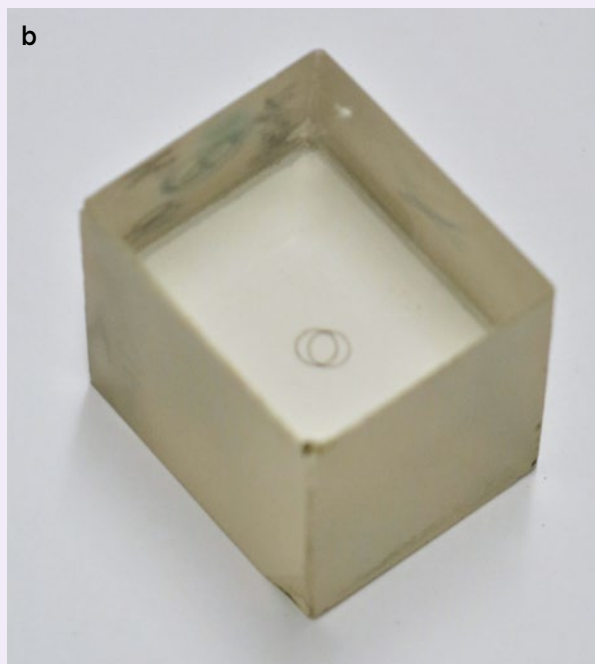


Figure 5: (a) This block of calcite has opposite polished faces (35 × 29 mm) that are cut parallel to the optic axis direction. It is viewed here perpendicular to the optic axis (through a thickness of 32 mm), and this orientation shows a single image of the circle on which the block stands. (b) Viewed obliquely, the same calcite block now shows two images of the circle. Photos by H. Killingback.



Figure 6: A calcite sphere (90 mm diameter) resting on a 4 mm diameter circle viewed perpendicular to the optic axis displays three concentric images of the circle: two near the centre and a third located near the periphery of the sphere. Another 4 mm circle is shown to the upper left of the sphere for comparison. Image of specimen BM.55140 courtesy of NHM London, © The Trustees of the Natural History Museum, London.

photo she supplied is shown in Figure 7. Again, three images of the circle are seen through the calcite.

There is of course an important difference between the spheres and the specimens with plane surfaces (i.e. the rhomb and the polished block): the interface between calcite and air at the top of a sphere is curved, not planar. This interface is also curved where the sphere stands on the underlying circle, but as the gap between them is so small, the magnification is principally due to the convex lens formed by the top surface of the sphere. Because this calcite lens has two RIs, it also has two powers of magnification, hence two images of different sizes are seen near the centre of the sphere. In this view, the larger of these two circles is produced by the ordinary ray. The smaller circle is due to the extraordinary ray which, at right angles to the optic axis, is at its minimum RI (calcite is optically negative). The axes of the sets of rays forming each image do indeed coincide and the images are concentric, but the magnifications are not the same. Using a circle as the subject being imaged through the sphere allows the viewer to see the larger image separately from the smaller one whereas, had an X been used, the smaller image would merely have reinforced the larger one (see Figure 8).

The ray diagram in Figure 9 was constructed using the highest and the lowest RIs of calcite. (A detailed description of the preparation of this diagram is given in the Appendix.) The lines represent diametrically



Figure 7: A view through a 40 mm diameter calcite sphere resting on a 4 mm diameter circle looking normal to the optic axis displays the same effect as seen in the larger sphere in Figure 6. Photo by Elise A. Skalwold.

opposite rays from the sets forming each circle. The ordinary rays are shown in green and the extraordinary rays in red. The diameter of the small circle on which the sphere rests is indicated by a-a. The rays leaving the sphere represent those seen by a distant observer, so they are shown as parallel lines. (In reality, the camera was relatively close, and the rays toward it were thus convergent, so the description here is only approximate.) The image formed by the extraordinary ray is represented by b-b and that due to the ordinary ray is c-c. There is also a third, weaker, image of the circle, represented by d-d, near the periphery of the sphere. It is caused by another refraction path for the ordinary ray, as shown. Theoretically, there could be a fourth image further out due to the extraordinary ray, but this is not visible to the camera because its viewpoint is too close to the sphere, and therefore the image is ‘over its horizon’.

During the preparation of this article, the author obtained the 31.4 mm diameter calcite sphere that is



Figure 8: A calcite sphere (31.4 mm diameter) has been positioned over an X mark and is viewed here at right angles to the optic axis. Two images of different size overlap, with the smaller image reinforcing the larger one. Photo by H. Killingback.

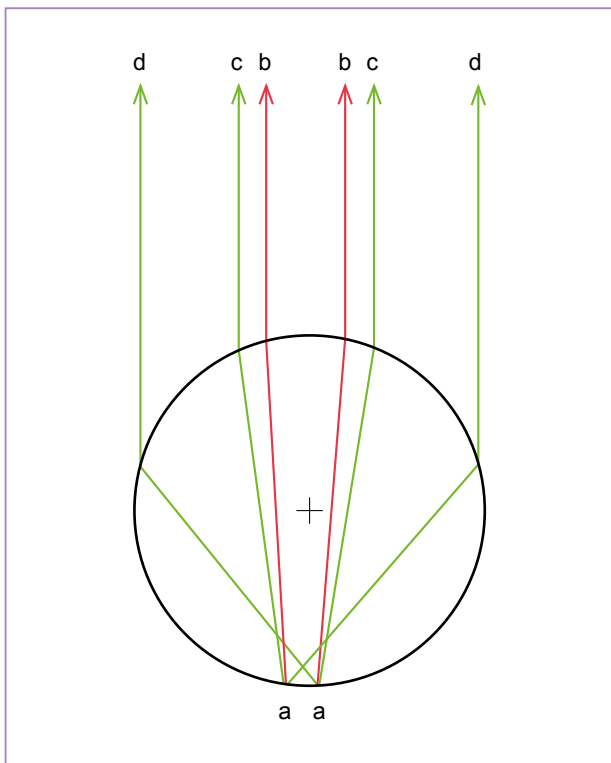


Figure 9: This simplified ray diagram shows a calcite sphere, with its optic axis horizontal, resting on a small circle (a-a). The green lines (d and c) represent the ordinary rays (RI = 1.658), and the red lines (b) are the extraordinary rays (RI = 1.486). The diagram demonstrates why we see three concentric images of the circle when viewed from above through the sphere.

depicted in Figure 10 (viewed at right angles to the optic axis). The sphere is shown resting on a circle of about 2 mm diameter. Another 2 mm circle is drawn to the upper left for comparison with the images seen through the sphere. Three images are visible, as with the other spheres, but the greater magnification resulting from the sharper curvature of this smaller sphere draws attention to the fact that the image due to the extraordinary ray is elliptical, rather than circular.

Figure 10a is taken at right angles to the optic axis, so the RI for the extraordinary ray is at its minimum, hence the smaller size of the central image. The shorter axis of the ellipse image lies in the direction of the optic axis (lowest RI, least magnification). Rotating the sphere on this axis does not alter the image seen, apart from the effects of cracks that come into view. However, if the calcite sphere is rotated a little, other than on the optic axis, the effects of differential magnification and of ray separation can both be seen, as shown in Figure 10b.

What if the Sphere Is Raised Above the Subject Circle?

When the sphere is raised above the surface on which the circle is drawn, the curvature of the lower surface of the sphere has a significant effect because then we are looking through a double convex lens. Figures 11 and 12 show views when the sphere is supported about 10 mm above a 2 mm diameter circle. Figure 11a shows the view when looking at right angles to the optic axis where the extraordinary ray has its lowest RI (1.486). Figure 11b is the same, with the addition of a London dichroscope, showing the two circle images are orthogonally polarised.

Figure 12 is a view along the optic axis, where the RIs of the ordinary and extraordinary rays are both the same (1.658), so there is only one image of the circle.

The ray paths were calculated by means like those described in the Appendix, extending the analysis to include refraction at the lower surface of the sphere. The result is portrayed in Figure 13, which shows that the larger of the central images is due to the extraordinary ray—not, as in Figure 9, to the ordinary ray. The calculated diameter of the image due to the extraordinary ray is 14.3 mm (i.e. a magnification of just over 7 \times) and that due to the ordinary ray is 6.3 mm (about 3 \times). The ratio of these diameters is 2.3. In the photo in Figure 11a, the

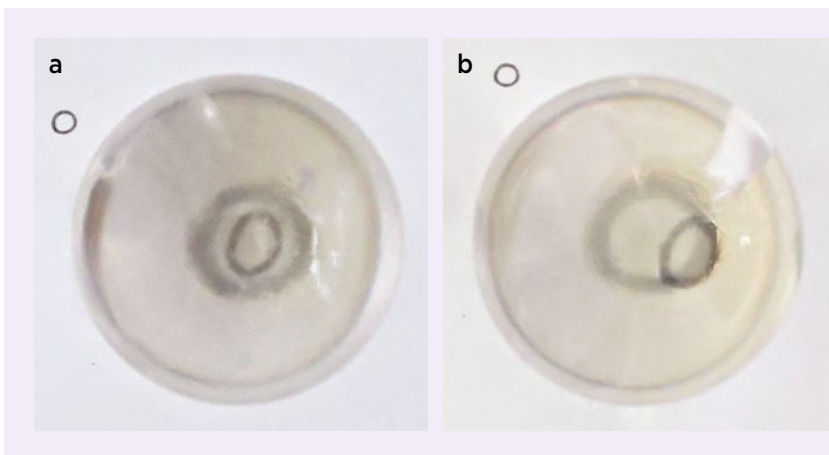


Figure 10: This 31.4 mm diameter calcite sphere is shown resting on a 2 mm circle. It is viewed (a) at right angles to the optic axis, and (b) after rotating the sphere slightly from being perpendicular to the optic axis, causing the extraordinary ray image to be offset. Photos by H. Killingback.

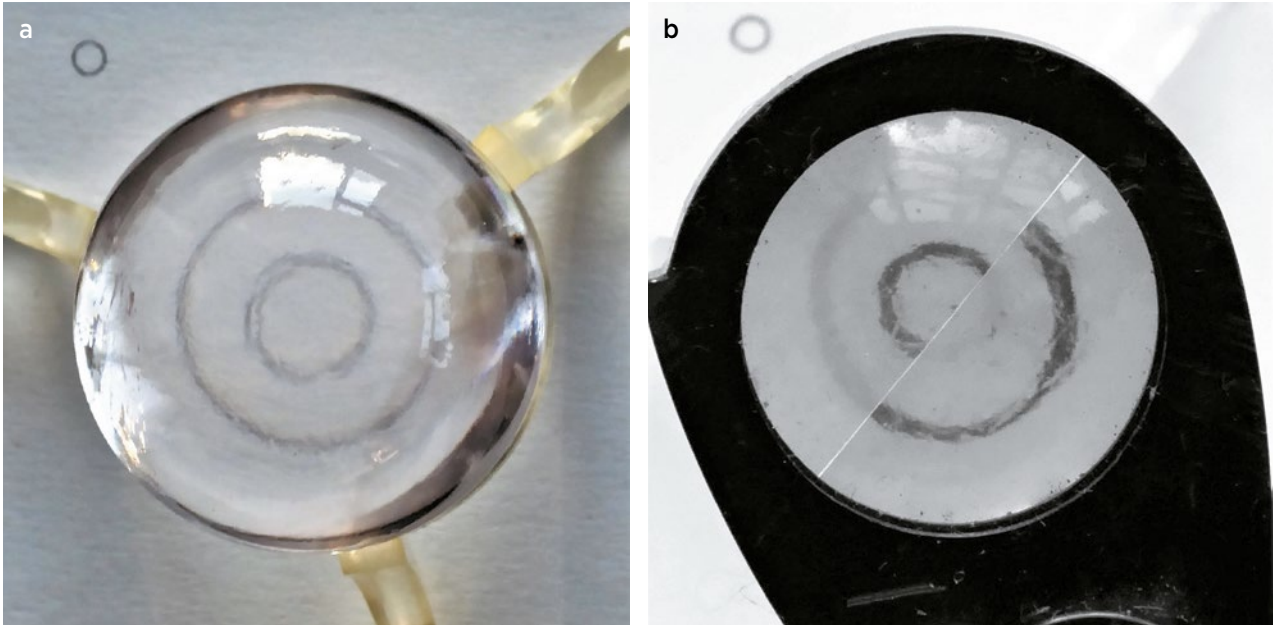


Figure 11: When the sphere is raised above the circle mark, the magnification of the circle images increases because the sphere acts like a double convex lens. (a) This is shown here for the 31.4 mm diameter calcite sphere, with the optic axis horizontal, which has been raised about 10 mm above a 2 mm circle. (b) Viewing the images through a London dichroscope confirms that the refracted rays are orthogonally polarised. Photos by H. Killingback.

ratio of these diameters is 2.6. In view of the acknowledged approximation of the basis for the calculations, these numbers are in sufficient agreement to provide confidence that Figure 13 gives an approximately true representation of the ray paths and allows us to visualise what is happening. Figure 13 does not include the possibility of images seen close to the periphery of the sphere.



Figure 12: Only one circle image is seen in the same sphere and setup as in Figure 11 but viewed in the direction of the optic axis, along which there is only one RI (1.658). Photo by H. Killingback.

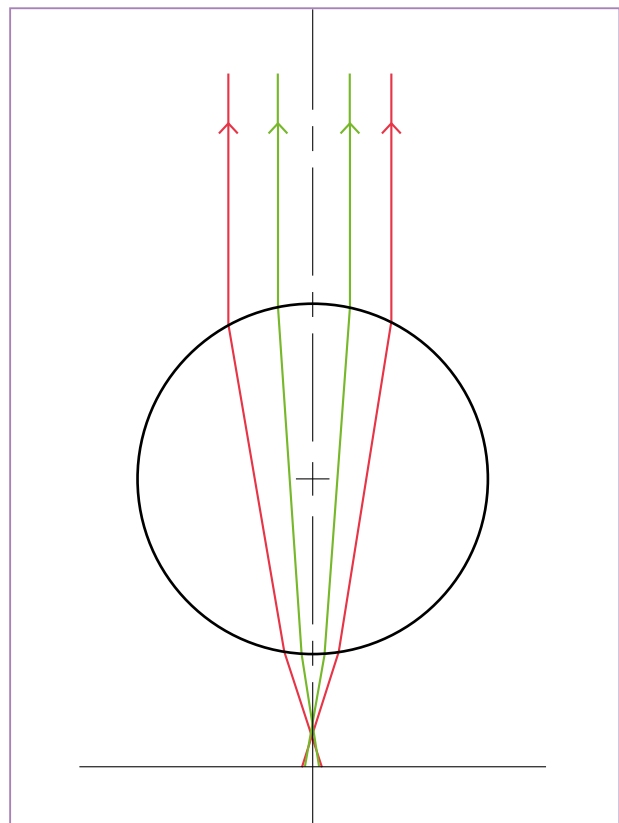


Figure 13: This diagram approximates the paths of the rays when the calcite sphere is raised above the circle mark. It demonstrates how the double-lens effect increases the magnification of the two concentric images of the circle. The larger image (red) is due to the extraordinary ray, rather than the ordinary ray (green); this is opposite to the positions of these rays seen in Figure 9.

CONCLUSIONS

When a light ray enters a birefringent uniaxial crystal at an angle other than along, or normal to, the optic axis, it is divided into two divergent rays. The maximum value of the separation angle between these rays is not determined by the value of either RI, nor by their difference (the birefringence), but by the ratio, Q , of the highest to the lowest RI, whether the crystal is optically positive or negative.

The rule that a double image cannot be seen when the crystal is viewed along or normal to the optic axis is not in question when the surface of the specimen is planar. It should be remembered, however, that if surfaces through which the rays pass are curved, the crystal acts as a lens, having two powers of magnification by virtue of its two RIs. For example, if a sphere with its optic axis horizontal stands on a circle mark, two concentric images of the circle are seen when

looking vertically downward. (A third, weaker image of the circle is seen near the periphery of the sphere, due to another refraction path for the ordinary ray.) It is recommended that when two or three concentric images are seen through a curved surface, the effect should not be referred to as *doubling* but rather as *differential magnification*.

From a practical viewpoint, this article may encourage authors of gemmological textbooks to provide a table of values of Q , not of birefringence. This article also provides a simple equation whereby an approximate value of the maximum angle of ray separation can be obtained for any transparent uniaxial crystal for which the maximum and minimum RIs are known. Finally, this article introduces the concept of differential magnification and warns against mistaking it for doubling when looking through a curved surface of any uniaxial stone.

REFERENCES

- Bartholini, E. 1669. *Experimenta Crystalli Islandici Disdiacastici Quibus Mira & Insolita Refractio Detegitur*. [Experiments on Doubly Refractive Crystals from Iceland in which Wonderful and Unusual Refraction Is Seen.] Hafniae (Copenhagen), Denmark, 60 pp.
- Killingback, H. 2014. The busy laser. *Gems&Jewellery*, **23**(3), 16–17.
- Skalwold, E.A. & Bassett, W.A. 2015. *Double Trouble: Navigating Birefringence*. Mineralogical Society of America, Chantilly, Virginia, USA, 20 pp.
- Sturman, D.B. & Back, M.E. 2002. Doubling of images in gemstones. *Journal of Gemmology*, **28**(4), 210–222, <http://doi.org/10.15506/JoG.2002.28.4.210>.

The Author

Harold Killingback FGA

Meadowside, 12 Church Lane, Brooke,
Oakham, Rutland, LE15 8RE
Email: haroldkillingback@btinternet.com

Acknowledgements

I am grateful to Robin Hansen (curator of Minerals and Gemstones, Natural History Museum, London) for contributing the photograph in Figure 6. Elise Skalwold (consulting gemmological curator, Earth and Atmospheric Sciences Department, Cornell University, Ithaca, New York, USA) is thanked for photographing the calcite sphere in Figure 7, and for her helpful comments as my work progressed. My thanks also go to Dr William A. Bassett (Professor Emeritus at Cornell University), who

contributed further comments. Marcus McCallum (Marcus McCallum, Hatton Garden, London) provided a rough piece of calcite and arranged for the 31.4 mm sphere in Figures 10–12 to be cut from it for this research. He also loaned the polished block of calcite shown in Figure 5. The anonymous reviewers of this paper made constructive suggestions that I was pleased to incorporate.

All this collaboration and support was most valuable for my research. As stated by John of Salisbury in 1159, ‘We are like dwarfs on the shoulders of giants, so that we can see more than they, and things at a greater distance, not by virtue of any sharpness of sight on our part, or any physical distinction, but because we are carried high and raised up by their giant size’ (as quoted in R. K. Merton’s *On the Shoulders of Giants*, 1965).

APPENDIX: CONSTRUCTION OF RAY DIAGRAMS FOR DIFFERENTIAL MAGNIFICATION

For simplicity, ray paths were calculated as seen by a distant observer. This means that the rays going to the observer were parallel to the line of sight. (In reality, the observer might be, say, 800 mm from the sphere, in which case the radius of the 31.4 mm diameter sphere would subtend an angle of 1.1° , which is not significantly different from 0° .)

Figure A-1 shows a ray A-B-C which could represent either rays a-b or a-c in Figure 9. Although what we see is light coming up through the calcite sphere, we can equally well envisage rays of light going down from the viewer's eye. Ray A-B, coming vertically down from a distant observer, meets the sphere at incident angle, i , or A-B-D. The angle of refraction, r (or C-B-O), can be calculated using Snell's Law, $n = \sin i / \sin r$, where n is the RI. Snell's Law was used for the extraordinary ray as well as for the ordinary ray because the views are perpendicular to the optic axis in this case.

Angle B-O-E = i , angle B-O-C = $180 - 2r$ and angle E-O-G = 180° , so angle COG is $2r - i$. Therefore C-G = O-C $\sin(2r - i)$. C-G is the radius of the circle on which the sphere rests. O-C is the radius of the sphere. The author made a guess of the incident angle, i , and calculated the angle of refraction, r , for each RI of calcite, and then worked out the associated values of C-G. This was repeated until a value of i was found that resulted in the correct radius for C-G. The light path is then A-B-C. (Because the sphere in this case is resting on the viewed circle, it is sufficiently accurate to ignore refraction at the lower interface. It is as if a circle of radius C-G were inscribed on the surface of the sphere.)

Figure 9 shows, in simplified form, the light paths A-B-C for both rays in the case of the 31.4 mm diameter sphere. It is resting on a 2 mm diameter circle, and we find i is approximately 19.0° for the ordinary ray and 10.7° for the extraordinary ray. The magnification produced at the top surface of the sphere is B-E / C-G. According to these calculations, this is about $5.1\times$ for the ordinary ray and $2.9\times$ for the extraordinary ray. Their ratio is about 1.75. The photos of this 31.4 mm diameter sphere in Figure 10 show rather fuzzy images and, as noted in the text, the circle image that is due to the extraordinary ray is elliptical. The observed ratios between the two images range from 1.7 to 2.0.

A similar geometric procedure was followed to investigate the circle d-d (ordinary ray) image in Figure 9. The calculated radius of this image is 15.15 mm—very close to the size of the radius of the sphere (15.70 mm). The radius of an image due to the extraordinary ray was calculated to be approximately 15.69 mm, so it is no wonder that it cannot be seen by the camera taking the photo in Figure 10, as it would be over the horizon.

By the same methods, the ray diagram in Figure 13 was constructed. It predicts the ordinary ray image diameter to be approximately 6.3 mm and that for the extraordinary ray image to be 14.3 mm, a ratio of 2.3. From Figure 11a, the ratio of the actual image sizes seen by the camera is 2.6.

Close agreement cannot be expected when comparing the results from photographs taken about 800 mm from the sphere with those calculated from simplified assumptions, including having the observer at an infinite distance from the sphere (rays between observer and sphere being parallel). The author suggests, however, that the ray diagrams are sufficiently accurate to allow us to visualise how the images are formed.

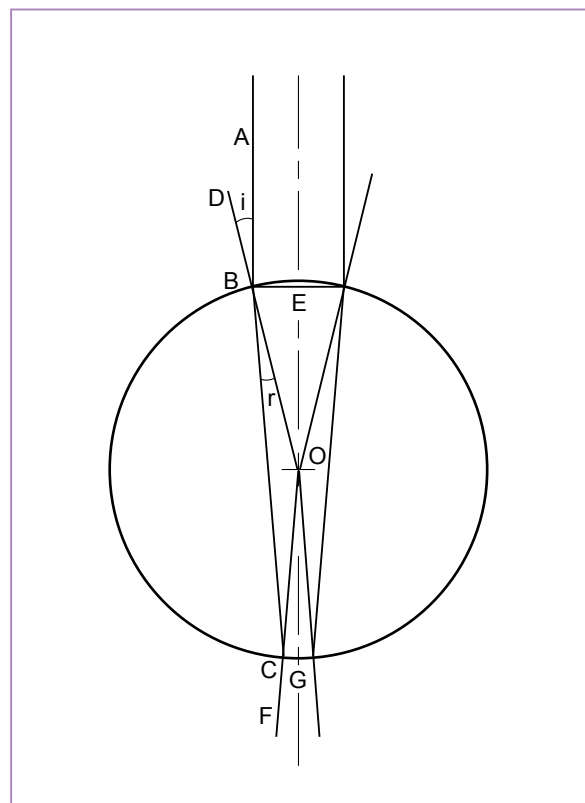


Figure A-1: This ray diagram shows in greater detail how Figure 9 was created.

An innovator in gemstone reporting

- Identification of colored gemstones • Country of origin determination • Full quality and color grading analysis



AMERICAN GEMOLOGICAL LABORATORIES



580 5th Ave • Suite 706 • New York, NY 10036, USA
www.aglgemlab.com • +1 (212) 704 - 0727

Conferences

SCOTTISH GEMMOLOGICAL ASSOCIATION 2019 CONFERENCE

The annual conference of the Scottish Gemmological Association (SGA) took place in Cumbernauld, Scotland, 3–6 May 2019. The conference was organised by the SGA board, and featured eight speakers and several workshop presenters (e.g. Figure 1). Attendance at the SGA conference has grown significantly in recent years, and this year achieved a new high of more than 120 delegates, not only from the UK but also many other countries.

A Friday night welcome cocktail reception was followed by an informative and entertaining talk by **John Benjamin** (John C. Benjamin Ltd, Aylesbury, Buckinghamshire), covering a broad range of jewellery history from Elizabeth I of England through Elizabeth Taylor. A familiar contributor to the popular British television programme *Antiques Roadshow*, Benjamin provided a number of humorous anecdotes as he guided the audience through centuries of jewellery history.

On Saturday morning, **Christopher Smith** (American Gemological Laboratories [AGL], New York, New York, USA)—the keynote speaker of this year's SGA conference—discussed the clarity enhancement of emeralds. There have been many debates and much misinformation

circulating about emerald treatments through the years, so this talk highlighting actual examples from AGL's case studies was helpful for sorting out points of confusion about these enhancements. Smith effectively educated gemmologists regarding filler types, as well as how they are added to stones by the treaters, their visual impact and their stability. His talk also covered how to identify the filler type and determine its effect on an emerald's apparent clarity.

The second presentation was given by **John Andrew**, curator of the Pearson Silver Collection, which is devoted to post-World War II British silver. He presented work from Maureen Edgar's enamelling career, which started in the 1950s. In the following decades, she became one of the best enamel artists in Scotland and produced an impressive collection of work until 2000. Some of her pieces were displayed during the conference for attendees to examine and enjoy.

Alex Grizenko (Lucent Diamonds Inc., Los Angeles, California, USA) presented an elaborate timeline of synthetic diamond production, starting with Lavoisier's diamond structure discovery in the 18th century. He continued through the failed attempts prior to World War II and, following the announcement of General Electric's success in the mid-1950s, the subsequent development of better synthesis methods, including a chronology of both



Figure 1: Members of the SGA board and some of the speakers/workshop presenters gather at the SGA conference's Saturday evening event (Ceilidh Night). From left to right, in the front row are Sylvia Gumpesberger, Dr Çiğdem Lüle, Alan Hodgkinson and Jan Calligan, and behind them are David Callaghan, Christopher Smith, Alex Grizenko, Stuart Robertson, Dr Jack Ogden, Ewen Taylor, Alistair Tait and Clare Blatherwick. Photo by Kim Rix.

HPHT and CVD growth technologies. He then reviewed synthetic diamond-producing companies and how their products were subject to colour treatments until colourless synthetic diamond was finally commercially produced in 2012. Grizenko also discussed identification challenges and techniques for synthetic diamonds.

Stuart Robertson (Gemworld International Inc., Glenview, Illinois, USA) gave an update on gem market trends, observations from the 2019 Tucson gem shows and the effects of the global economy on the gem industry. His presentation covered not only the gem side of the business but also some of the people, especially small-scale miners, who are involved in the global market. The growing awareness of 'fair trade' goods and ethical mining is important to the market, but it is also giving rise to unintended consequences. While some attempts and practices hit the target, others seem to exist as added-value labels devoid of any meaningful action. And still others are leading to a consolidation of the supply chain that could freeze out participation by the small-scale miners altogether. Therefore, Robertson indicated, it may be wise to ask, 'Fair trade? Fair for whom?'

Sylvia Gumpesberger (Toronto, Ontario, Canada) gave an engaging presentation on the use of light sources with various filters throughout gemmological history and how today's LED technology affects our daily work. She discussed the pros and cons of LED illumination, and demonstrated several applications in which LED lighting is suitable for gemmology. The audience then joined in to experiment with diffraction-grating glasses and various light sources. Encouraged by the practicality and low cost of LED lighting options, gemmologists should be aware of the benefits as well as the limits of LEDs when using them with basic tools.

The day concluded with an engrossing presentation by **Dr Jack Ogden** (Society of Jewellery Historians, London). He started with a history of diamond mining and emphasised how important diamonds were for reasons other than adornment. He provided a detailed history of many famous diamonds, such as the Pigot, Hornby and Nassak, including their questionable journeys to London from India, and how they ended up in early lottery schemes to generate money, were presented as diplomatic gifts, and even used in bribery.

The second day of the conference (Sunday) began with a presentation on developments in colour communication for gemmology given by **Christopher Smith**. He discussed his new colour-reference system called ColorCodex, which after more than three years in development provides an innovative system for describing the colour of transparent faceted coloured gemstones. He explained

the challenges of colour communication in gemmology and the limitations of previous attempts at producing comprehensive colour systems for the trade. ColorCodex offers a unique approach by addressing the depth and internal reflections of a faceted stone. It provides an intuitive comparison environment with well-defined numeric codes rather than ambiguous colour names.

Clare Blatherwick (independent jewellery consultant, Edinburgh, Scotland) gave a vibrant and enchanting presentation on how jewellery making has been inspired by nature (especially flowers) through millennia. Techniques and cultural meanings might have changed over time, but humans have continuously been inspired by their surroundings and natural habitat.

Sunday morning's programme closed with an award ceremony for gemmology students and GemSet 2019 winners. This jewellery design competition encourages many young people to join the gem industry.

As in the past, this year's SGA conference concluded with Sunday afternoon workshops. Ranging from specialised talks to hands-on sessions, they were well attended. The workshop presenters included **David Callaghan, Kerry Gregory, Pat Daly, Tammy Cohen, Tatiana Conte** and **this author**, as well as many of the speakers from the previous day. An optional excursion on Monday visited the recently opened V&A museum branch in Dundee, Scotland, which features Scotland's design heritage.

*Dr Çiğdem Lüle FGA DGA
(clule@kybelellc.com)
Kybele LLC, Buffalo Grove,
Illinois, USA*

5TH MEDITERRANEAN GEM AND JEWELLERY CONFERENCE

The 5th Mediterranean Gem and Jewellery Conference (MGJC) was held under the Mediterranean sun of Limassol, Cyprus, 17–19 May 2019. As in previous years (i.e. in Greece, Spain, Italy and Montenegro), the conference was organised by **George Spyromilios** (Independent Gemological Laboratory, Athens, Greece) and **Branko Deljanin** (CGL-GRS Swiss Canadian Gemlab, Vancouver, British Columbia, Canada). The event attracted 75 gemmologists, appraisers, traders and others interested in the gem industry. Those who arrived early were introduced to some of the island's history with a visit to Roman ruins at Kurion, where a 'bonus' was provided by an army battalion being photographed in the amphitheatre.

Half-day workshops were held before and after the conference. This year an opal workshop (Figure 2) was instructed by **Gail Brett Levine** and **Travis Lejman** (National Association of Jewelry Appraisers, Rego Park, New York, USA), with many samples available that allowed participants to examine different types of opal—including material from different sources, as well as treated and synthetic specimens. An afternoon workshop on ruby, sapphire and emerald, presented by **Branko Deljanin**, focused on treatments and synthetics. As the sun set, a welcome cocktail party by the conference hotel pool saw delegates from 24 countries meeting friends old and new.

The next morning, the conference opened with an overview of previous MGJCs by **Branko Deljanin**. **Yianni Melas** (Limassol, Cyprus) chaired this year's conference, introducing speakers and adding anecdotes of his experiences with them. He is known in the trade for sourcing gem material from remote localities and championing fair trade for artisanal miners.

Olga Okhrimenko (OctoNus, Moscow, Russia) outlined what she believes is the reason for a stagnating diamond industry: most customers only purchase a diamond once in their lifetime. Okhrimenko postulated that with the vast majority of diamonds being round brilliants, consumers are not educated about the variety of shapes and cuts that can generate different levels of brilliance, fire and scintillation. Such awareness, she believes, would excite consumers to return for repeat purchases. **Roman Serov** (OctoNus) followed with proposed solutions in the form of in-store displays to educate consumers about cut options, although he conceded that the stock carried by most jewellery stores consists exclusively of round brilliants, with no option to 'test drive' alternative cuts.

This author described the various processes that a rough diamond undergoes during its transformation to a faceted gem. He highlighted how technology and lasers have transformed the industry for cut planning as well as sawing/cleaving and bruting operations, and how polishing on scaifes remains the most time-consuming step of the process. He also showed how the processing time varies as a function of rough diamond size and type.

Dr Michael Schlamadinger (Swarovski, Wattens, Austria) reviewed the synthetic diamond industry, starting with a snapshot of how China now produces 10 billion carats annually from more than 10,000 presses. While they are typically of industrial quality, the addition of a 'nitrogen getter' into the growth medium can enable the growth of colourless synthetic diamonds. CVD production has become a force in the industry, with WD Lab Grown Diamonds (Washington DC, USA) boasting



Figure 2: Held just prior to the MGJC, a workshop on opals was conducted by Gail Brett Levine (standing centre) and Travis Lejman (standing right). Photo by Branko Deljanin.

more than 200 reactors. Dr Schlamadinger cited a study that found the energy needed to mine diamonds is about twice that for growing synthetics. An overview of the technical applications for synthetic diamonds showed various alternatives to gem use.

Garry Holloway (Holloway Diamonds, Melbourne, Australia) described his new parameter for judging diamond cut: 'looks like' as a measure of the apparent diameter of a faceted diamond, which can be affected by the amount of light reflection near the periphery of a stone. Poorly cut diamonds look smaller than they actually are, as can be measured using computer simulations. To demonstrate the message, he handed participants two CZs of the same weight. One was a Tolkowsky-cut brilliant while the other had a deeper pavilion, resulting in a physically smaller diameter but also lower light return near the periphery. Relying on a 'Triple X' cut grade is no assurance of a good cut, as was illustrated by a diamond with a 65% height that showed poor periphery reflection.

Dr Katrien De Corte (HRD Antwerp, Belgium) delivered a short 'sponsor' talk on detecting near-colourless CVD-grown synthetic diamonds. A notable characteristic is an absorption and PL peak at 737 nm attributed to silicon, but it is not always present or conspicuous. However, in an HRD study of 150 samples at liquid-nitrogen temperature, a PL peak at 467 nm was always present in these CVD synthetics. DiamondView images showed blue, orange and red fluorescence, with the blue not always exhibiting phosphorescence.

Sergey Buks (Alrosa, Moscow, Russia) also gave a short 'sponsor' presentation on the Alrosa Diamond Inspector, a recent addition to his company's line of instruments for detecting synthetic diamonds. Their system is based on three spectroscopic measurements applicable to individual 0.03–10 ct colourless diamonds and simulants, both loose and mounted.

After lunch, **Dr Stefanos Karampelas** (Bahrain Institute for Pearls & Gemstones [DANAT], Manama) reported on how his lab collects and labels samples for their research database. The lab's activities are not limited to pearls, and Dr Karampelas also reported research on the heat treatment of amber at 180–220°C.

Edward Boehm (Rare Source Gems, Chattanooga, Tennessee, USA), explored the sustainability of the gem industry. He noted that 80% of coloured-stone production comes from artisanal diggers, while only 20% is derived from large-scale mining. Origin is an important consideration for consumers and there are several methods to assess it, including gemmological evidence (e.g. inclusions) and blockchain technology. However, blockchains do not support artisanal miners, and trade anonymity along the supply chain is compromised.

Abeer Al-Alawi (DANAT), with **Dr Stefanos Karampelas**, focused on the Bahrain pearl industry, which dates back centuries, to the oldest documented pearl being from 5500 BCE. The industry there is protected by prohibiting the trade of cultured pearls, which make up 99.8% of global production. In 2018, 2 million pearls were harvested in Bahrain, with only one in 100 molluscs bearing a pearl. The formation of natural pearls is stimulated not by an irritating grain of sand (as is commonly believed), but by a malfunctioning organ. Karampelas gave an overview of pearl colour, lustre, shape and surface texture—the last potentially enhanced by ‘pearl doctors’ who can transform a damaged surface by sanding and polishing.

Stefan Müller (DSEF German Gem Lab, Idar-Oberstein, Germany) described various items seen in his laboratory. He noted that emeralds from Ethiopia can be separated from those of other deposits such as Zambia and Brazil by their trace elements measured with EDXRF, and that the majority of rubies currently in the trade are from Mozambique. The main treatments applied to gem corundum are heating and fracture filling with borax, glass, oil or resins. In some instances, the heat of a lamp can cause bubbles to form within oiled fissures, as was clearly shown in a video clip. He also shared cautionary experiences with a garnet-glass doublet, rough diamond imitations and a foil-backed beryl.

Dr Clemens Schwarzingger (Johannes Kepler University, Linz, Austria) is a master cutter and gave some insights into precision gem cutting, an art rarely recognised in a trade that pays by the carat. He showed examples of poor cuts, and blamed inferior equipment for asymmetric outlines and bad facet ‘meet points’. He receives inspiration for his award-winning designs from plants and architecture, while the smoothest

finishes are achieved by polishing with 250 nm grit, which produces ‘scratches’ with widths less than the wavelength of visible light. Soft gems are harder to polish, while other challenges are presented by complex stones such as colour-zoned tourmaline, which can show a brown appearance if faceted incorrectly. He lamented that precision cutting is unlikely to be recognised as long as there is no grading system for gemstone cuts that rewards cutters financially. Dr Schwarzingger brought several of his gemstones to show the audience during conference breaks (Figure 3).

Dr Gamini Zoysa (Ceylon Gemmological Services, Colombo, Sri Lanka) shared his expertise on ruby and sapphire and their value. He showed examples of rubies from different deposits, of which the Thai/Cambodian ones are almost exhausted. Rubies from his Sri Lankan homeland show distinctive photoluminescence compared to those from Mozambique, which dominate the market. He stated that generally all basaltic sapphires are heat treated. Yellow sapphires can be much larger than blue, being up to 40–50 ct, but their prices are about one-third those for blue sapphires. Photos of violet, purple and colour-change sapphires were shown along with price tables and auction examples.



Figure 3: Master cutter Dr Clemens Schwarzingger exhibited a collection of his precision-cut gemstones at the MGJC. Photo by J. Chapman.

Two short talks followed, with **Yuri Shelementiev** (MSU Gemological Center, Moscow, Russia) announcing a gem excursion to the Ural Mountains that will be held in 2020, and **Elena Deljanin** (Gemmological Research Industries Inc., Vancouver, Canada) describing ‘philosophical stones’ polished by master cutter Victor Tuzlukov. **Mark Cullinan** (Cullinan Diamonds, Monaco) took the podium briefly to describe the background of the Cullinan diamond. He passed around a model of the 3,106 ct rough diamond for participants to examine.

The last speaking event was a round-table discussion on ‘Manufacturing Gems and Diamonds in the 21st Century’, which included panellists **Garry Holloway**, **Sergey Sivovolenko** (OctoNus, Finland), **Yuri Shelementiev**, **Clemens Schwarzing** and Israeli diamond polisher **Moish Lempel**. **This author** acted as moderator, and initiated discussions surrounding gem cuts, including whether price guides rather than beauty dictate polishers’ choices, and how consumers could be better educated to appreciate cut. Discussions considered lab reports, consumer engagement, online sales, experiences selling fancy cuts and retailer knowledge. **Antoinette Matlins** (South Woodstock, Vermont, USA) from the audience was vocal on her views about how customers perceive diamonds, so she was invited to join the panel.

Sunday featured more workshops. **Sergey Sivovolenko** and **Roman Serov** demonstrated the factors that affect a faceted diamond’s beauty, with the aid of custom lighting and viewing equipment. **Branko Deljanin** ran concurrent workshops on identifying synthetic and treated diamonds with the use of standard and advanced instruments.

Some delegates joined a post-conference tour to the capital of Cyprus, Nicosia. In addition, a group of 20 people continued on a special three-day tour to Israel, guided by **Branko Deljanin** and **Moish Lempel**. Participants had a chance to see large diamonds being cut at the DDS factory in Ramat Gan, followed by a tour of Sarine Technology by the manager, **David Block**. They also visited the trading floor at the Israeli Diamond Bourse, where Deljanin delivered a talk on the provenance of pink diamonds and synthetic diamonds to about 100 bourse members. A tour of Jerusalem and a local CVD growth facility completed the week-long conference events.

The next MGJC will be held in Greece, on 15–17 May 2020. Details will be posted on the conference website (www.gemconference.com) as they become available.

*John Chapman (john@gemetrix.com.au)
Gematrix, Perth, Australia*

AGA LAS VEGAS

The Accredited Gemologists Association’s (AGA) 2019 Las Vegas conference took place on 31 May during the JCK Show in Nevada, USA. This year’s event was attended by 58 people and featured three speakers. The conference was opened by AGA past-president **Donna Hawrelko**, whilst AGA president **Stuart Robertson** introduced the speakers.

Shane McClure (Gemological Institute of America [GIA], Carlsbad, California, USA) described the visual characteristics of heat treatment in gem corundum according to three different temperature categories: low (up to 1,200°C, when rutile needles start to be affected), high (1,200–1,700°C) and extreme (1,700–1,850°C). Corundum heated under extreme temperature is easy to identify because the inclusions are pervasively damaged. Furthermore, high-temperature heat treatment is not difficult to distinguish if certain features are present, such as dissolved rutile (leaving lines of points and/or blotchy colour zoning), ‘snowballs’ (indicating former uraninite crystals) and glassy discoid fractures. Low-temperature heating may not be possible to detect visually unless damage is evident in carbonate or diaspore inclusions. McClure also described some recent low-temperature heating experiments on Mozambique ruby, as well as low- to high-temperature experiments on blue sapphires (including heating with pressure).

Dr Thomas Hainschwang (GGTL Laboratories, Balzers, Liechtenstein) reviewed diamond colour treatments and then provided an update on his ambitious project to record detailed measurements on a wide variety of diamond types before and after irradiation, annealing and/or HPHT processing. Importantly, the creation of the N3 centre (and resulting blue fluorescence) provides a clue for HPHT treatment in both natural and synthetic type Ib diamonds.

Dror Yehuda (YehudaDiamond Co., New York, New York, USA; Figure 4) described various diamond testers/detectors and gave some results for several instruments that have been evaluated so far by the Assure Program. (*Editor’s note:* See the article on pp. 606–619 of this issue for more on this topic.) He then focused on diamond testing with his company’s Sherlock Holmes 2.0 device. The instrument uses fluorescence and phosphorescence to distinguish between natural and synthetic diamonds, as well as some simulants (cubic zirconia and synthetic moissanite). The results require some interpretation from the user, although red markings shown on the device’s screen make it relatively straightforward to detect the presence of synthetics and simulants in loose parcels and mounted jewellery.



Figure 4: Dror Yehuda delivers his presentation at the AGA Las Vegas conference. Photo by B. M. Laurs.

The conference concluded with hands-on opportunities for attendees to examine natural and synthetic diamonds using various instruments, including the GemmoRaman-532SG by Magilabs, the Diamond Inspector by Alrosa, the D•Secure by DRC Techno and the Sherlock Holmes 2.0.

Brendan M. Laurs FGA

EUROPEAN GEMMOLOGICAL SYMPOSIUM 2019

The 7th European Gemmological Symposium took place on 24–26 May 2019 in Idar-Oberstein, Germany, and was attended by 200 participants from more than 20 countries. The conference was hosted by the German Gemmological Association (Deutsche Gemmologische Gesellschaft E.V., or DGemG) and the German Foundation for Gemstone Research (Deutsche Stiftung Edelsteinforschung/DSEF German Gem Lab), and celebrated the 50th anniversary of the DSEF German Gem Lab. The programme featured 17 invited speakers (Figure 5) who delivered presentations over a two-day period.

The opening ceremony included three lectures. **Dr Thomas Lind** (president of DGemG and chairman of the board of the DSEF German Gem Lab) recounted the history of DGemG and the DSEF German Gem Lab, and also chronicled the European Gemmological Symposium—which initially took place in Idar-Oberstein in 2007 to mark the 75th anniversary of DGemG.

Next, **Frank Frühauf** (Lord Mayor of Idar-Oberstein and patron of the conference) welcomed the attendees to the beautiful town of Idar-Oberstein. Then **Dr Gaetano Cavaliere** (president of CIBJO—The World Jewellery Confederation) described the history of CIBJO and its role as the ‘United Nations of the jewellery industry’, in which it represents 20 countries and nearly 100 million people who are working in the gem and jewellery business.

Hans-Jürgen Henn (Henn GmbH, Idar-Oberstein) gave the keynote speech, titled ‘A Gem of a Life’, in which he described how gems are brought to market by recounting his personal experiences with sourcing coloured stones from around the world. Timeliness, luck and financial liquidity through partnerships with others have all benefited his dealings. One of his proudest accomplishments was sourcing a 26 kg aquamarine from Teófilo Otoni, Brazil, which was subsequently carved into the ‘Dom Pedro’ by Bernd Munsteiner and donated to the Smithsonian Institution in Washington DC, USA, where it is seen by millions of people annually.

Dr James Shigley (GIA, Carlsbad, California, USA) discussed synthetic diamonds, including their types, characteristics and identification. He indicated that the main concerns surrounding these products are their accurate identification, disclosure in the supply chain and appropriate pricing. The three main categories of synthetic diamonds include those larger than 5 ct (which are quite rare in the market), those ranging from 0.2 to 2.5 ct (i.e. commercial sizes that are commonly submitted to gemmological laboratories) and melee (<0.20 ct, which pose the greatest identification challenge to the industry).

generation of large tourmalines followed by a second generation of smaller crystals that are less abundant but of higher quality. Most of the rubellite-bearing granitic pegmatites are rather small, although one famous locality—the Anjanabonoina pegmatite—is quite large, and in 2018 it produced well-formed rubellite crystals weighing up to 26 kg.

Dr Tobias Häger and co-authors (Institute of Geosciences, Johannes Gutenberg University Mainz, Germany) reviewed the localities and gemmological properties of Colombian emeralds. He showed photomicrographs of characteristic three-phase inclusions and explained how UV-Vis-NIR spectra indicate that type I H₂O is much more abundant than type II H₂O in these emeralds. While it is not currently possible to differentiate emeralds according to individual mines, in the future stones from different belts in Colombia may be distinguishable.

Dr Daniel Nyfeler (Gübelin Gem Lab, Lucerne, Switzerland) described technologies for tracing and tracking gems along the supply chain, including the Emerald Paternity Test and Provenance Proof blockchain (see Conferences section of *The Journal*, Vol. 36, No. 5, 2019, p. 472).

Dr Claudio Milisenda (DSEF German Gem Lab) provided a review of spectroscopic research at DGemG and the DSEF German Gem Lab. The early history included contributions by Georg O. Wild, Prof. Dr Karl Schlossmacher and Prof. Dr Hermann Bank, and also involved collaborations with Heidelberg University and the German state of Rhineland-Palatinate. More recently, work has focused on the photoluminescence spectroscopy of alexandrite and Cu-bearing tourmaline, as well as the UV-Vis-NIR spectroscopy of Santa Maria-type aquamarine, spessartine from Namibia and rhodolite from various localities.

Dr Michael Krzemnicki (Swiss Gemmological Institute SSEF, Basel) explained how his lab differentiates between different colour varieties of gems. SSEF distinguishes some gems based only on colour (ruby vs. pink sapphire and padparadscha vs. pink, orange or fancy-colour sapphire), and others based on colour and spectroscopy (Co-spinel vs. blue spinel, emerald vs. green beryl and alexandrite vs. chrysoberyl). Such differentiations depend on employing standard procedures regarding the light source and observer, and the use of internal standards (e.g. master stones or colour charts) that correspond to the gem variety being observed.

Tom Stephan (DGemG) discussed his Ph.D. research on the role of V³⁺ in gems that are mainly coloured by Cr³⁺. He used spectral fitting to subdivide overlapping absorption bands and to describe/calculate colour in ruby and emerald. He found that V³⁺ intensifies the colour of

both gem varieties, while also producing a more violetish hue in ruby and a purer green hue in emerald.

Kenneth Scarratt (Bahrain Institute for Pearls & Gemstones [DANAT], Manama) described an October 2018 trip by two of his co-authors to acquire and characterise natural pearls from Australia. They joined a commercial shell- and meat-gathering expedition for *Pinctada maxima* near Darwin, where the processing of 6,837 molluscs yielded 793 natural pearls. The pearls formed in various parts of the molluscs, including the hinge, adductor muscle, mantle lip and gut areas.

Dr Ahmadjan Abduriyim (Tokyo Gem Science, Tokyo, Japan) summarised the history and gemmological characteristics of freshwater cultured pearls from Lake Kasumigaura, Japan. Currently 37 kg/year are produced from three farms, and the cultured pearls range from 11 to 15 mm with a nacre thickness of ~3 mm. Similar cultured pearls from China can be differentiated by plotting their Ga vs. Ba content.

The conference also featured a diploma ceremony for current DGemG graduates that was conducted by **Dr Thomas Lind**. At the end of the graduation ceremony, DGemG's coveted Golden Needle of Honour was presented to **Prof. Dr Henry Hänni** by **Dr Thomas Lind** and **Dr Ulrich Henn** (Figure 6).

Brendan M. Laurs FGA



Figure 6: Dr Ulrich Henn (left) and Dr Thomas Lind (right) present the Golden Needle of Honour award to Prof. Dr Henry Hänni. Photo by B. M. Laurs.

Gem-A Notices

Gifts to the Association

Gem-A is most grateful to the following for their generous donations that will support continued research and teaching:

Rui Galopim de Carvalho, Portugal, for a selection of jewellery, rocks and minerals.

Roland Naftule, USA, for eight synthetic sapphire/strontium titanate doublets.

Olivier Segura, France, for four books: *For the Love of Jewelry* by Jean-Noël Mouret; *The Art of the Jeweller* by Guillaume Glorieux; *Flora, The Art of Jewelry* by Patrick Maurières and Évelyne Possémé; and *Fauna, The Art of Jewelry* by Patrick Maurières and Évelyne Possémé.

Ian Thomson, UK, for a selection of 20 carved pillboxes, two carved resin figures imitating ivory and an original boxed Rayner UV lamp set.

Kathryn Wyatt, Australia, for three publications: *A Field Guide to Australian Rocks, Minerals & Gemstones* by Wolf Mayer; *Collecting Australian Gemstones* by Bill James; and an issue of *Australian Gemmologist*.

We are also particularly thankful to the family of the late **Mr Irwood** of West Finchley, London, who donated an extensive collection of fluorescent minerals, amounting to 111 in total, along with four publications: *Journal of the Fluorescent Mineral Society 1977*, *Ultraviolet Guide to Minerals* by Sterling Gleason, *Collecting Fluorescent Minerals* by Stuart Schneider and *The Story of Fluorescence* by Harry Wain.

Gem-A Confirms Oldest-Known Carved Tourmaline at the Ashmolean Museum, Oxford

In July 2019, Gem-A Tutor Pat Daly FGA and Operations Manager Charles Evans FGA DGA visited Oxford's Ashmolean Museum to study a unique and highly significant carved tourmaline. Gem-A's expertise had been requested by Gloria Staebler (co-founder of the mineralogy publishing house, Lithographie), who had been researching the piece for an upcoming publication titled *Rubellite—Tourmaline Rouge*.

The 2.4 cm-wide intaglio depicting Alexander the Great in profile was suspected to be a carved tourmaline, although the stone had never been subjected to gemmological testing. Based on the quality and accuracy of the portrait, along with the presence of an ancient Indian script in the carving, the intaglio is thought to date to the period of the famed king's reign (circa 334–323 BCE).

The study at the Ashmolean Museum brought about a landmark gemmological finding as observations by Daly and Evans, aided by a GemmoRaman spectrometer, confirmed that the stone was indeed a red-yellow tourmaline, making it the earliest known use of tourmaline as an ornament. For further information on the Ashmolean Museum's historic intaglio and Gem-A's involvement in the research visit <https://gem-a.com/news-publications/news-blogs/news/industry/gem-a-confirms-oldest-known-carved-tourmaline-intaglio>.



A red-yellow tourmaline intaglio depicts the profile of Alexander the Great. Photo by Charles Evans.

Gem-A Annual General Meeting

The Gem-A AGM will be held Wednesday 30 October 2019 at etc.venues The Hatton, 51–53 Hatton Garden, London, EC1N 8HN. We look forward to welcoming Gem-A Members to the Emerald Suite on the second floor for drinks from 18:00. The AGM will commence at 18:30.

No further action is required at this stage but please add this date to your diary. AGM documentation and nomination for election information will be released soon.

Gem-A's Webinar Debut

On 18 July 2019 Gem-A hosted its first of a series of brand new webinar sessions live from our London headquarters. Gem-A Tutor Pat Daly FGA presented 'Introduction

to Gemstones', a beginner's gemmology lesson, which explained the physical characteristics, origins and vital care techniques of popular gems including sapphire, emerald and ruby. The 45-minute session was followed by a 15-minute Q&A and provided a free taster of our renowned gemmology courses to attendees across the world, reaching as far afield as Brazil, Indonesia and Australia.

Our next webinar, 'Introduction to Diamonds', will be held 10 October 2019 and will explain how diamonds are formed, what makes them special, and how to assess their value and qualities using the 4Cs: cut, colour, clarity and carat weight. This beginner's session will be ideal for a diamond enthusiast who has no prior gemmological knowledge. Keep an eye on our website for details on how to register.

Obituary

Professor Dr Hermann Bank 19 January 1928 – 14 August 2019



The esteemed member of the global gemmological community, published author and proactive member of the German Gemmological Association passed away in August 2019.

The Journal of Gemmology is saddened to announce the passing of Professor Dr Hermann Bank. Born in Idar-Oberstein in January 1928, Prof. Dr Bank was inspired by the gemmological heritage of his hometown and chose to study both geology and mineralogy at Johannes Gutenberg University in Mainz, Germany, and at ETH Zurich (Swiss Federal Institute of Technology) in Switzerland. In 1953, Prof. Dr Bank secured a Ph.D. in geology and was named the very first German Fellow of the Gemmological Association of Great Britain, before later being awarded honorary membership.

Following the completion of his Ph.D., Prof. Dr Bank became a leading light within the European gemmological community. The 1960s were a particularly exciting decade: he became partner and managing director of gemstone-cutting company Gebrüder Bank; joined the International Gemmological Conference (IGC) committee; and was named president of the German Gemmological Association and chairman of the German Foundation for Gemstone Research.

Prof. Dr Bank continued to lend his efforts to leading and inspiring those around him, while encouraging a sense of cooperation among European and global gemmological organisations. In 1996, he was named chairman of the Federation for European Education in Gemmology (FEEG), and by 2003 was honorary president of both the German Gemmological Association and FEEG. His honorary memberships were vast, including gemmological associations and gem trade organisations in Japan, the United States, Brazil, France and Poland. His passionate dedication to gemmological education and continued learning was an inspiration to his colleagues, peers and contemporaries, including Gem-A staff and Members.

For a man with such impressive accolades and achievements, including two Crosses of the Order of Merit of the Federal Republic of Germany, more than 1,000 published articles and seven books, Prof. Dr Bank never lost sight of his broader goals: to connect the gem and jewellery sectors with the science of gemmology. He envisioned the popularisation of gemmology in a way that furthered understanding for all, and eagerly pursued his own research projects while teaching the next generation. Friends and colleagues fondly remember his 'gemmological brooch'—a simple mounting he used to transport topical stones to conferences across the world and share his insights with others.

Gem-A would like to express our sincere condolences to Prof. Dr Bank's family and friends. His enthusiasm, passion and significant contribution to the field of gemmology has created a multi-faceted legacy that will continue to benefit further generations of gemmologists.

Learning Opportunities

CONFERENCES AND SEMINARS

12th Annual Portland Jewelry Symposium

29–30 September 2019
Portland, Oregon, USA
<https://portlandjewelrysymposium.com>

International Colored Gemstone Association (ICA) Congress

12–15 October 2019
Bangkok, Thailand
<http://icacongress2019.com>

Chicago Responsible Jewelry Conference

25–26 October 2019
Chicago, Illinois, USA
www.chioresponsiblejewelryconference.com

Munich Show: Mineralientage München

25–27 October 2019
Munich, Germany
<https://munichshow.de/2019/06/26/2019-forum-minerale/?lang=en>
Note: Includes a seminar programme

Gem-A Conference 2019

2–3 November 2019
London
<https://gem-a.com/event/conference-2019>

2019 China International Gems & Jewelry Academic Conference

13–14 November 2019
Beijing, China
Email ngtcyjb@163.com

MAESA 2019: 2nd International Conference on Applied Earth Sciences

29 November–1 December 2019
Yangon, Myanmar
www.maesa.org/info_2019.html
Notes: A conference theme is ‘Mineralogy, Gemology and Genesis of Gem Deposits’. A post-conference excursion on 2–7 December will include a visit to Mogok.

Jewelry History Series

3–4 January 2020
Miami, Florida, USA
<https://originalmiamibeachantiqueshow.com/show/jewelry-history-series>
Note: This conference is part of The Original Miami Beach Antique Show.

22nd FEEG Symposium

24–27 January 2020
Schoonhoven, The Netherlands
www.feeg-education.com/symposium

NAJA 53rd ACE® IT Annual Winter Conference

2–3 February 2020
Tucson, Arizona, USA
www.najaappraisers.com/html/conferences.html

AGTA Gemfair Tucson

4–9 February 2020
Tucson, Arizona, USA
<https://agta.org/seminars>
Note: Includes a seminar programme

AGA Tucson Conference

5 February 2020
Tucson, Arizona, USA
<https://accreditedgemologists.org/currevent.php>

Tucson Gem and Mineral Show

13–16 February 2020
Tucson, Arizona, USA
www.tgms.org/show
Note: Includes a seminar programme

Inhorgenta Munich

14–17 February 2020
Munich, Germany
www.inhorgenta.com/index.html
Note: Includes a seminar programme

Prospectors & Developers Association of Canada PDAC 2020

1–4 March 2020
 Toronto, Ontario, Canada
www.pdac.ca/convention/programming/technical-program

Theme of interest: The Business of Diamonds: From Rock to Ring

36th International Geological Congress

2–8 March 2020
 New Delhi, India
www.36igc.org

Sessions of interest: Geology and Gemstones; Advances in Synthetic Gemstones; Diamonds Today; Gem Species and their Varieties

MJSA Expo

15–17 March 2020
 New York, New York, USA
https://mjsa.org/eventsprograms/mjsa_expo
Note: Includes a seminar programme

Amberif

18–21 March 2020
 Gdańsk, Poland
<http://amberif.amberexpo.pl/title,Jezyk,lang,2.html>
Note: Includes a seminar programme

10th National Opal Symposium

8–9 April 2020
 Coober Pedy, Australia
www.opalsymposium.org

inArt 2020: 4th International Conference on Innovation in Art Research and Technology

14–17 April 2020
 Paris, France
<https://inart2020.sciencesconf.org>

47th Rochester Mineralogical Symposium

23–26 April 2020
 Rochester, New York, USA
www.rasny.org/minsymp

American Gem Society Conclave

27–29 April 2020
 Denver, Colorado, USA
www.americangemsociety.org/mpage/conclave2020-home
Note: Includes a seminar programme

Diamonds – Source to Use 2020

9–11 June 2020
 Johannesburg, South Africa
www.saimm.co.za/saimm-events/upcoming-events/diamonds-source-to-use-2020

9th International Conference Mineralogy and Museums

5–7 July 2020
 Sofia, Bulgaria
www.bgminsoc.bg
Note: Gem minerals will be covered in a session titled ‘Mineralogical Research and Museums’.

25th Congress and General Assembly of the International Union of Crystallography

22–30 August 2020
 Prague, Czech Republic
www.xray.cz/iucr
Sessions of interest: Science Meets Art: Crystallography and Cultural Heritage; X-ray Spectrometry and X-ray Diffraction in Art and Archaeology; Superhard Materials: Status & Prospects

OTHER EDUCATIONAL OPPORTUNITIES**Gem-A Workshops and Courses**

Gem-A, London
<https://gem-a.com/education>

AIGS Mogok Mines, Market & Culture Tour

Mogok, Myanmar
 17–21 October 2019
www.aigsthailand.com/Mogok-Trip-Register/1/EN
Note: After the ICA Congress, visit gem mines and markets in the Mogok area with the Asian Institute of Gemological Sciences.

Lectures with Gem-A's Midlands Branch

Fellows Auctioneers, Augusta House, Birmingham
Email louiseludlam@hotmail.com

- Miranda Wells—The Changing Face of Tourmaline
27 September 2019
- Shirley Mitchell—Becoming A Valuer & the Part Gemmology Plays
25 October 2019
- Richard Maymon—Pearls
29 November 2019
- Dr Maria MacLennan—Forensic Jewellery
28 February 2020
- Peter Buckie—The Treasures Seen by an Expert Valuer
27 March 2020
- Roy Starkey—Minerals of the English Midlands
24 April 2020

Lectures with The Society of Jewellery Historians

Society of Antiquaries of London,
Burlington House, London
www.societyofjewelleryhistorians.ac.uk/current_lectures

- Sarah Steele, Léonard Pouy and Sigrid van Roode—New Research on Jewellery
22 October 2019
- Rachel Church—Brooches, Badges and Pins at the Victoria and Albert Museum
26 November 2019
- Thomas Holman—A Box Full of Buttons: The Life and Work of Frederick James Partridge (1877–1945)
28 January 2020
- Stephen Whittaker—TBA
25 February 2020
- Carol Michaelson—Chinese Jade Jewellery and Ornaments from the Neolithic to the Present
24 March 2020

Gem-A
THE GEMMOLOGICAL ASSOCIATION OF GREAT BRITAIN

Do you follow Gem-A on social media?

Stay up-to-date with Gem-A @GemAofGB



PAUL WILD

EXCELLENCE IN
GEMSTONE INNOVATION



TSAVORITE

Known for its great brilliance, clarity and radiant colour, the spectacular tsavorite is an exquisite investment for the true connoisseur.

MINING • CUTTING • CREATION

PAUL WILD OHG • AUF DER LAY 2 • 55743 KIRSCHWEILER • GERMANY
T: +49.(0)67 81.93 43-0 • F: +49.(0)67 81.93 43-43 • E-MAIL: INFO@PAUL-WILD.DE • WWW.PAUL-WILD.DE

VISIT US AT

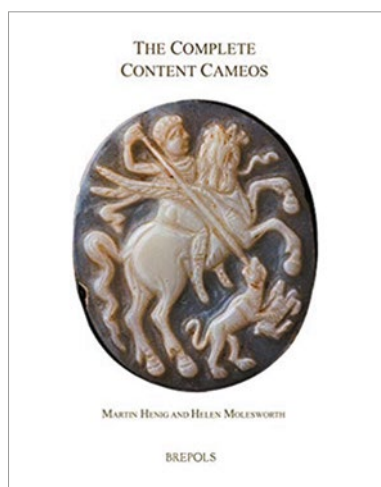
The Munich Show
Mineralientage München



GEMWORLD
MUNICH

MUNICH SHOW BOOTH NO. B6.441
OCTOBER 25 – 27, 2019

New Media



The Complete Content Cameos

By Martin Henig and Helen Molesworth, 2018.
Brepols Publishers, Turnhout, Belgium,
www.brepols.net/Pages/ShowProduct.aspx?prod_id=IS-9782503578965-1,
iv+407 pages, illus., ISBN 978-2503578965.
EUR150.00 hardcover.

Note: the correct year is 1990.

Derek Content's collection of hardstone cameos is, as far as is known, the largest in private hands. Between 1900 and 2000 the Ashmolean Museum displayed the collection, as it was then, in a specially built case, with an accompanying catalogue. The collection is now very much larger and is extraordinarily comprehensive. In view of the additions and the greatly increased scholarly knowledge of cameos (due in part to several recent catalogues of other collections), this new catalogue was called for. Over a number of years Martin Henig, one of the world's great engraved gem scholars, together with Helen Molesworth, an archaeologist and gemmologist, compiled this magnificent volume with contributions from other specialists, including Christopher Cavey, Jeffrey Spier and Content himself. It is beautifully produced on heavy art paper with stunning photographs. Although Content says in the preface that 'it is time to consider the collection a closed entity', he is still, unsurprisingly, collecting; perhaps there will be a supplemental volume in the future.

Cameos were for many years considered poor relations of intaglios, although the skills involved in deep three-

Note: The correct number is 441.

dimensional carving of very difficult materials, using the different colour layers, were quite extraordinary.

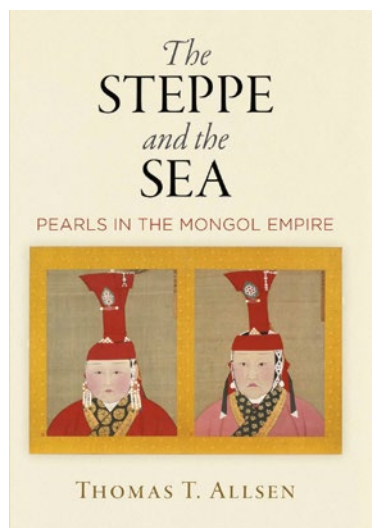
The 425 cameos dealt with in this book range from the 9th century BCE to the 18th century CE. The ancient specimens are presented mostly in chapters by theme, rather than strictly chronologically, including Portraits, Deities and Myths, Dionysiac, Eros, Gorgoneia, Animals, Daily Life, Theatre and Music, and Legends. Separate chapters cover important periods (Hellenistic, Byzantine and Medieval, and Renaissance and Later), followed by a chapter on less-common countries of origin and one titled 'Carvings in the Round'. The book ends with an essay on ancient mountings; indexes by subject, material, mountings and provenance; and an extremely comprehensive bibliography.

The number of published cameos now available for comparative study allowed the authors to examine the popularity of particular subjects during various periods, together with the development of styles and techniques, and the use of gem materials. The authors attempted to date every item, although they admit this is an inexact science. Indeed, it is inevitable that more international research will result in the need to revise some attributions. It is hoped that this publication will spur such research and encourage some of the great institutions to produce comparable catalogues of their collections. (The British Museum catalogue is still the rather cursory 1926 listing by H. B. Walters!)

It is a great pity that a DVD of the images was not included with the book (as has been done with some recent catalogues). This would have greatly enhanced the ability to study these superb cameos. Also, as great as the photographs are, two-dimensional images cannot really give the feel of deeply carved objects. Modern technology—such as high-definition three-dimensional scanning—would enable the cameos to be turned and viewed in all orientations on a screen.

This really splendid publication will remain, however, a major standard reference work for the foreseeable future, and it is currently the only major modern publication in English on ancient cameos. Indeed, it is extremely difficult to imagine that any future serious research into hardstone cameos could be conducted without reference to it.

Nigel Israel FGA DGA
London



The Steppe and the Sea: Pearls in the Mongol Empire

By Thomas T. Allsen, 2019. University of Pennsylvania Press, Philadelphia, Pennsylvania, USA, www.upenn.edu/pennpress/book/15970.html, 240 pages, illus., ISBN 978-0812251173. USD45.00 hardcover or USD36.00 eBook.

This volume is part of the ‘Encounters with Asia’ series from the University of Pennsylvania Press, and its author was professor emeritus of The College of New Jersey. The ‘was’ is sadly significant, because Prof. Allsen passed away in February 2019, shortly before this book was published. Allsen was a highly respected expert and author on medieval Eurasia and the Mongol Empire. It is gratifying that he directed his erudite attention to a gem material—the pearl—and looked at it in the context of its trade and importance in and across the Mongol Empire from 1206 to 1370. Even those not familiar with the Mongol Empire will know of its founder, Genghis Khan. At its height in the late 1200s, before it began to split under Genghis’s grandsons, the Mongol Empire was the largest contiguous land empire the world has yet seen, stretching from what is now Eastern Europe across to China. It also extended as far south as the Persian Gulf, with trade routes directly linking the Chinese court with the Arabian pearl beds.

At the outset, it must be stated that this book is a highly academic work, the fruit of very extensive research and clear evidence of Prof. Allsen’s proficiency in the Chinese, Persian, Arabic and Russian languages. It is a valuable addition to information we have about pearls and their value, symbolism and trade in the past, supplementing Robin Donkin’s monumental and essential *Beyond Price: Pearls and Pearl Fishing* (1998). It is neither a light read nor particularly visually appealing; it is a

reference work. It is amusing to note that the publishers, presumably hoping to widen its appeal, begin the inside dust-jacket blurb with mention of a female prisoner in 1221 who confessed to having swallowed her pearls, only to be killed and eviscerated on the spot.

The book itself proves less sensationalist generally, of course, but despite the tight focus on history and the myriad textual sources, Allsen wears his scholarship lightly and consummately puts pearls within a very human context. At one point, for example, he refers to the ‘price fixing, kickbacks, gross mismanagement and outright theft’ within the pearl-loving Mongol court. In another case he notes, with regard to the diminishment of a treasury as a result of lax guarding and bribery, ‘What happened in those instances would now be called a breakdown of inventory control, though it is fairly obvious that little if any control was ever exercised.’ Referring to the sad susceptibility of pearls to decay with time, he notes succinctly, ‘While diamonds are forever, pearls are not.’

The wealth of textual information Allsen has gathered from across the Mongol world is distilled into chapters that cover everything from pearl fishing and processing to prices and counterfeits. With regard to the latter, he notes that the culturing of pearls in China dates back to as early as the ninth century—much sooner than I thought.

The lack of illustrations in the book is a huge shame. There are just four, all in greyscale (apart from the dust jacket). There are no images of actual pearl-set jewellery. The closest are two images of early gold jewellery that have nothing to do with Mongol culture and are included because they illustrate spherical gold components that are resourcefully described as ‘pearl shaped’. Even in a scholarly book that concentrates on the historical aspects of pearls, a few choice illustrations would have been good. Photos of some impressive Mongol gold jewellery have been published in recent years, including pearl-set pieces, as seen in Mikhail Piotrovskii’s beautifully illustrated *The Treasures of the Golden Horde* (2000).

According to the dust jacket, Jos Gommans, professor of Colonial and Global History at Leiden University, The Netherlands, described this book as offering ‘new insights into the wider socioeconomic and cultural history of the Mongol Empire’. Since this review is in a gemmological publication, I will simply plagiarise this statement with a slight modification and say that this book offers new insights into the wider socioeconomic and cultural history of *the pearl*. It is a welcome addition to the gem or jewellery historian’s bookshelf.

Dr Jack M. Ogden FGA
London

Other Book Titles

CULTURAL HERITAGE

All That Glittered: Britain's Most Precious Metal from Adam Smith to the Gold Rush

By Timothy Alborn, 2019. Oxford University Press, New York, New York, 276 pages, ISBN 978-0190603519. USD35.00 hardcover or USD23.99 Kindle edn.

Masterpieces in Miniature: Engraved Gems from Prehistory to the Present

By Claudia Wagner and John Boardman, 2018. Philip Wilson Publishers, London, 304 pages, ISBN 978-1781300626. GBP40.00 hardcover.

GENERAL REFERENCE

The Science of Gemstones

By Ahmadjan Abduriyim, 2019. Ark Publishing Inc., 271 pages, ISBN 978-4860592066 (in Japanese). JPY2,500.00 softcover.

INSTRUMENTATION

Handbook of Advanced Non-Destructive Evaluation

Ed. by Nathan Ida and Norbert Meyendorf, 2019. Springer, Cham, Switzerland, 1,626 pages, ISBN 978-3319265520 (print), 978-3319265537 (eBook) or 978-3319301228 (print plus eBook). EUR727.99 hardcover, EUR832.99 eBook or EUR1,143.99 hardcover plus eBook (in two volumes, not available separately).

JEWELLERY HISTORY

Chaumet en Majesté: Joyaux de Souveraines Depuis 1780

By Stéphane Bern and Christophe Vachaud, 2019. Flammarion, Paris, France, 288 pages, ISBN 978-82081489349 (in French). EUR30.00 softcover.

Designers and Jewellery 1850–1940

By Helen Ritchie, 2018. Philip Wilson Publishers, London, 176 pages, ISBN 978-1781300671. GBP16.95 softcover.

JEWELLERY AND OBJETS D'ART

The Art of the Jeweler: Excellence and Craftsmanship

By Guillaume Glorieux, 2019. Éditions Gallimard, Paris, France, 76 pages, ISBN 978-2072822605. EUR14.50 softcover.

Bejeweled: The World of Ethical Jewelry

By Kyle Roderick, 2019. Rizzoli, New York, New York, USA, 224 pages, ISBN 978-0847865888. USD65.00 hardcover.

Brooches and Badges

By Rachel Church, 2019. Thames & Hudson, New York, New York, USA, 160 pages, ISBN 978-0500480359. USD24.95 hardcover.

Bulgari: The Perfume of Gems

By Brian Eno, Annick Le Guerier, Chiara Gamberale and Renato Bruni, 2018. Rizzoli, New York, New York, USA, 272 pages, ISBN 978-0847865383. USD150.00 hardcover.

Bulgari: Stories of Gems and Jewels

Ed. by Lucia Boscaini and Chiara Ottaviano, 2019. Rizzoli, New York, New York, USA, 352 pages, ISBN 978-8891824325. USD65.00 hardcover.

Diamond Jewelry: 700 Years of Glory and Glamour

By Diana Scarisbrick, 2019. Thames & Hudson, New York, New York, USA, 256 pages, ISBN 978-0500021507. USD75.00 hardcover.

Marie-Helene de Taillac: Gold and Gems

By Marie-Helene de Taillac and Eric Deroo, 2019. Rizzoli, New York, New York, USA, 224 pages, ISBN 978-0847865376. USD85.00 hardcover.

Masters of New Jewellery Design: Eclat

By Carlos Pastor, 2019. Promopress, Barcelona, Spain, 236 pages, ISBN 978-8492810970. EUR29.00 softcover.

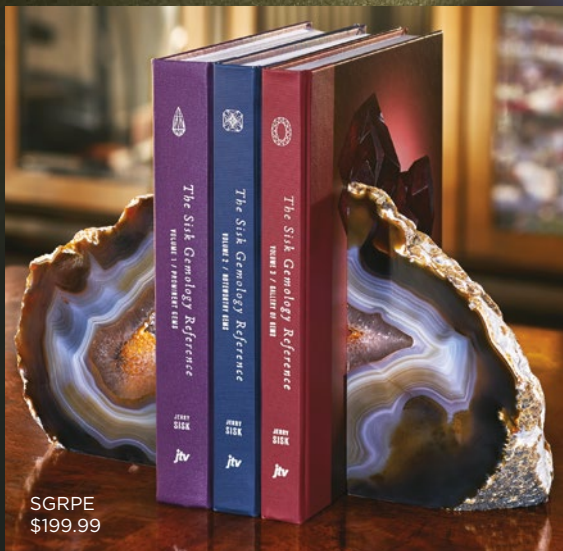
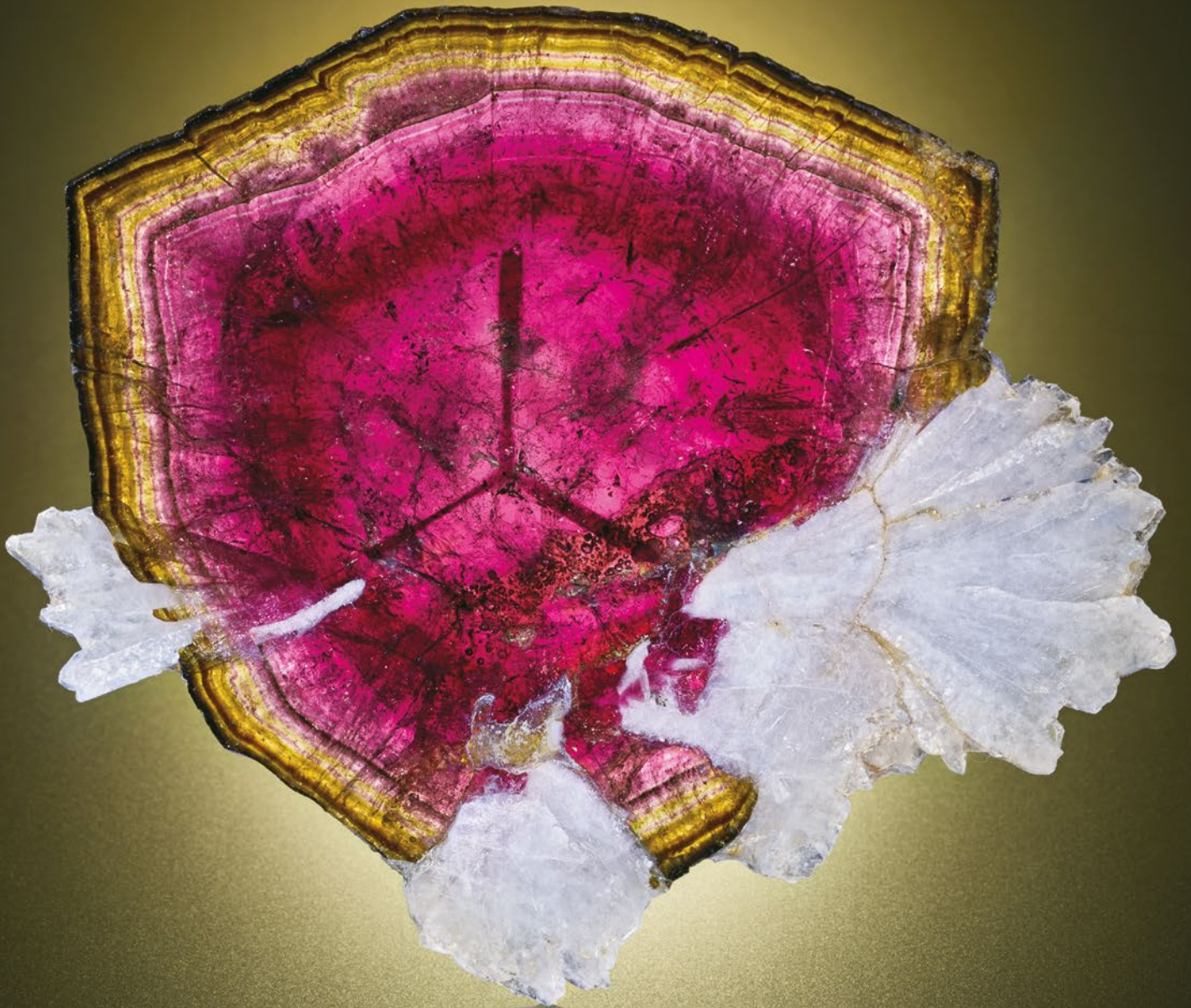
Museo del Gioiello di Vicenza:

Gioiello & Jewellery 3

Ed. by Alba Cappellieri, 2018. Silvana Editoriale, Milan, Italy, 344 pages, ISBN 978-8836642205 (in English and Italian). EUR34.00 hardcover.

New Necklaces: 400 Designs in Contemporary Jewellery

By Nicolás Estrada, 2019. Promopress, Barcelona, Spain, 240 pages, ISBN 978-8417412432. EUR29.00 hardcover.



SGRPE
\$199.99

The Sisk Gemology Reference by Jerry Sisk Professional Edition

A comprehensive and visual gemology resource
featuring prominent and noteworthy gemstones.

jtv[®]
jewelry love
jtv.com/sgr

Literature of Interest

COLOURED STONES

Almandine gemstone—A review. N. Sultana and S.P. Podila, *International Journal of Recent Scientific Research*, **9**(10B), 2018, 29204–29209.

Bixbite: The rarest common gem in the world. M. Macrì, *Rivista Italiana di Gemmologia/Italian Gemmological Review*, No. 7, 2019, 47–55.

Black nephrite jade from Guangxi, southern China. Q. Zhong, Z. Liao, L. Qi and Z. Zhou, *Gems & Gemology*, **55**(2), 2019, 198–215, <http://doi.org/10.5741/GEMS.55.2.198>.*

Characteristics of faceted-quality ruby from Longido, Tanzania. T. Leelawatanasuk, N. Susawee and P. Bupparenoo, *Bulletin of Earth Sciences of Thailand*, **9**, 2018, 1–7, <http://tinyurl.com/y8pzxf3m>.*

Color mechanisms in spinel: A multi-analytical investigation of natural crystals with a wide range of coloration. G.B. Andreozzi, V. D'Ippolito, H. Skogby, U. Hålenius and F. Bosi, *Physics and Chemistry of Minerals*, **46**(4), 2018, 343–360, <http://doi.org/10.1007/s00269-018-1007-5>.

A comparative study of element content and UV–VIS spectroscopy characteristics of rubies from Burma and Mozambique. K. Guo, Z. Zhou, Q. Zhong, M. Lai, H. Wang, Y. Li, X. Qiao and P. Nong, *Acta Petrologica et Mineralogica*, **37**(6), 2018, 1002–1010 (in Chinese with English abstract).

Les différentes facettes du jade [The different facets of jade]. Tay Thye Sun, *Revue de Gemmologie A.F.G.*, Nos. 204–205, 2018, 53–58 (in French).

Fingerprinting Paranesti rubies through oxygen isotopes. K. Wang, I. Graham, L. Martin, P. Voudouris, G. Giuliani, A. Lay, S. Harris and A. Fallick, *Minerals*, **9**(2), 2019, article 91 (14 pp.), <http://doi.org/10.3390/min9020091>.*

Flickering flames over the Libyan desert [Libyan desert glass]? J.M. Saul, *International Geology Review*, 2018, **61**(11), 1340–1369, <http://doi.org/10.1080/00206814.2018.1512057>.

Gemmological characteristic of “crystal opal” from Coober Pedy, Australia. W. Peng and T. Jiang, *Journal of Gems & Gemmology*, **20**(Supp.), 2018, 122–128 (in Chinese with English abstract).

The gemmological characteristics of Guatemalan jade. L. Li, Y. Xiong, N. Liu and Y. Cao, *Superhard Material Engineering*, **30**(3), 2018, 55–59 (in Chinese with English abstract).

Genetic significance of the 867 cm⁻¹ out-of-plane Raman mode in graphite associated with V-bearing green grossular. R. Thomas, A. Rericha, W.L. Pohl and P. Davidson, *Mineralogy and Petrology*, **112**(5), 2018, 633–645, <http://doi.org/10.1007/s00710-018-0563-1>.

Inclusions in natural, treated, synthetic, and imitation opal [chart]. N.D. Renfro, J.I. Koivula, J. Muyal, S.F. McClure, K. Schumacher and J.E. Shigley, *Gems & Gemology*, **55**(2), 2019, 244–245 plus chart, <http://doi.org/10.5741/GEMS.55.2.244>.*

Masters of green: Chromium and vanadium. K. Feral, *Gemmology Today*, March 2019, 28–32, www.worldgemfoundation.com/GTMARCH2019DV/html5forpc.html?page=28.*

Masters of green: Chromium and vanadium (part two). K. Feral, *Gemmology Today*, June 2019, 38–45, www.worldgemfoundation.com/GTJUNE2019DV/html5forpc.html?page=38.*

The power of cobalt [spinel]. G. Dominy, *Gemmology Today*, June 2019, 34–37, www.worldgemfoundation.com/GTJUNE2019DV/html5forpc.html?page=34.*

The siren’s call [Siren of Serendip 422.66 ct blue sapphire necklace]. R. Galopim de Carvalho, *Gems&Jewellery*, **28**(3), 2019, 36–37.

The story of Blue John. E.Z. Karlin, *Adornment*, **12**(1), 2019, 28–44.

Study on mineralogy and spectroscopy of turquoises from Hami, Xinjiang. X. Liu, C. Lin, D. Li, L. Zhu, S. Song, Y. Liu and S. Chong-hui, *Spectroscopy and Spectral Analysis*, **38**(4), 2018, 1231–1239 (in Chinese with English abstract).

Tenebrescence of sapphire. B. Zhao, Y. Zhi, X. Lyu and Y. Wang, *Journal of Gems & Gemmology*, **20**(5), 2018, 1–14 (in Chinese with English abstract).

Wearable wulfenite. M. Mauthner, *Rocks & Minerals*, **94**(1), 2019, 32–33, <http://doi.org/10.1080/00357529.2019.1519670>.

CULTURAL HERITAGE

The digital microscope and multi-scale observation in the study of lapidary manufacturing techniques: A methodological approach for the preliminary phase of analysis in situ. E. Morero, H. Procopiou, J. Johns, R. Vargiolu and H. Zahouani, in K. Kelley and R.K.L. Wood, Eds., *Digital Imaging of Artefacts: Developments in Methods and Aims*. Archaeopress Publishing Ltd, Sommertown, Oxford, 2018, 75–100, <https://eprints.soton.ac.uk/426431/1/seals2018.pdf#page=89>.*

The importance of jade in the Mughal court. T. Schneider, *Gems&Jewellery*, **28**(3), 2019, 32–35.

Making history [Christie's sale of Mughal treasures from the Al Thani Collection]. J. Ogden, *Gems&Jewellery*, **28**(3), 2019, 22–25.

Objets préhistoriques en jade-néphrite (VII^e au V^e millénaires Av. J.-C.) de Bulgarie et des Balkans [Prehistoric jade-nephrite objects (7th-5th millennium BC) from Bulgaria and the Balkans]. R.I. Kostov, *Revue de Gemmologie A.F.G.*, Nos. 204–205, 2018, 36–42 (in French with English abstract).

Poly-material ornaments: The Iron Age amber fibulae. N.L. Saldalamacchia, *Rivista Italiana di Gemmologia/Italian Gemological Review*, No. 7, 2019, 65–68.

Unveiling the art of René Lalique with XRF and Raman spectroscopy – Technological innovation in jewellery production. I. Tissot, M. Manso and M.F. Guerra, *Journal of Cultural Heritage*, **33**, 2018, 83–89, <http://doi.org/10.1016/j.culher.2018.03.014>.

DIAMONDS

The 709 carat diamond, Rapaport, ethics and auctions in Sierra Leone. D. Angelino, *Rivista Italiana di Gemmologia/Italian Gemological Review*, No. 7, 2019, 41–44.

Diamonds from the deep—Kimberlites: Earth's diamond delivery system. K.V. Smit and S.B. Shirey, *Gems & Gemology*, **55**(2), 2019, 270–276, www.gia.edu/gems-gemology/summer-2019-kimberlites-earths-diamond-delivery-system.*

Identifying and valuing Old European cut diamonds. R.B. Drucker, *GemGuide*, **38**(4), 2019, 4–7.

Jwaneng – The untold story of the discovery of the world's richest diamond mine. N. Lock, *Journal of the Southern African Institute of Mining and Metallurgy*, **119**(2), 2019, 155–164, <http://doi.org/10.17159/2411-9717/2019/v119n2a8>.*

A quantitative testing method for the evaluation of diamond color. Y. Cheng, C. Fan, Y. Wang, C. Zhang, H. Zhu and S. Chen, *Spectroscopy and Spectral Analysis*, **39**(5), 2019, 1643–1647 (in Chinese with English abstract).

A record-breaking jewel [cutting the 1,109 ct Lesedi La Rona rough diamond]. Anonymous, *Gems&Jewellery*, **28**(2), 2019, 39–41.

GEM LOCALITIES

Amethyst occurrences in Tertiary volcanic rocks of Greece: Mineralogical, fluid inclusion and oxygen isotope constraints on their genesis. P. Voudouris, V. Melfos, C. Mavrogonatos, A. Tarantola, J. Götze, D. Alfieris, V. Maneta and I. Psimis, *Minerals*, **8**(8), 2018, article 324 (26 pp.), <http://doi.org/10.3390/min8080324>.*

A decade of ruby from Mozambique: A review. W. Vertriest and S. Saeseaw, *Gems & Gemology*, **55**(2), 2019, 162–183, <http://doi.org/10.5741/GEMS.55.2.162>.*

Gems of Italy [prehnite to dendritic spessartine].

E. Amore, R. Appiani, V. Bordoni, M. Campos Venuti, G. Cattaneo, F. Caucia, G. Conti-Vecchi, E. Costa, C. Ghisoli, A. Guizzardi, D. Leoni, M. Macrì, A. Maras, L. Marinoni, M. Mauri, L.M. Pich, A. Mottana, P. Stara, S. Tegani and F. Troilo, *Rivista Italiana di Gemmologia/Italian Gemological Review*, No. 7, 2019, 22–33.

Geochemical characteristics and Ar-Ar dating of different nephrite deposits in Qinghai Province.

H. Yu, Q. Ruan, B. Liao and D. Li, *Acta Mineralogica Sinica*, **38**(4), 2018, 655–668 (in Chinese with English abstract).

The Malkhan pegmatite district, Krasny Chikoy, Transbaikalia, eastern Siberian region, Russia.

J. Kynický, J. Kynický, B. Lees, W. Song, M. Kotlanova, G. Wagner and P. Persson, *Mineralogical Record*, **50**(3), 2019, 235–324.

Mighty Montepuez [ruby mine in Mozambique].

M. Dettmer, *Gems&Jewellery*, **28**(2), 2019, 22–25.

Modern discovery of Aappaluttoq [Greenland ruby].

D. Turner, W. Rohtert, M. Ritchie and B. Wilson, *Gems&Jewellery*, **28**(2), 2019, 14–17.

Trace elements and U-Pb ages of zircons from Myanmar jadeite-jade by LA-ICP-MS: Constraints for its genesis. S. Cai and E. Zhang, *Spectroscopy and Spectral Analysis*, **38**(6), 2018, 1896–1903 (in Chinese with English abstract).

INSTRUMENTATION**3D imaging of gems and minerals by multiphoton microscopy.**

B. Cromey, R.J. Knox and K. Kieu, *Optical Materials Express*, **9**(2), 2019, 516–525, <http://doi.org/10.1364/ome.9.000516>.*

The characterization of natural gemstones using non-invasive FT-IR spectroscopy: New data on tourmalines.

M. Mercurio, M. Rossi, F. Izzo, P. Cappelletti, C. Germinario, C. Grifa, M. Petrelli, A. Vergara and A. Langella, *Talanta*, **178**, 2018, 147–159, <http://doi.org/10.1016/j.talanta.2017.09.030>.

Sensitive and rapid oxygen isotopic analysis of nephrite jade using large-geometry SIMS.

A. Schmitt, M.-C. Liu and I. Kohl, *Journal of Analytical Atomic Spectrometry*, **34**(3), 2019, 561–569, <http://doi.org/10.1039/c8ja00424b>.

MISCELLANEOUS

An analysis on branded gemstones. Ç. Lüle, *GemGuide*, **38**(3), 2019, 4–8.

The art of photomicrography. D. Pregun, *Gems&Jewellery*, **28**(2), 2019, 34–37.

Jewellery: From material to affection. A. Passos, *Journal of Jewellery Research*, **2**, 2019, 16 pp., www.journalofjewelleryresearch.org/download/ana-passos.*

The local translation of global norms: The Sierra Leonean diamond market. N. Engwicht, *Conflict, Security & Development*, **18**(6), 2018, 463–492, <http://doi.org/10.1080/14678802.2018.1532639>.*

Man-made diamonds are diamonds too. This new extended definition isolates the FTC from European standards. P. Minieri, *Rivista Italiana di Gemmologia/Italian Gemological Review*, No. 7, 2019, 34–38.

Valuation considerations, home and abroad. S. Mitchell, *GemGuide*, **38**(3), 2019, 9–12.

ORGANIC/BIOGENIC GEMS

L'Ambre birman : la redécouverte d'un ancien gisement, son trésor de fossils [Burmese Amber: The rediscovery of a former deposit, its treasure of fossils]. S. Ellenberger, *Revue de Gemmologie A.F.G.*, Nos. 204–205, 2018, 63–71 (in French).

Can DNA be extracted from amber?

K. Szawaryn, *Bursztynisko (The Amber Magazine)*, No. 43, 2019, 96–97, https://issuu.com/internationalamberassociation/docs/bursztynisko_43/98 (in English and Polish).*

Inclusions [in amber]: Imagination vs. reality.

A.K.-K.E. Sontag, *Bursztynisko (The Amber Magazine)*, No. 43, 2019, 92–94, https://issuu.com/internationalamberassociation/docs/bursztynisko_43/94 (in English and Polish).*

Infrared spectroscopic characteristics of Borneo and Madagascar copal resins and rapid identification between them and ambers with similar appearances.

L. Dai, G. Shi, Y. Yuan, M. Wang and Y. Wang, *Spectroscopy and Spectral Analysis*, **38**(7), 2018, 2123–2131 (in Chinese with English abstract).

PEARLS

Un aperçu sur les perles d'eau douce d'Amérique du Nord [An overview of freshwater pearls from North America]. G. Latendresse, *Revue de Gemmologie A.F.G.*, Nos. 204–205, 2018, 59–62 (in French).

Component analysis and identification of black Tahitian cultured pearls from the oyster *Pinctada margaritifera* using spectroscopic techniques. L. Shi, Y. Wang, X. Liu and J. Mao, *Journal of Applied Spectroscopy*, **85**(1), 2018, 98–102, <http://doi.org/10.1007/s10812-018-0618-4>.

Evidence of rotation in flame-structure pearls from bivalves of the Tridacnidae family. J.-P. Gauthier, J. Fereire and T.N. Bui, *Gems & Gemology*, **55**(2), 2019, 216–228, <http://doi.org/10.5741/GEMS.55.2.216>.*

The optical characteristics of cultured akoya pearl are influenced by both donor and recipient oysters. T. Iwai, M. Takahashi, C. Miura and T. Miura, in K. Endo, T. Kogure & H. Nagasawa, Eds., *Biom mineralization*, Springer, Singapore, 2018, 113–119, http://doi.org/10.1007/978-981-13-1002-7_12.*

A pearl identification challenge. N. Sturman, L.M. Otter, A. Homkrajae, A. Manustrong, N. Nilpetploy, K. Lawanwong, P. Kessrapong, K.P. Jochum, B. Stoll, H. Götz and D.E. Jacob, *Gems & Gemology*, **55**(2), 2019, 229–243, <http://doi.org/10.5741/GEMS.55.2.229>.*

Pearl varieties. K. Gregory, *GemGuide*, **38**(2), 2019, 8–11.

SYNTHETICS

10x – From the analyst's notebook. An investigation on a red faceted stone [synthetic ruby]. C. Cumo, *Rivista Italiana di Gemmologia/Italian Gemological Review*, No. 7, 2019, 7–13.

Crystallography 101 – A seven-sided emerald crystal [hydrothermal synthetic emerald]?

J.-M. Arlabosse, *Gemmology Today*, June 2019, 5–8, www.worldgemfoundation.com/GTJUNE2019DV/html5forpc.html?page=4.*

Research on laboratory testing features of chemical vapor deposition in overgrowth diamonds. S. Tang,

J. Su, T. Lu, Y. Ma, J. Ke, Z. Song, J. Zhang, X. Zhang, H. Dai, H. Li, J. Zhang, X. Wu and H. Liu, *Rock and Mineral Analysis*, **38**(1), 2019, 62–70 (in Chinese with English abstract).

TREATMENTS

Aesthetic improvement of transparent natural quartz by heat treatment at different temperature. R.K. Sahoo, B. Dhal, S.K. Singh and B.K. Mishra, *International Journal of Nano and Biomaterials*, **7**(3), 2018, 231–241, <http://doi.org/10.1504/ijnbm.2018.094251>.

Behandelte Korunde - Einführung in die Thematik [Treated corundum - Introduction to the topic]. T. Lind, *Gemmologie: Zeitschrift der Deutschen Gemmologischen Gesellschaft*, **67**(3/4), 2018, 1–10 (in German).

Diffusions- und Oberflächenbehandlung bei Korunden [Diffusion and surface treatment of corundum]. U. Henn, C.C. Milisenda, T. Stephan and B. Huaysan, *Gemmologie: Zeitschrift der Deutschen Gemmologischen Gesellschaft*, **67**(3/4), 2018, 47–60 (in German with English abstract).

Effect of heat treatment on the luminescence properties of natural apatite. P. Chindudsadeegul and M. Jamkratoke, *Spectrochimica Acta Part A: Molecular and Biomolecular Spectroscopy*, **204**, 2018, 276–280, <http://doi.org/10.1016/j.saa.2018.06.056>.

Madagascar sapphire: Low-temperature heat treatment experiments. E.B. Hughes and R. Perkins, *Gems & Gemology*, **55**(2), 2019, 184–197, <http://doi.org/10.5741/GEMS.55.2.184>.*

Nachweis der Temperaturbehandlung von Korund [Identification of the heat treatment of corundum]. T. Stephan and S. Müller, *Gemmologie: Zeitschrift der Deutschen Gemmologischen Gesellschaft*, **67**(3/4), 2018, 21–36 (in German with English abstract).

Reinheitsverbesserung von Korunden durch Rissbehandlung [Clarity enhancement of corundum by fissure treatment]. T. Stephan and U. Henn, *Gemmologie: Zeitschrift der Deutschen Gemmologischen Gesellschaft*, **67**(3/4), 2018, 37–46 (in German with English abstract).

Temperaturbehandlung von Korund [Heat treatment of corundum]. T. Häger, *Gemmologie: Zeitschrift der Deutschen Gemmologischen Gesellschaft*, 67(3/4), 2018, 11–20 (in German with English abstract).

Titanium – Heating rutile is never futile.

G. Dominy, *Gemmology Today*, March 2019, 22–26, www.worldgemfoundation.com/GTMARCH2019DV/html5forpc.html?page=22.*

COMPILATIONS

G&G Micro-World. Intergrown emerald specimen from Chivor • Purple fluorite inclusion in Russian emerald • Helical inclusion in Colombian emerald • Mexican opal with large fluid inclusion • Pyrope-almandine in sapphire • Euhedral phantom sapphire in sapphire • Curved banding in flame-fusion synthetic sapphires • Iridescent Tabasco (Mexico) geode • Inclusion-rich black topaz from the Thomas Mountains, Utah, USA • Diopside in and on quartz. *Gems & Gemology*, 55(2), 2019, 260–269, www.gia.edu/gg-issue-search?ggissueid=1495287212844&articlesubtype=microworld.*

Gem News International. Plume agate from Iran • Jadeite from the Polar Urals • Natural freshwater pearls from the Mississippi River system • Trapiche quartz • Rubies from Rock Creek, Montana • Glass-filled polki-cut CVD synthetic diamonds • Low-temperature heat treatment of pink sapphire • Tagua nut as a sustainable replacement for ivory. *Gems & Gemology*, 55(2), 2019, 278–292, www.gia.edu/gg-issue-search?ggissueid=1495287212844&articlesubtype=gni.*

Lab Notes. Resin-coated and clarity-enhanced aquamarine pendant • Rough diamond with fake green ‘radiation stains’ • Separation of kornerupine and prismatic • Faceted milarite • ‘Hollow’ pearl filled with foreign materials • Dyed serpentine imitating sugilite • Color-change spessartine • Spurrite cabochon • Natural-looking exsolved particles in flux-grown pink synthetic sapphire. *Gems & Gemology*, 55(2), 2019, 246–259, www.gia.edu/gg-issue-search?ggissueid=1495287212844&articlesubtype=labnotes.*

*Article freely available for download, as of press time



SAVE THE DATE
Gem-A's Big Gem Bash,
Tucson 2020

THURSDAY 6 FEBRUARY 2020
Scottish Rite Cathedral, 160 S Scott Ave, Tucson, AZ 85701
6:30 – 8:30pm

Calling all gemmologists!
Don't miss the best networking event in town!
REGISTRATION OPENS SOON.



Gem-A

THE GEMMOLOGICAL ASSOCIATION
OF GREAT BRITAIN

BOOK NOW!

Gem-A Conference 2019

November 2-3

etc.venues County Hall, London



Bringing together the greatest minds in Gemmology



REASONS TO ATTEND

- ◆ An amazing line-up of speakers from all corners of gemmology.
- ◆ Network with some of the leaders in the field during the Conference breaks and the Saturday evening dinner.
- ◆ Learn from speakers and fellow delegates.
- ◆ Exclusive workshops and trips including private viewings.
- ◆ Join us for dinner on the 2 November at the House of Commons, an iconic venue that forms part of the Palace of Westminster.

Register your place: gem-a.com/event/conference

Gem-A Members and Students! You have been sent an email with a link to book the members/student rate. Contact events@gem-a.com if you haven't received the email.

Creating gemmologists since 1908



Color is a power which directly influences the soul
— *Wassily Kandinsky*



Pala International

PalaGems.com / PalaMinerals.com

+1 800 854 1598 / +1 760 728 9121

Chartreuse tourmaline • 43.40 ct • Spessartine • 33.48 ct • Purple tourmaline from Mozambique • 18.17 ct

Blooms from Pala International Grounds • Photo: Mia Dixon